FORECASTING SUMMER/FALL EL NIÑO-SOUTHERN OSCILLATION EVENTS AT 6-11 MONTH LEAD TIMES

Stacey A. Seseske

Principal Investigator: William M. Gray

Department of Atmospheric Science

Colorado State University

Fort Collins, Colorado 80523

June, 2004

ATS Paper No. 749

ABSTRACT

Accurately predicting El Niño-Southern Oscillation (ENSO) events is an important yet challenging task, especially at the extended range of 6-11 months. This research offers a new methodology for forecasting extended range ENSO events, utilizing global data and a statistical model. Most ENSO forecasts utilize data local to the Pacific Ocean basin. This research uses an all-subsets technique to select from an inclusive pool of global predictors that are able to capture useful ENSO precursor signals beyond the Pacific basin. A multiple linear regression using the best five predictors produced a December 1 forecast for the June-July-August (6-8 month forecast) and the September-October-November (9-11 month forecast) Sea Surface Temperature Anomaly (SSTA) in the Niño 3.4 region (5°N-5°S, 120-170°W). The performance of each forecast was then compared to the analogous 1 December ENSO-CLIPER (Knaff and Landsea 1997) forecast which is held as a benchmark for specifying ENSO forecast skill.

Results for the 6-8 month forecast (1 December to JJA) show that the scheme presented in this research (herein referred to as SG) explains more variance than that of the ENSO-CLIPER scheme. The SG scheme accounts for 58 percent of the variance for the period 1952-2002, while the ENSO-CLIPER model explains only 14 percent for the same period.

The 9-11 month forecast (1 December to SON) shows that SG only improves slightly upon ENSO-CLIPER. The SG forecast explained 36 percent of the variance for the 1950-2002 period, while ENSO-CLIPER explained 25 percent. However, by combining the two schemes (SG + ENSO-CLIPER) it is possible to explain over 50 percent of the variance in the SON SSTA timeseries 9-11 months in advance.

TABLE OF CONTENTS

LIST OF SYMBOLS AND ACRONYMS

CDC: Climate Diagnostics Center, Boulder, Colorado

El Niño: When anomalously warm sea surface temperatures greater than 0.4°C occur in the Niño 3.4 region of the Pacific for at least six months.

ENSO: El Niño-Southern Oscillation - A global climate phenomenon related to the shift of atmospheric pressure between Darwin, Australia and Tahiti that influences the sea surface temperatures in the tropical Pacific.

ENSO-CLIPER: Statistical ENSO forecast model that is used as a benchmark of skill in forecasting ENSO events

GZ: Geopotential Height - The height of the given pressure level.

JJA: June-July-August

La Niña: When anomalously cool sea surface temperatures less than -0.4°C occur in the Niño 3.4 region of the Pacific for at least six months.

MB: Millibar - Unit of measure for air pressure

NCEP: National Centers for Environmental Prediction, Washington, D.C.

Niño 3.4: The region in the Pacific (5°N-5°S, 120-170°W) used to define ENSO events.

Obs: Observations

PDO: Pacific Decadal Oscillation

RMSE: Root mean squared error

SG: Statistical ENSO forecast model presented in this thesis (abbreviation for Seseske-Gray)

SLP: Sea Level Pressure

SO: Southern Oscillation

SON: September-October-November

SST: Sea surface temperature

SSTA: Sea surface temperature anomaly

U: Zonal Wind - The u-component of the wind, which blows in the east-west direction.

Chapter 1

INTRODUCTION

Although many attempts have been made to forecast the variability of the El Niño-Southern Oscillation (ENSO) six to twelve months in advance, the results thus far have not proven consistent or reliable (Fig. 1.1). The focus of this study is to explore the possibility of producing a more accurate and dependable statistical ENSO forecast by making use of global climate data. This study is a preliminary effort to explore the extent to which the global atmosphere and oceanic systems have long-range precursor signals. Results of this research show that it is indeed possible to produce an extended-range ENSO prediction scheme that is able to surpass the rigorous benchmark test of ENSO-CLIPER (Knaff and Landsea 1997) in hindcast skill over a 51-year period. This new scheme has the potential to produce more accurate ENSO forecasts, in particular, the ability to forecast changes in ENSO over the difficult forecast barrier between the Northern Hemisphere spring (March-May) and summer (July-September).

1.1 Background on El Niño Southern Oscillation

The El Niño-Southern Oscillation (ENSO) is an oceanic-atmospheric feature based in the Pacific Ocean that is well known for its large impact on global climate. Warm and cool ENSO phases alternate on yearly and interdecadal time scales, with the duration and strength of each warm and cool event depending on many global atmospheric and oceanic factors. An El Niño (warm) event has been formally defined by Trenberth (1997) as when the sea surface temperature anomaly in the Niño 3.4 region (5°N-5°S, 120-170°W) has an amplitude greater than 0.4°C for six continuous months or more. La Niña (cool) events are distinguished similarly, when the SSTA remains less than -0.4°C for six continuous

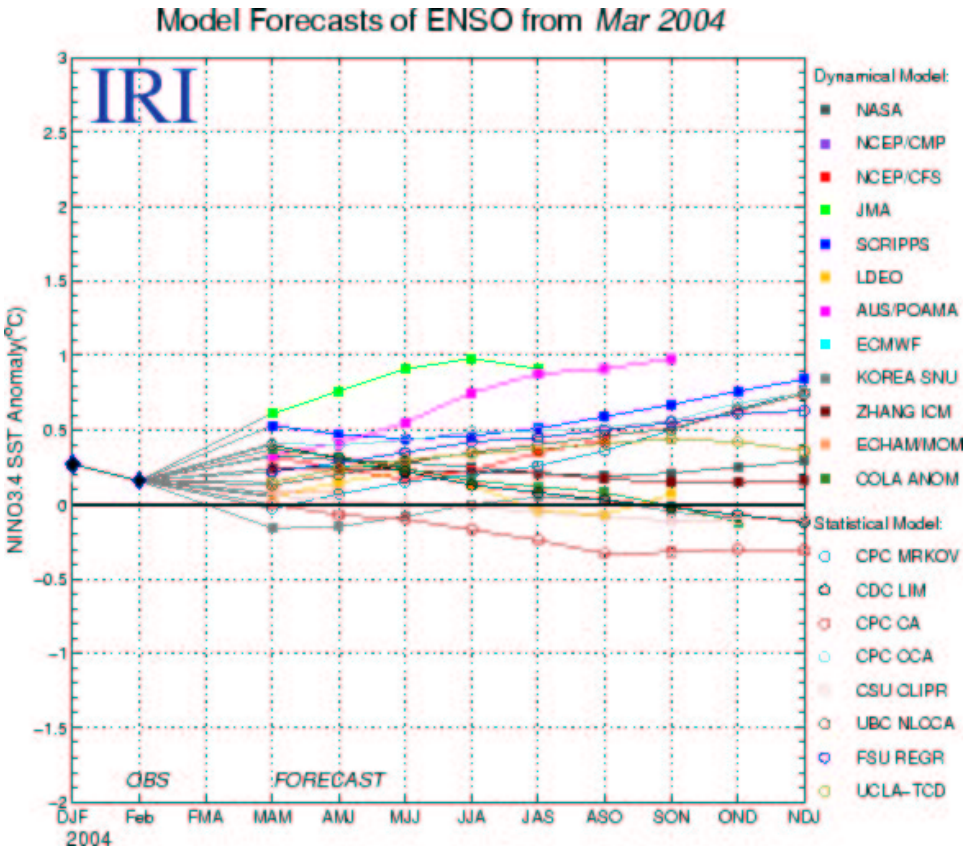

Figure 1.1: Statistical and dynamical forecasts for the Niño 3.4 SSTA are shown. These forecasts were made in late February and early March 2004. Note the degree of disagreement between the models. From the International Research Institute (IRI) for Climate Prediction. http://iri.columbia.edu/climate/ENSO/

months. Although there are five Niño regions in the Pacific (Niño 1, 2, 3, 4 and 3.4), the Niño 3.4 region has been accepted as a critical area in the Pacific basin for defining El Niño events. Forecasters often make predictions for the sea surface temperature in this region (Fig. 1.2).

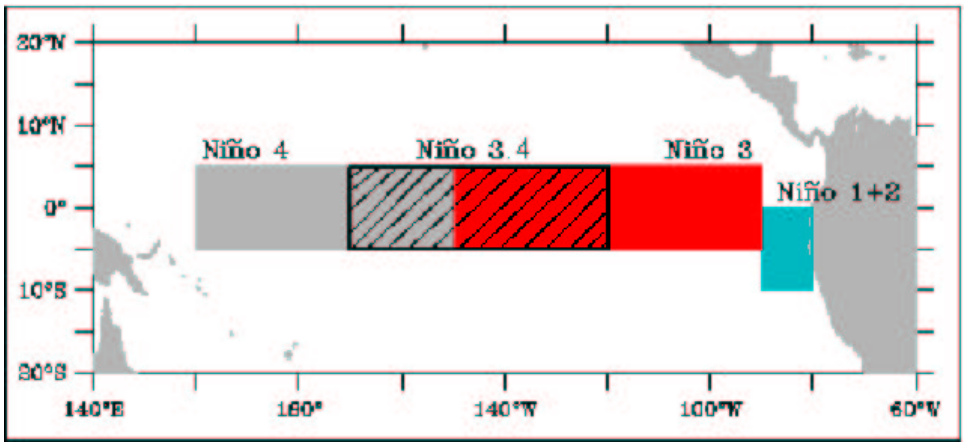

Figure 1.2: Geographic location of the Niño regions.

To appreciate the complexity of the mechanisms behind ENSO events, it is imperative to have at least a simple understanding of the atmospheric and oceanic dynamics in the equatorial Pacific Ocean. Under normal conditions, equatorial easterly winds prevail in the Pacific Ocean. This flow pattern aids in the formation of a deep pool of warm water (greater than 29°C) in the western part of the basin. This collection of warm water is a vast energy source, fueling deep convection and causing the copious precipitation observed in the western Pacific. Corresponding low atmospheric pressure is present in the west, resulting in a pressure gradient across the Pacific basin (Fig. 1.3). Eastern Pacific high pressure resulting from cooler SSTs produces tropospheric subsidence in this area. This surface pressure dipole is indicative of the positive phase of the Southern Oscillation, which maintains high surface pressure in the east Pacific and low surface pressure in the west Pacific. Atmospheric surface pressure shifts back and forth between Darwin, Australia and Tahiti, depending on the phase of the Southern Oscillation. The high pressure in the east Pacific causes air to sink, establishing a dry climate and creating oceanic divergence. Upwelling along the South American west coast and the equatorial Pacific occur due to

the surface easterly winds that are usually present. Oceanic upwelling draws cold water from depth up to the surface, causing the waters in the eastern Pacific to be cooler than in the western Pacific (Fig. 1.4).

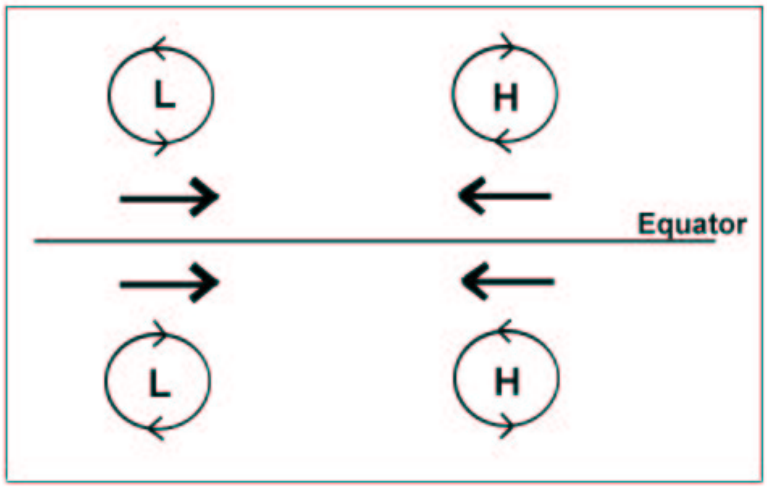

Figure 1.3: This schematic shows how subtropical high and low pressure systems can influence lower-level winds in the equatorial tropics and cause east-west temperature advection and Ekman induced up-and-downwelling.

During an El Niño event, the easterly winds across the Pacific basin are weakened, which affects the flow of surface waters of the ocean. This causes the gradient of the ocean temperatures to shift, allowing the warm water that has accumulated in the west Pacific to move eastward as multiple packets of Kelvin waves on the ocean thermocline. A large reduction in the east to west SST gradient occurs. The area of low pressure and deep convection that was once in the west Pacific shifts to the east, causing the equatorial Pacific and the west coast of South America to experience heavy rainfall. This shift in atmospheric pressure causes a shift in the Southern Oscillation, changing it into its negative phase. The upwelling of nutrient-rich water along the coast of the South American continent is greatly reduced or ceases as the low atmospheric pressure causes greatly reduced trade winds and a large reduction in eastern Pacific upwelling (Rasmusson and Carpenter 1982).

La Niña episodes feature cooler sea surface temperatures throughout the central and eastern Pacific as a result of the strengthening of the prevailing easterly winds. Ekman

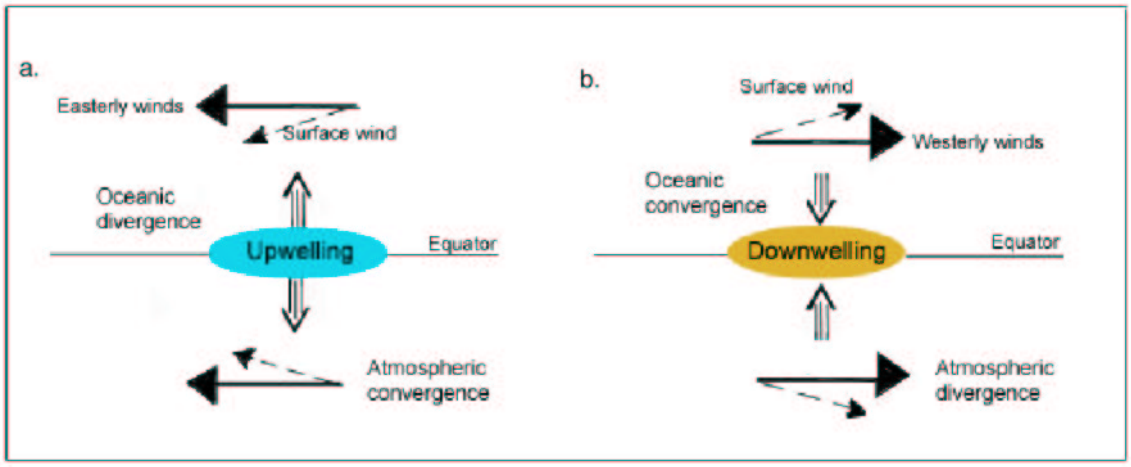

Figure 1.4: This schematic shows how a.) easterly winds over the equatorial Pacific Ocean cause oceanic divergence and atmospheric convergence and b.) westerly winds over the equatorial Pacific Ocean cause oceanic convergence and atmospheric divergence.

forcing is responsible for the enhanced ocean upwelling that occurs during La Niña events. With easterly winds in place along the equator, the surface winds converge along the equator. This atmospheric convergence causes an opposite divergence in the ocean surface waters along the equator, pulling up cooler water from depth (Fig. 1.4). This results in the cool SSTs that are observed in the Pacific Ocean during La Niña events.

While the variations caused by ENSO are most dramatic near the equatorial Eastern Pacific Ocean where the phenomenon is witnessed, the climate at many locations around the globe also feels the effects of these events. Global teleconnections, or physical links between climate variations occurring simultaneously, were explored in a seminal paper by Trenberth et al. in 1982. When warm SSTs shift locations in the Pacific Ocean basin, the location and intensity of convection also shifts along with them, causing a change in where heating, precipitation and upper tropospheric divergence occur. Wave propagation is also recognized as a way in which changes in tropical heating can achieve global influence. In these ways, changes in SST patterns in the Pacific Ocean can impact the global atmosphere

It is generally accepted that El Niño development typically occurs as a consequence of the formation of a number of successive Madden-Julian Oscillation (MJO) events in the equatorial Indian and West Pacific Oceans (Madden and Julian 1971). It is necessary

that these MJO events be able to propagate into the eastern Pacific for an El Niño event to occur. The MJO events act to trigger ocean thermocline level Kelvin wave generation. These Kelvin waves move eastward along the thermocline and bring low-level westerly wind anomalies and the upwelling of warm eastern equatorial Pacific water. Eastern equatorial Pacific deep convection and heavy rainfall occur as a response to the resulting increased east Pacific SSTs.

It is observed that more frequent and stronger MJOs and Kelvin wave formtion events in El Niño years and move further eastward as compared with La Niña years. It is the conjecture of this paper that global (not Pacific basin alone) atmospheric and ocean conditions contribute to the development of equatorial western Pacific and Indian Ocean conditions conducive to the formation and further eastward propagation of MJO events. The inhibiting of MJO frequency and intensity, and/or a lack of eastward propagation, is typically associated with neutral or La Niña years. One must thus look to current and recent past global atmospheric and ocean conditions to determine when global conditions will be more or be less conducive to the formation of MJO events. The favorable conditions for the formation and eastward propagation of El Niño events is hypothesized to occur in response to specific global atmosphere and ocean conditions to be discussed in this paper.

To obtain a background idea of what is occurring globally during El Niño and La Niña events, composites of several global fields during warm and cool years in the Pacific offer a view of what is occurring outside of the tropics. Ten years in which the Niño 3.4 region of the Pacific warmed throughout the year were composited for several different global fields, including SST, SLP, surface zonal wind (u), 500-mb zonal wind (u), and 200-mb gZ. The same was done for years in which the region cooled throughout the year. Figures 1.5, 1.6 and 1.8 shows these composites.

In years when the Niño 3.4 region warmed, it appears that the 200-mb height field (Fig. 1.5) shows low heights, on average, throughout the tropics and subtropics. Conversely, during cooling years, the heights are anomalously high throughout the same region. Generally, high heights aloft are associated with El Niño events, but this atmospheric

response can take several months to occur. The composite of warming years shows the 200-mb heights starting to rise in the Pacific, but the response has not been fully realized in this map, which is averaged over the year. The same explanation is valid for the composite of the cooling years. The heights are high when averaged over the entire year; the atmospheric response to the warming cannot be clearly seen in the Jan-Dec. average. Typically, though, low 200-mb heights are an expected response to La Niña events.

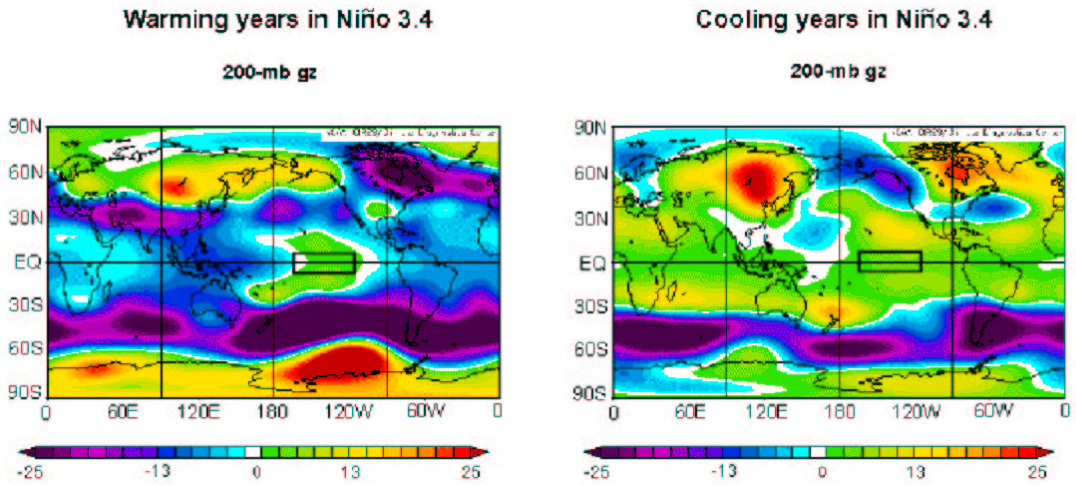

Figure 1.5: Composites of 200-mb gZ anomalies for ENSO warming and cooling events (Jan-Dec averages) in the Niño 3.4 region (see the black box). Warming years are 1951, 1957, 1963, 1965, 1972, 1976, 1982, 1986, 1997, and 2002. Cooling years are 1954, 1955, 1964, 1970, 1973, 1983, 1988, 1992, 1995, and 1998.

The composite of SSTs in warming years in Niño 3.4 show warm surface waters in the east Pacific and cool surface waters in the west Pacific (Fig. 1.6). Physically, this makes sense, as El Niño events are marked by the eastward shift of the warm pool in the Pacific Ocean basin. As expected, the composite for cooling years in Niño 3.4 show cool SSTs in the east and central Pacific.

The SLP composite for the warming years (Fig. 1.6) shows low pressure over the east Pacific and high pressure over the west. When the surface is warm, as it is during El Niño events, the pressure in the east Pacific decreases. Hence, it makes sense that when the east and central Pacific are warm, the sea level pressure there will become lower. Note that the extratropics show low SLP over the continents of Africa, central Asia, and Europe during

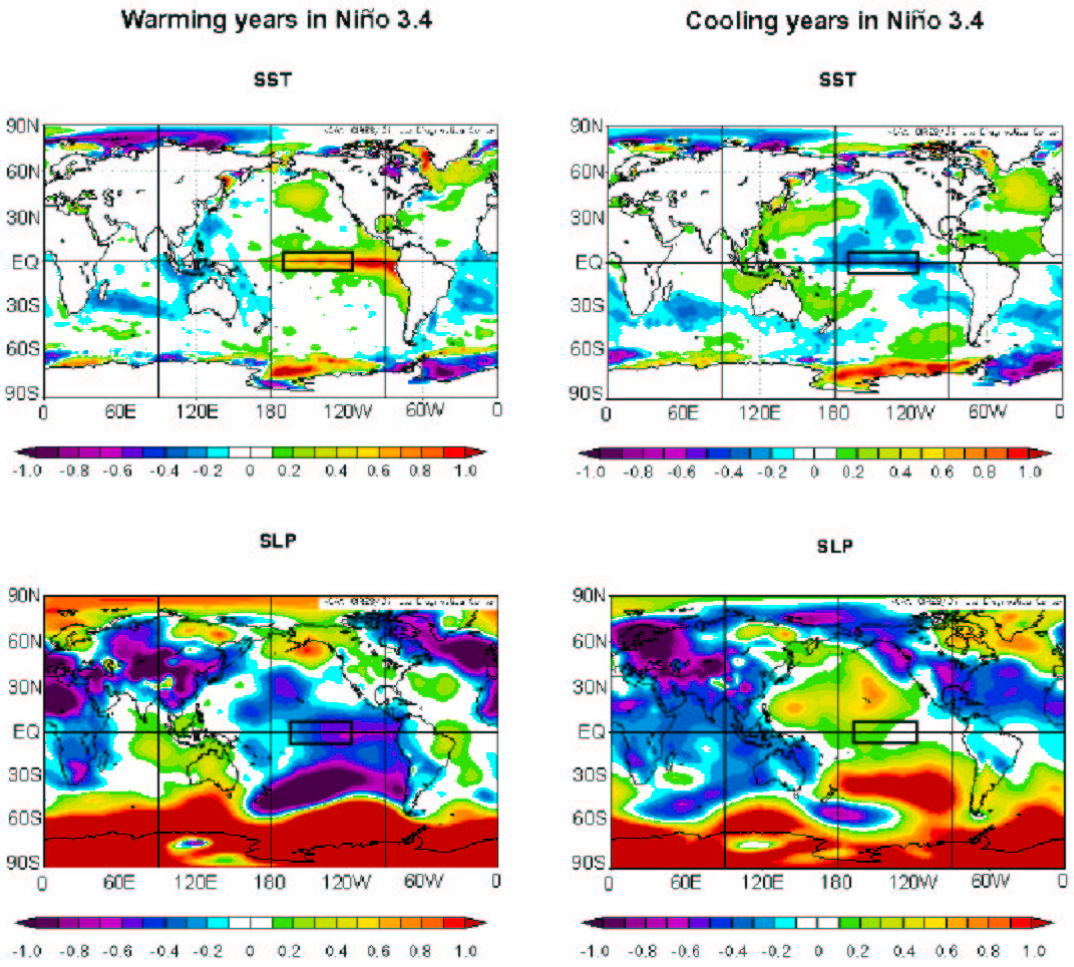

Figure 1.6: Composites of SST and SLP for ENSO warming and cooling events (Jan-Dec averages) in the Niño 3.4 region. Warming years are 1951, 1957, 1963, 1965, 1972, 1976, 1982, 1986, 1997, and 2002. Cooling years are 1954, 1955, 1964, 1970, 1973, 1983, 1988, 1992, 1995, and 1998.

El Niño years. In comparison, the composite for the cooling years shows relatively high pressure in the central and east Pacific, where cooler waters remain. Note that over the warm pool in the west Pacific, the SLP is low. Figure 1.7 shows the relationship between the pressure heights aloft and at the surface for warm and cool conditions in the Eastern equatorial Pacific.

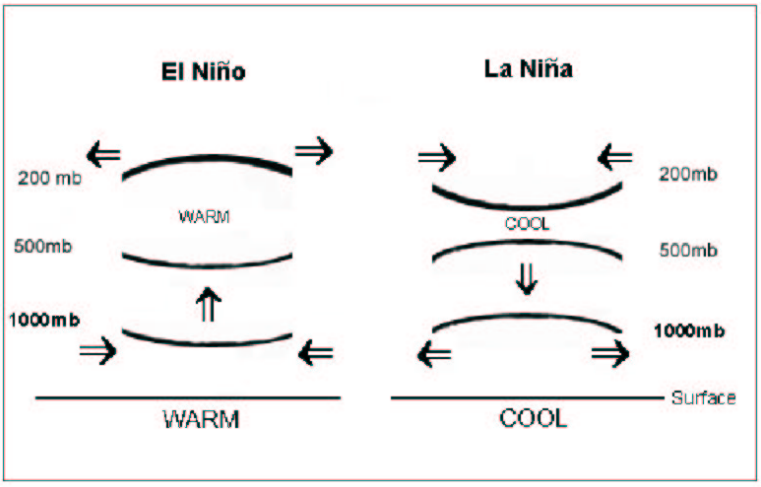

Figure 1.7: This schematic shows the typical pressure heights in the Eastern equatorial Pacific that are associated with El Niño (warm) and La Niña (cool) conditions.

The surface zonal wind (u) in warming years (Fig. 1.8) shows westerly winds over the west and central Pacific. Anomalous westerly winds are expected in this region, as they aid in the eastward progression of the warm pool that occurs during El Niño events. Also note that the warming composite features have anomalous westerlies in the southern Pacific (20-40°S, 120-180°W) and adjacent to that, there is a large region of anomalous easterly winds (45-65°S, 170°E-80°W). During cooling years there are easterly surface winds along the equator in the west Pacific. Note that the zonal winds in the Southern Hemisphere are opposite to what they are for the warming years; there are now easterly winds where the westerly winds prevailed during the warming years (20-40°S, 120-180°W) and just south of that region there are now westerly winds where once there were easterlies.

The 500-mb zonal wind composites (Fig. 1.8) show opposite conditions along the equator for warming and cooling years. Anomalous westerly surface winds dominate the

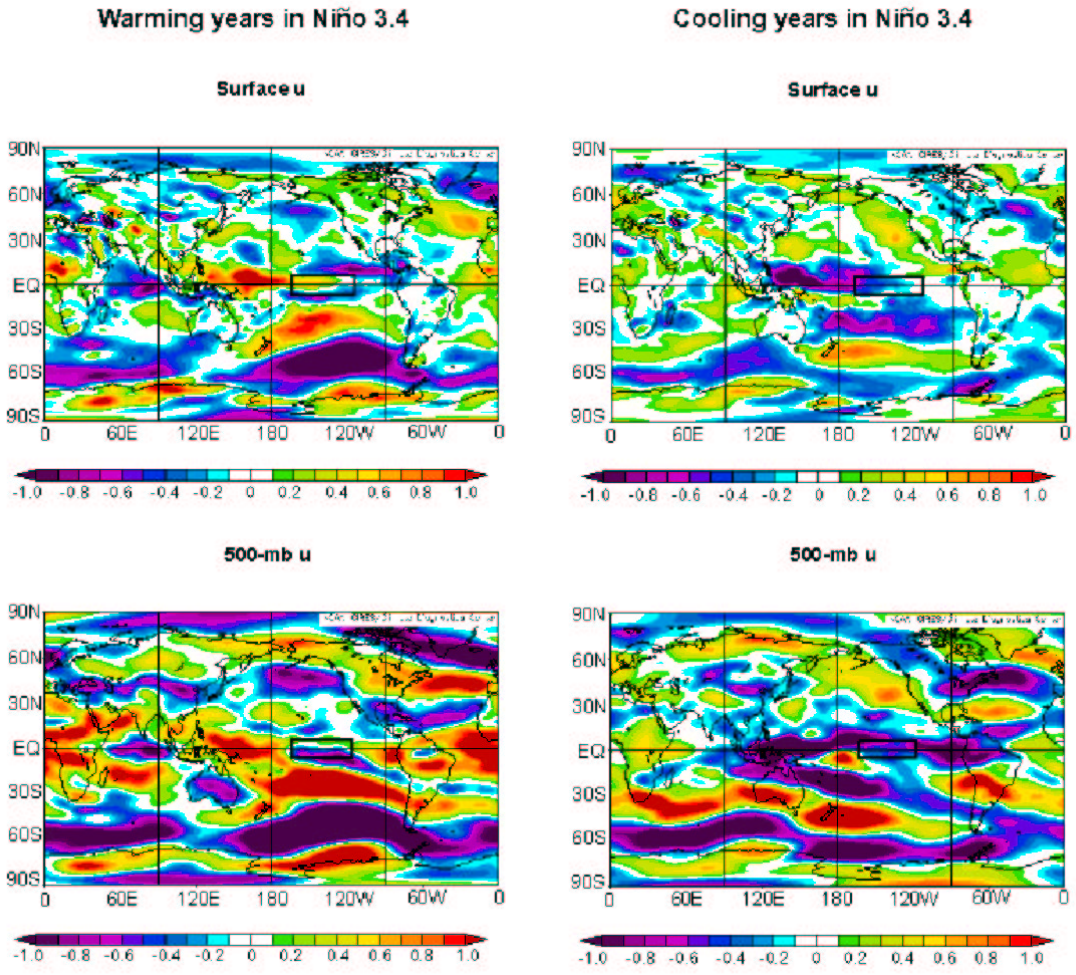

Figure 1.8: Composites of surface and 500-mb zonal winds for ENSO warming and cooling events (Jan-Dec averages) in the Niño 3.4 region. Warming years are 1951, 1957, 1963, 1965, 1972, 1976, 1982, 1986, 1997, and 2002. Cooling years are 1954, 1955, 1964, 1970, 1973, 1983, 1988, 1992, 1995, and 1998.

tropics during warming years and easterly surface winds occur throughout the tropical Pacific in the cooling years. The warmth at the surface alters the height fields, which in turn affects zonal winds aloft. Therefore, the winds at 500-mb are connected to ENSO, even though they are not in direct contact with the surface where the events take place.

Figure 1.9 shows the difference in the 500-mb heights in the Northern Hemisphere winter for El Niño and La Niña years. El Niño years typically show a strong low centered over the north east Pacific Ocean and a high pressure system in the west Pacific, creating westerly flow in the middle atmosphere over the equatorial Pacific (see arrow in Fig. 1.9). As discussed previously, this westerly equatorial flow is associated with El Niño events. During La Niña years, the strong low pressure that was in the east Pacific during El Niño events shifts eastward, and a large area of high pressure sets up in the central north Pacific. Easterly flow occurs in the central Pacific, enhancing surface easterly winds and causing cool conditions in the Pacific.

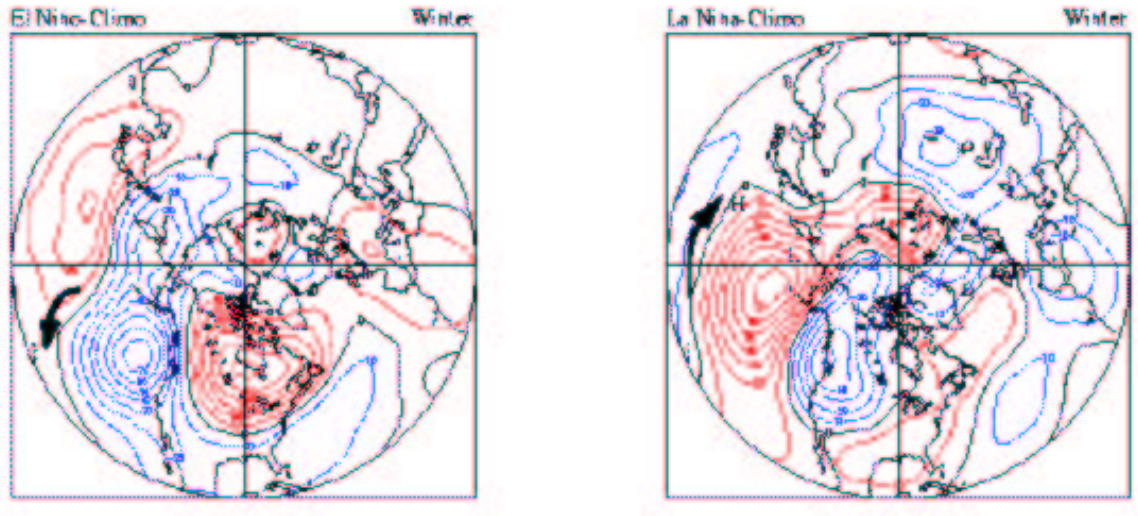

Figure 1.9: Composites of 500-mb heights during El Niño and La Niña conditions. Adapted from the CDC's website http://www.cdc.noaa.gov/ENSO.

1.2 Forecasting El Niño events

Producing an accurate El Niño-Southern Oscillation forecast is worthwhile because of the severe global impacts these events can have on climate, the environment, and humans.

Increased understanding of these events will also provide a better understanding of global climate and how it is affected by ENSO. However, studies have shown the current quality of El Niño forecasts, statistical and dynamical, to be poor in most aspects (Landsea and Knaff 2000, Barnston et al. 1999).

The exact physical mechanisms behind El Niño events are still not well understood, and scientists are still unable to predict ENSO events with much skill. However, it is generally accepted that El Niño events are often triggered by westerly wind bursts from successive Madden-Julian Oscillation (MJO) events. Despite this knowledge, it is difficult to foresee the onset, duration, and strength of these MJO events because they occur on short time scales (a few days to a few weeks in duration).

Another difficulty in predicting ENSO events is the Spring Predictability Barrier (Webster and Yang 1992; Gray et al. 1994). The largest SST changes typically occur in the Northern Hemisphere spring, from April-June (Fig. 1.10). The ENSO predictability barrier is notoriously difficult to forecast across, as sudden changes often occur in the Pacific SSTs during this time. The mechanisms behind the rapid onset of ENSO events in the Northern Hemisphere spring are not well understood and therefore, forecasting these changes in the Pacific remains very difficult.

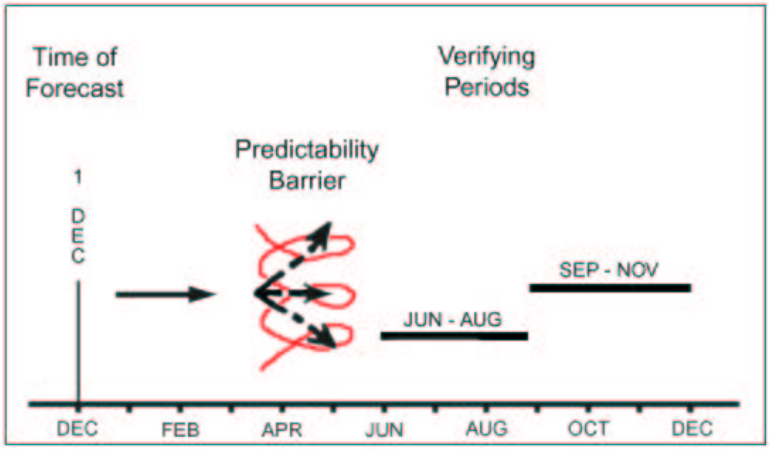

Figure 1.10: Schematic showing the time frame for making predictions of ENSO, the "predictability barrier" and the two verification periods.

Because of the difficulties in predicting ENSO events, a question arose as to whether they are predictable at all. Fedorov (2003) suggested that probabilistic forecasts based on an ensemble of forecast models may be better for forecasting El Niño events than initial value deterministic predictions, which give only one possible outcome. The probabilistic forecast is therefore based on the results of many years of coupled ocean-atmosphere behavior.

1.3 ENSO-CLIPER - The Benchmark of ENSO Forecasts

In an attempt to create a more stringent standard for ENSO forecasts, Knaff and Landsea (1997) produced ENSO-CLIPER, a statistical forecast that predicts the sea surface temperature anomaly throughout the Niño regions in the Pacific Ocean. The authors argue that persistence is not a rigorous enough test for skill when forecasting ENSO events. Instead, they propose that a combination of trend, climatology, and persistence makes a much better baseline for establishing skill. The ENSO-CLIPER forecast was designed to encompass these three elements. If a scheme produces more accurate forecasts than ENSO-CLIPER, then that scheme is said to have skill.

The ENSO-CLIPER forecast scheme uses multiple linear regression to produce predictive equations for all Niño regions and the Southern Oscillation Index. Specifically, the "leaps and bounds" technique is utilized to select one to four of the best predictors from a pool of fourteen predictors. Predictors that may be selected by ENSO-CLIPER include the 1-, 3-, or 5-month averages of anomalies in both the initial conditions and the trend of the specific region being predicted, and also the three month average of both the initial conditions and the trend in the other four predictands. Table 1.1 lists the pool of predictors used by ENSO-CLIPER to forecast the Niño 3.4 SSTA. Each forecast predicts a three month period, and seven of these forecasts are issued by ENSO-CLIPER each month. Adjustments are made to the predictions to account for expected degradation in forecasts made for independent data years.

As expected, the results from ENSO-CLIPER show that it does indeed produce more accurate forecasts than persistence alone. Because the performance of the model is affected

Table 1.1: Pool of 14 predictors used by ENSO-CLIPER in forecasting the Niño 3.4 SSTA (Knaff and Landsea 1997).

1.	Initial Niño 3.4 Conditions (1 month)
2.	Initial Niño 3.4 Conditions (3 month)
3.	Initial Niño 3.4 Conditions (5 month)
4.	Trend of Niño 3.4 Conditions (1 month)
5.	Trend of Niño 3.4 Conditions (3 month)
6.	Trend of Niño 3.4 Conditions (5 month)
7.	Initial Niño 1+2 Conditions (3 month)
8.	Trend of Niño 1+2 Conditions (3 month)
9.	Initial Niño 3 Conditions (3 month)
10.	Trend of Niño 3 Conditions (3 month)
11.	Initial Niño 4 Conditions (3 month)
12.	Trend of Niño 4 Conditions (3 month)
13.	Initial SOI Conditions (3 months)
14.	Trend of SOI Conditions (3 months)

by the starting point of the forecast, a 12-month average of the explained amount of variance best shows the model's proficiency. The average percentages of variance explained for the zero- through seven-season lead time predictions are shown in Table 1.2 (for example, a zero-lead time forecast made on 1 August is a forecast for August-September-October). By itself, persistence yields notably lower percentages for every forecast. Adding climatology and trend to persistence explains more variance at an extended range and therefore offers a more skillful forecast.

Table 1.2: Variance explained (r^2) by persistence alone and ENSO-CLIPER (persistence plus climatology) for 0-7 season lead times (Knaff and Landsea 1997).

Lead Time (seasons)	0	1	2	3	4	5	6	7
Percent Variance Explained by ENSO-CLIPER	81	55	34	24	18	18	12	7
Percent Variance Explained by Persistence Alone	74	34	7	0	3	6	8	6

Although ENSO events typically last about 12-18 months, unusual warm conditions may persist, as they did in the Pacific basin from 1990 to early 1995. The extended El Niño conditions may be partially responsible for the poor performance of ENSO models in the early 1990s. The ENSO-CLIPER forecasts for independent data years (1993-1996) were

worse than expected, but remained better than most models. At the time of their 1997 paper, Knaff and Landsea showed that the ENSO-CLIPER model performed better than (or at least comparable to) other statistical and numerical models. Although their model is shown to be the best at forecasting ENSO, there remains a problem with forecasting using independent data: beyond one-season lead time, only a small percentage of the observed variance is accounted for. Producing good mid- to long-range forecasts with independent data remains a challenge for all ENSO models.

1.4 Evaluation of ENSO models for the 1997-1998 El Niño Episode

Landsea and Knaff (2000) examined the usefulness and skill of several statistical and dynamical ENSO models for the 1997-1998 El Niño event, using ENSO-CLIPER as a baseline for establishing skill. Usefulness, as the authors define it, is based on the ability of the model to distinguish between the phases of ENSO and the magnitude of the event. Skill is attributed to models that perform better than ENSO-CLIPER. The models that were evaluated for performance in forecasting the SSTA are the Niño 3 and 3.4 regions as listed in Table 1.3. The models were also examined specifically for the onset (the first three-month period when the SSTA exceeded $+0.4^{\circ}$C) and decay (first three-month period when the SSTA averaged lower than $+0.4^{\circ}$C) periods. Models were evaluated by categories based on forecast length, short being 0-1 seasons (0-5 mo.), medium being 2-3 seasons (6-11 mo.), and long being 4-7 seasons (12-23 mo.).

Only the following models were able to perform better than ENSO-CLIPER in predicting the onset of the '97-'98 El Niño, which occurred during March-May 1997. Short range forecasts that possessed skill and were useful for the onset were: BMRC, CCA, COLA, LIM, and SSA/MEM. Medium range forecasts with both of these qualities were: ANALOG, BMRC, COLA, CONSOL, LIM, NCEP, and SSA/MEM. For the long range, only BMRC was able to beat ENSO-CLIPER. The NCEP model had the best forecast for the Niño 3.4 region, with a RMSE that was 31 percent lower than ENSO-CLIPER. Also note that some of the models were skillful at medium range forecasting but not at the short time periods (e.g., ANALOG, CONSOL, NCEP). The decay period of the '97-'98

Table 1.3: Listing of the statistical and dynamical ENSO models evaluated by Landsea and Knaff (2000).

ENSO Model	Niño Region	Author	Year of Publication
ENSO-CLIPER	3, 3.4	Knaff and Landsea	1997
ANALOG	3.4	Van den Dool	1994
CONSOL	3.4	Unger et al.	1996
NCEP	3.4	Ji et al.	1996
SCR/MPI	3.4	Barnett et al.	1993
CCA	3.4	Barnston and Ropelewski	1992
OXFORD	3.4	Balmaseda et al.	1994
BMRC	3	Kleeman et al.	1995
COLA	3	Kirtman et al.	1997
LDEO	3	Zebiak and Cane	1987
SSA/MEM	3	Keppenne and Ghil	1992
LIM	3	Penland and Magorian	1993

El Niño occurred in April-June 1998. For the short range, only ANALOG and CCA were both useful and showed skill for this period.

At the medium range, ANALOG, COLA and LIM fit these two requirements. There were no long range forecasts that could both beat ENSO-CLIPER and be useful for the decay period of the El Niño. LIM improved upon ENSO-CLIPER's RMSE by 22 percent, making it the most skillful medium range forecast for the Niño 3 region.

Table 1.4: Lists the ENSO forecasts that showed both skill and usefulness in predicting both the onset and decay of the 1997-1998 El Niño event.

	Onset (March-May 1997)	Decay (April-June 1998)
Short range forecast	BMRC, CCA, COLA, LIM, SSA/MEM	ANALOG, CCA
Medium range forecast	ANALOG, BMRC, COLA, CONSOL, LIM, NCEP, SSA/MEM	ANALOG, COLA, LIM
Long range forecasts	BMRC	none

Not many models were useful for the duration of the '97-'98 El Niño event. Only short range forecasts show usefulness (ANALOG, BMRC, CCA, COLA, ENSO-CLIPER, NCEP, NEURAL, and SSA/MEM); there were no medium or long range forecasts that were useful. There were no short range models that provided skillful forecasts, but the same three models (ANALOG, CCA, and COLA) were able to show skill for both medium

and long range. However, none of the models for any range of forecasts provided both useful and skillful forecasts for the length of the 1997-1998 El Niño event (Landsea and Knaff 2000). Landsea and Knaff conclude that none of the models they evaluated were both useful and skillful for the extent of the 1997-1998 El Niño event. They found that ENSO-CLIPER performed better than all of the more complicated models for zero- to two-season lead times (0-9 months).

1.5 Purpose of This Thesis: A Better Extended-Range ENSO Forecast

The focus of this study is to produce a skilful and reliable statistical ENSO forecast using global atmospheric and oceanic data. The prominent difference between the proposed SG model and other ENSO forecast models is the utilization of global predictors by the SG model ENSO-CLIPER, established as a benchmark of skill for ENSO forecasts, uses predictors only from the region in the Pacific where the ENSO events occur. By using predictors that are local to the Pacific basin, ENSO-CLIPER closes itself off to other possibly important global predictors that may influence ENSO formation or termination. Also, the predictors employed by ENSO-CLIPER are limited to sea surface temperature and surface pressure anomalies in the various Niño regions. While this does indeed provide useful data for forecasting El Niño events, there are also many other valuable global variables that should be included in the pool of predictors. A forecast that included several fields of global predictors would appear to make a more inclusive prediction of ENSO events and likely have more skill.

Instead of limiting the possible predictors to the Pacific basin, the forecast presented in this thesis selects predictors from a pool that was drawn from various global locations. This difference from the ENSO-CLIPER model allows for teleconnections from ENSO to be included. Many studies have shown the existence of teleconnections between ENSO and global climate (Trenberth et al. 1982; Hoerling et al 1997; Enfield and Mestas-Nũnez 1999). As ENSO influences the global climate, it stands to reason that the global climate would in turn influence ENSO. Therefore, signals in global climate may foretell future

changes in the Pacific basin. This is a preliminary study in utilizing global hindcast data to forecast ENSO events at 6-11 months lead time.

Chapter 2

DATA AND METHODOLOGY

2.1 Data

Data were made available by the NOAA-CIRES Climate Diagnostics Center (CDC) website (http://www.cdc.noaa.gov/cdc/reanalysis/), which provided NCEP/NCAR Reanalysis data for January 1948 to September 2003. The NCEP/NCAR Reanalysis Project collected data from several sources and then utilized a global data assimilation system to produce 55 years of reanalysis data (Kalnay et al. 1996). A model similar to the NCEP global operational model (1991) was used to produce data on a 2.5° by 2.5° global grid. The CDC website also featured several tools for accessing the data, enabling a user to produce correlations, regressions, composites, or simply access the raw data. This resource was especially useful because of the ease of production of global maps for monthly mean composites and linear monthly correlations. The CDC's NCEP/NCAR Reanalysis internet tools were an essential part of this research.

2.2 Methodology

An inclusive group of global predictors was created from which the best final predictors were selected for producing forecasts. The predictors for the forecasts were selected by studying correlations between atmospheric and oceanic variables and ENSO. Specifically, some fields that were examined included geopotential height at various pressure levels, zonal and meridional wind at various pressure levels, SLP, and SST. The NCEP/NCAR Reanalysis data were used to produce global correlation maps, which gave insight to areas that were well-correlated with the Niño 3.4 sea surface temperature anomalies. El Niño and La Niña years were also composited for several fields to give insight into other potential

predictors for the forecast. These relationships were studied for all months and years but were eventually narrowed down to produce a 1 December forecast based on 1950-1990 data. The most recent 12 years were excluded from the data set in order to leave some years as independent data to test the forecast scheme. Averaged October and November data were used to predict the following year's June-July-August and September-October-November Niño 3.4 sea surface temperature anomalies. In this way, hindcast data were used to forecast these climate events. Predictors using October-only and November-only data were tested, but it was found that in most cases it was more beneficial to average the data values for the two months for the forecast. Another benefit of using a predictor averaged over two months is that any effects from the Madden-Julian Oscillation (approximately a 30-50 day time period) are averaged out. Time series for each predictor were obtained from the CDC website.

After an extensive pool of predictors was established, five predictors that produced the highest percent of variance explained were selected using an all-subsets technique. A multiple linear regression was then performed with these best five predictors and the desired Niño 3.4 anomaly time series. The predictive equations formed by this method used October-November predictors to formulate a 1 December forecast for both the June-July-August (6-8 month forecast) and September-October-November (9-11 month forecast) Niño 3.4 sea surface temperature anomaly. Equation 2.1 (2.2) shows the formula used to produce the 1 December JJA (SON) SG forecast. The formula for the SON Combination (SG + ENSO-CLIPER) forecast is shown in Equation 2.3. Statistics on the results of these equations can be found in Appendix C.1.

$$JJA\ SG\ Forecast\ =\ y_{int} + a_1x_1 + a_2x_2 - a_3x_3 - a_4x_4 - a_5x_5 \tag{2.1}$$

where $y_{int} = 85.235$, $a_1 = 0.082$, $x_1 =$ South Pacific 500-mb u, $a_2 = 0.149$, $x_2 =$ Equatorial Pacific 500-mb u, $a_3 = 0.095$, $x_3 =$ Lake Baikal 500-mb u, $a_4 = 0.072$, $x_4 =$ South Atlantic 200-mb gZ and $a_5 = 0.660$, $x_5 =$ South Atlantic Surface u.

$$SON\ SG\ Forecast\ =\ y_{int} - b_1 y_1 + b_2 y_2 - b_3 y_3 + b_4 y_4 + b_5 y_5 \tag{2.2}$$

where $y_{int} = 147.923$, $b_1 = 0.176$, y_1 = South Atlantic 200-mb gZ, $b_2 = 0.200$, y_2 = Lake Baikal SLP, $b_3 = 0.137$, y_3 = South Pacific SLP, $b_4 = 0.202$, y_4 = North Atlantic SST, and $b_5 = 0.386$, y_5 = PDO Index

$$SON\ Combination\ Forecast\ =\ y_{int} - c_1 z_1 + c_2 z_2 \tag{2.3}$$

where $y_{int} = 0.022$, $c_1 = 0.751$, z_1 = SON SG Forecast and $c_2 = 0.704$, z_2 = SON ENSO-CLIPER Forecast

Niño 3.4 SSTA forecasts were produced from 1 December for the following JJA and SON for the years from 1950 to the present using the multiple regression equations for the best predictors. Errors were calculated and analyzed for each year and decade. The performance of each forecast was then compared to the analogous 1 December ENSO-CLIPER forecast. The following chapters discuss the skill of these forecast equations.

Chapter 3

RESULTS

The best predictors were selected for each forecast to give the highest possible percentage of variance explained. They were selected from a group of thirty possible predictors for the JJA forecast and from a possible twenty-two predictors for the SON forecast (listed in Appendix A.3 and A.4). From these predictors, a prognostic equation was formed via multiple linear regression for each of the forecast periods. Each equation was then used to produce a Niño 3.4 anomaly forecast for JJA and SON from 1950 to the present. The performance of each forecast was compared to the analogous 1 December ENSO-CLIPER forecast. Below are the chosen predictors for each forecast and suggested explanations as to why they were selected for forecasting ENSO events.

3.1 1 December Forecast for JJA Niño 3.4 SSTA

The best predictors for the JJA Forecast were selected from a group of thirty possible predictors. Table 3.1 lists the best one through five predictors and the percent variance each combination explains. The locations of these predictors are shown in Fig. 3.1.

It is also interesting to examine the correlation and variance for other ranges of years. To better assess the performance of this forecast, the model is tested on independent data from 1991-2002. For these years of independent data, the SSTA predicted by this scheme correlates at 0.59 with the observed JJA Niño 3.4 SSTA, explaining 35 percent of the variance. For all possible years, 1952-2002, the prediction correlates at 0.76 and explains 58 percent of the variance.

For 1952-2002, the ENSO-CLIPER prediction correlates at 0.38 with the observed JJA Niño 3.4 SSTA and hence explains 14 percent of the variance. The correlation and

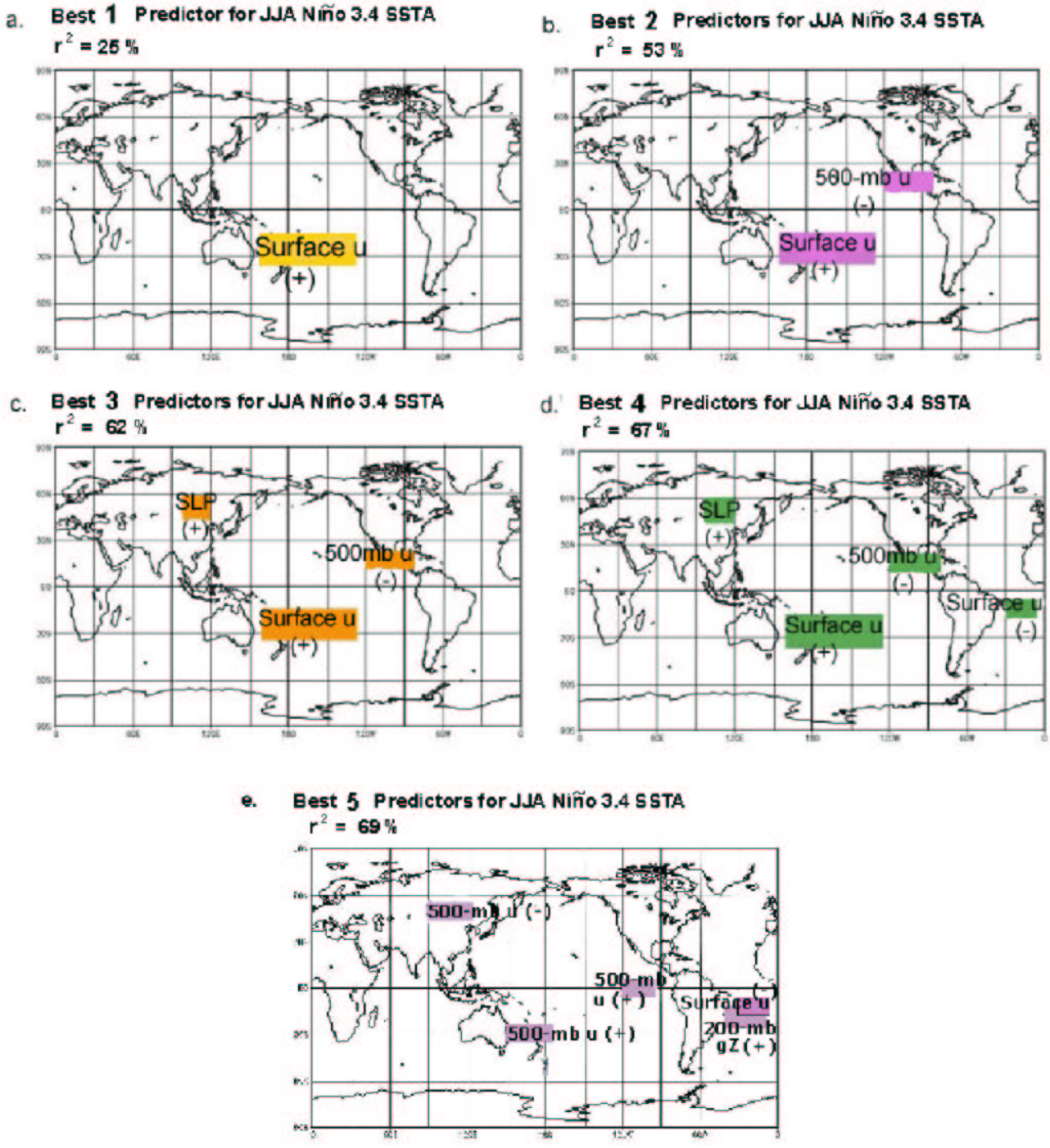

Figure 3.1: Shows the best Oct/Nov predictors (and sign of correlation) for the 1 December Niño 3.4 forecast of the following JJA. Positive (negative) sign indicates positive (negative) correlation with warm SSTA in Niño 3.4.

Table 3.1: Best predictors (all Oct/Nov values) for the 1 December SG JJA Forecast and the corresponding variance they explain (1950-1990).

Predictors	Predictors Chosen	Latitude, Longitude	r^2 1950-1990
Best 1	E. of Australia Surface u	(15-30°S, 160°-125°E)	0.25
Best 2	E. of Australia Surface u	(15-30°S, 160°-125°E)	0.53
	Mexico 500-mb u	(15-25°N, 80-120°W)	
Best 3	E. of Australia Surface u	(15-30°S, 160°-125°E)	0.62
	Mexico 500-mb u	(15-25°N, 80-120°W)	
	Lake Baikal SLP	(45-60°N, 100-125°E)	
Best 4	E. of Australia Surface u	(15-30°S, 160°-125°E)	0.67
	Mexico 500-mb u	(15-25°N, 80-120°W)	
	Lake Baikal SLP	(45-60°N, 100-125°E)	
	South Pacific Surface u	(5-15°S, 5-30°W)	
Best 5	Lake Baikal 500-mb u	(45-55°N, 90-125°E)	0.69
	Equatorial Pacific 500-mb u	(5°N-5°S, 95-120°W)	
	E. of Australia 500-mb u	(25-35°S, 150°E-175°W)	
	South Atlantic 200-mb gZ	(10-25°S, 10-40°W)	
	South Atlantic Surface u	(5-15°S, 5-30°W)	

Table 3.2: Percent variance explained (r^2) for SG, ENSO-CLIPER, and the combination of the two for both the JJA and SON forecast periods.

Forecast period	Model	1952-1990	1992-2002	All Years 1952-2002
JJA	SG	69	35	58
	ENSO-CLIPER	15	17	14
SON	SG	47	23	36
	ENSO-CLIPER	32	15	25
	COMBINATION	57	51	50

variance explained, respectively, for 1992-2002 are 0.44 and 17 percent. It should be noted that the ENSO-CLIPER forecast scheme was based on data from 1950-1994, so when comparing statistical measures for "independent data years," the range of years would be different for this forecast scheme (1992-2002) and ENSO-CLIPER (1995-2002). The correlation and variance for independent years (1995-2002) for ENSO-CLIPER are 0.50 and 25 percent, respectively.

The percent variance explained by each of the predictors individually is listed in Table 3.3. The sum of the variances is not equal to the percent explained by the total, as the combination of predictors sometimes explains more variance than the sum of the individual predictors themselves. For example, the best two predictors for the JJA Forecast (Table 3.1) explain 53 percent of the variance together. Yet individually, the E. of Australia Surface u predictor explains 25 percent and the Mexico 500-mb u predictor explains 18 percent, which sums to 43 percent. This sum of the individual predictors is ten percent less than the percentage of variance explained by the two predictors combined. It is uncertain as to the physical processes that cause this surprising rise in variance explained beyond the sum of the individual variances. This increased variance likely occurs as a consequence of the enhancement of variance due to the product of the two variables acting together.

The opposite situation is more likely to occur in statistical models where the percent variance explained by a combination of predictors is less than the sum of the variances explained by each predictor individually. For example, the best five predictors for the JJA SG forecast explain 69 percent of the variance together, but the sum of the variances explained by each of the five predictors individually amount to 99 percent. This difference can be explained by the inter-correlation or redundancy between variables.

3.2 Best 5 Predictors for the 1 December Forecast for JJA Niño SSTA

The five October/November predictors that were selected to forecast the JJA Niño 3.4 sea surface temperature anomaly are: South Pacific 500-mb zonal wind (25-35°S, 150-180°E), Equatorial Pacific 500-mb zonal wind (5°N-5°S, 95-120°W), Lake Baikal 500-mb zonal wind (45-55°N, 90-125°E), South Atlantic Surface Zonal Wind (5-15°S, 5-30°W), and

Table 3.3: Shows the correlation (r) with the 1950-1990 Niño 3.4 SSTA and variance explained (r^2) for each of the best JJA predictors (listed in Table 3.1), individually.

Predictor	Correlation (r) 1950-1990	Variance (r^2) 1950-1990
South Pacific 500-mb u	0.46	0.21
Equatorial Pacific 500-mb u	0.46	0.21
Lake Baikal 500-mb u	-0.38	0.14
South Atlantic 200-mb gZ	-0.44	0.19
South Atlantic Surface u	-0.49	0.24
East of Australia Surface u	0.50	0.25
Mexico 500-mb u	-0.43	0.18
Lake Baikal SLP	0.47	0.22

South Atlantic 200-mb geopotential height (10-25°S, 10-40°W). These predictors correlate at 0.83 with the Niño 3.4 SSTA record for 1950-1990 (the years on which the scheme was based) and explain 69 percent of the variance.

1. **South Pacific 500-mb Zonal Wind (u) Predictor (25-35°S, 150-180°E)**. This predictor is located over the Pacific Ocean, just east of Australia. The correlations between the October/November 500-mb zonal wind and the Niño 3.4 SSTA in JJA the following year are strong (r = 0.44 for 1950-2002). When the zonal winds at 500-mb are from the west in this region in October/November, there tends to be a warm Niño 3.4 anomaly the following JJA.

2. **Equatorial Pacific 500-mb Zonal Wind Predictor (5°N-5°S, 95-120°W)**. The region for this predictor straddles the equatorial Pacific Ocean just west of South America. In this area, westerly wind anomalies in October/November are correlated with a warm SSTA in the Niño 3.4 region during the following JJA (r = 0.38 for 1950-2002). This predictor captures the westward wind anomalies that are related to the warming in the eastern Pacific as an El Niño event is established.

3. **Lake Baikal 500-mb Zonal Wind Predictor (45-55°N, 90-125°E)**. Zonal winds at the 500-mb height level in October/November are negatively correlated (r = -0.34 for 1950-2002) with the JJA Niño 3.4 SSTA the next year in this eastern Asia

region. When easterly winds are present in this region during October/November, cooler conditions prevail in the Pacific the following year.

4. **South Atlantic 200-mb Geopotential Height Predictor (10-25°S, 10-40°W)**. The October/November 200-mb heights in the region over the Atlantic Ocean just east of Brazil correlate negatively (r = -0.46 for 1950-2002) with the SSTA of the Niño 3.4 region during JJA of the following year. When low heights are present at this location during October/November, cooler conditions are likely the next year in the Pacific.

5. **South Atlantic Surface Zonal Wind Predictor (5-15°S, 5-30°W)**. The zonal wind at the surface southeast of Brazil shows a negative correlation (r = -0.49 for 1950-2002) with the JJA Niño 3.4 SSTA. Easterly surface winds in this region are associated with cold Niño 3.4 SSTA in JJA the following year.

3.3 1 December Forecast for SON Niño 3.4 SSTA

The best predictors for the SON Forecast were selected from a group of twenty-two possible predictors, which are listed in Appendix A.4. Table 3.4 lists the best one through five predictors and the percent variance explained. The locations of these predictors are shown in Fig. 3.2.

The percent variance explained by each of the predictors individually is listed in Table 3.5. As expected, the sum of the variances is significantly higher than the combination total. There is overlap and redundancy between the combination of variables. However, as with the JJA prediction, the combination of the best two predictors gives a variance explained of 53 percent while the sum of the variance explained by the two variables themselves gives a total of only 22 percent. Again, the product of two variables rather than their sum appears to be the primary predictive element.

Table 3.4: Best predictors (Oct/Nov values) for the 1 December SG SON Forecast and the corresponding variance explained (1950-1990).

Predictors	Predictors Chosen	Latitude, Longitude	r^2 1950-1990
Best 1	West Pacific SST	(5-30°N, 90°-125°E)	0.28
Best 2	South Atlantic 200-mb gZ	(10-20°S, 15°-40°W)	0.52
	PDO Index	Oct/Nov PDO Index	
Best 3	S. Hemisphere 200-mb gZ	(10-20°S, 5-100°W)	0.66
	Lake Baikal SLP	(40-60°N, 90-125°E)	
	PDO Index	Oct/Nov PDO Index	
Best 4	South Atlantic 200-mb gZ	(10-20°S, 15°-40°W)	0.71
	Lake Baikal SLP	(40-60°N, 90-125°E)	
	South Pacific SLP	(25-45°S, 160°E-160°W)	
	PDO Index	Oct/Nov PDO Index	
Best 5	South Atlantic 200-mb gZ	(10-20°S, 15°-40°W)	0.73
	Lake Baikal SLP	(40-60°N, 90-125°E)	
	South Pacific SLP	(25-45°S, 160°E-160°W)	
	North Pacific SST	(35-45°N, 150-170°W)	
	PDO Index	Oct/Nov PDO Index	

Table 3.5: Shows the correlation (r) with the 1950-1990 Niño 3.4 SSTA and variance explained (r^2) for each of the best SON predictors (listed in Table 3.4) individually.

Predictor	Correlation (r) 1950-1990	Variance Explained (r^2) 1950-1990
South Atlantic 200-mb gZ	-0.45	0.20
Lake Baikal SLP	0.45	0.20
South Pacific SLP	-0.50	0.25
North Pacific SST	0.24	0.06
PDO	-0.13	0.02
West Pacific SST	-0.50	0.25
S. Hemisphere 200-mb gZ	-0.38	0.14

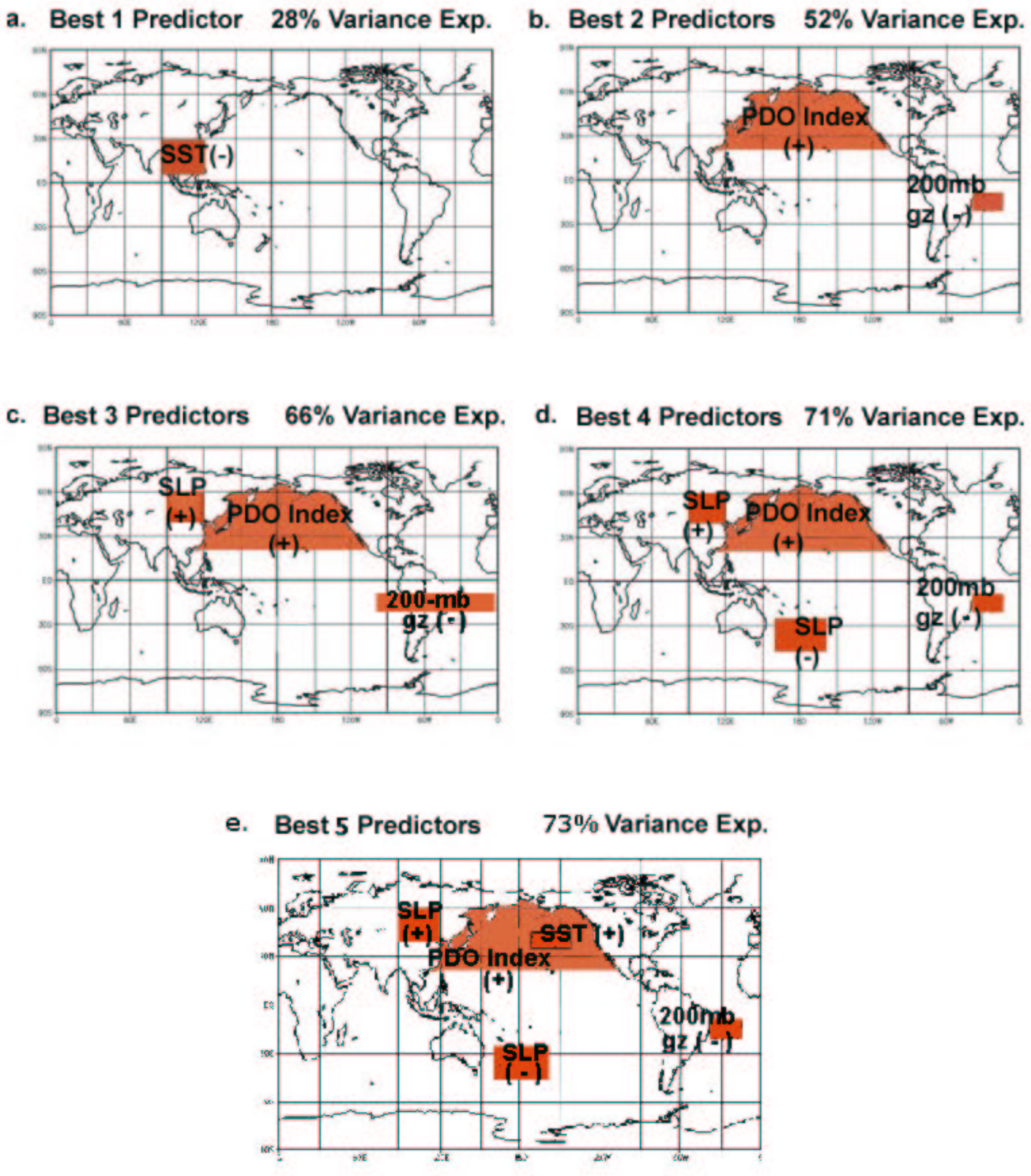

Figure 3.2: The best Oct/Nov predictors (and sign of correlation) used to make the 1 December Niño 3.4 Forecast for the following SON and the variance each combination explains. Positive (negative) sign indicates positive (negative) correlation with warm SSTA in Niño 3.4.

3.4 Best 5 Predictors for the 1 December Forecast for SON Niño 3.4 SSTA

The five October/November predictors that were selected to forecast the SON Niño 3.4 sea surface temperature anomaly are: South Atlantic 200-mb Geopotential Height (10-20°S, 15-40°W), Lake Baikal SLP Predictor (40-60°N, 90-120°E), South Pacific SLP Predictor (25-45°S, 160°E-160°W), North Pacific SST Predictor (35-45°N, 150-170°W), and the PDO Index Predictor (SSTA in Pacific basin, poleward of 20°N). These predictors correlate at 0.83 with the SON Niño 3.4 SSTA record for 1950-1990 (the years on which the scheme was based) and explain 73 percent of the variance.

1. **South Atlantic 200-mb Geopotential Height Predictor (10-20°S, 15-40°W)**. This predictor is located over the Southern Atlantic Ocean, just east of Brazil. The correlation between the October/November 200-mb geopotential height and the Niño 3.4 SSTA in SON the following year are negative (r = -0.45 for 1950-2002). When the 200-mb heights are high in this region in October/November, there tends to be a negative SST anomaly the following SON in the Niño 3.4 region. This accounts for the frequently observed biannual oscillation of ENSO.

2. **Lake Baikal SLP Predictor (40-60°N, 90-120°E)**. Sea level pressure in October/November in this region is correlated with the SON Niño 3.4 SSTA the next year in this region, located in eastern Asia. For the years that the forecast was developed on (1950-1990), the predictor correlates at 0.45 with the SON Niño 3.4 and for the entire period (1950-2002), the correlation is 0.41. When high pressure was present in this region during October/November, warm conditions tended to prevail in the Pacific the following year.

3. **South Pacific SLP Predictor (25-45°S, 160°E-160°W)**. The sea level pressure just southeast of New Zealand shows a significant negative correlation with the SON Niño 3.4 SSTA, correlating at -0.43 for 1950-2002. Low sea level pressure in this region is associated with warm Niño 3.4 SSTA in SON the following year.

4. **North Pacific SST Predictor (35-45°N, 150-170°W)**. The sea surface temperature in the northern Pacific Ocean is positively correlated with the SON Niño 3.4 SSTA. This predictor and the SON Niño 3.4 SSTA correlate at 0.22 for 1950-2002. Warm SSTs in the northern Pacific in October/November are correlated with warm SSTs in the Niño 3.4 region the following SON.

5. **PDO Index Predictor (SSTA in Pacific basin, poleward of 20°N)**. The PDO Index is positively correlated with a concurrent El Niño but is negatively correlated with the following year's SON Niño 3.4 SSTA. This means that when the sea surface temperatures are anomalously warm northward of 20°N in the Pacific Ocean in October/November, warm conditions are also in place in the equatorial Pacific. The negative correlation with the SON Niño 3.4 SSTA suggests that when anomalously warm conditions occur in the North Pacific in Oct/Nov, cool conditions should occur in the Niño 3.4 region the following SON (Horel and Wallace 1981). This predictor accounts for the reverse in SST conditions in the Pacific that is often observed one year later. Although the correlation with the SON Niño 3.4 SSTA is somewhat low, the PDO Index remains a significant component of the SON forecast.

Chapter 4

DISCUSSION OF 1 DECEMBER FORECAST FOR JJA NIÑO 3.4 SSTA

4.1 Relation of JJA Predictors to Global Fields

To show how the predictors are related to the El Niño-Southern Oscillation, correlation maps between the predictor and several atmospheric variables were made. The most relevant correlation maps are discussed and shown in this chapter. Correlations were made between each predictor (all having October-November values) with the current October-November global variable (for example, SLP). Also, the time series for each specific predictor region was correlated with a global field 6-8 months later (June-July-August). On each map, red implies a strong positive correlation and on the other end of the spectrum, purple stands for a strong negative correlation. For the wind maps, reds indicate westerly winds and purples indicate easterly winds. On height maps, reds are high heights and purples are low heights.

1. **Lake Baikal 500-mb Zonal Wind Predictor**. Figure 4.1 shows the correlation between the October-November 500-mb zonal wind predictor over the Lake Baikal region (45-55°N, 90-125°E) and the October-November SSTs. The strong positive correlation throughout the equatorial Pacific Ocean signifies an El Niño event is in place. The correlation map between the Oct-Nov predictor and the Oct-Nov sea level pressure shows that the Southern Oscillation (SO) is in its negative phase (Fig. 4.1). The negative phase of the SO is associated with El Niño conditions. Clearly, this predictor is correlated with the Southern Oscillation and is therefore useful in predicting ENSO events.

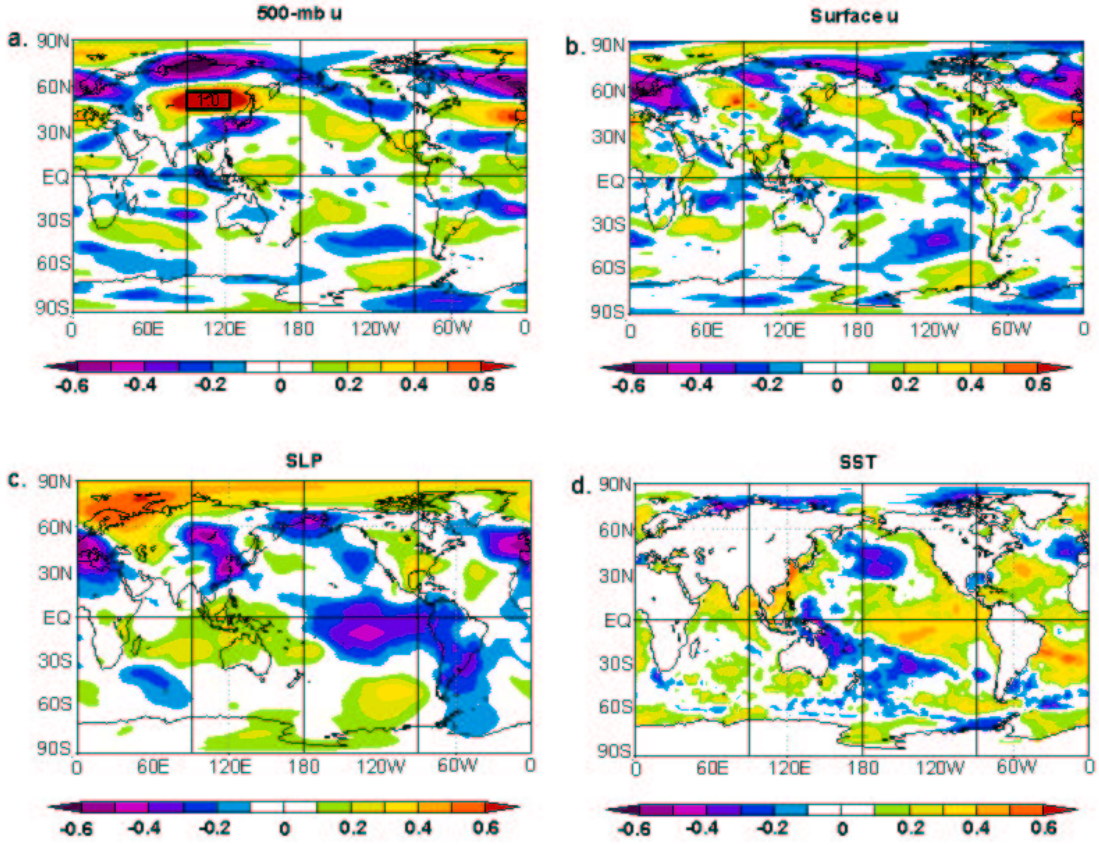

Figure 4.1: Lake Baikal Oct/Nov 500-mb zonal wind normalized anomalies in the region 45-55°N, 90-125°E (see black box in diagram a.) correlated with the **current Oct/Nov** global anomaly fields of a.) 500-mb u, b.) surface u, c.) SLP, and d.) SST. Correlations based on 1950-1990 data.

Several fields show how this predictor is related to ENSO. Figure 4.2 shows the correlation between the predictor and the June-July-August sea level pressure. The strong negative correlation throughout the equatorial Pacific shows that there are cooler SSTs in the region, representing a La Niña event. The correlation between the predictor and the JJA sea level pressure shows that the Southern Oscillation in its positive phase. The positive phase of the Southern Oscillation has been linked to La Niña conditions.

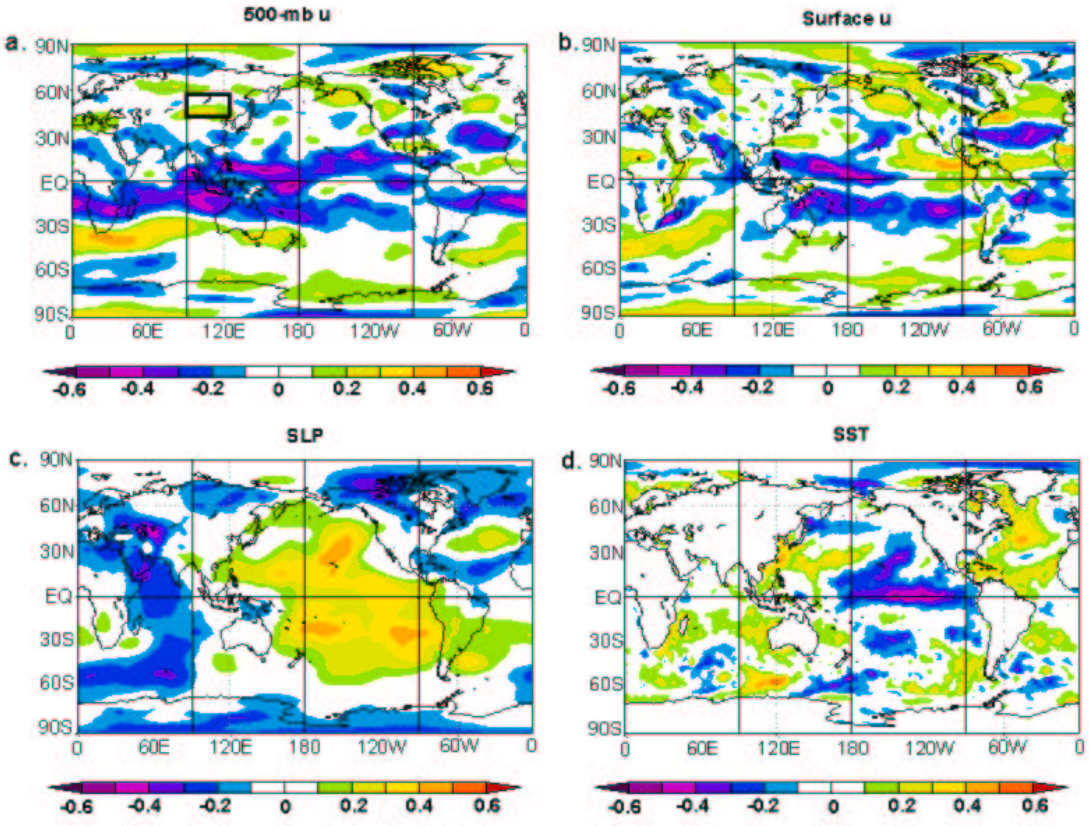

Figure 4.2: Lake Baikal Oct/Nov 500-mb zonal wind normalized anomalies in the region 45-55°N, 90-125°E (see black box in diagram a.) correlated with the **following year's JJA** global anomaly fields of a.) 500-mb u, b.) surface u, c.) SLP, and d.) SST. Correlations based on 1950-1990 data.

The 500-mb zonal wind field also shows support for this predictor. Figure 4.2 shows the correlation between the October-November 500-mb zonal wind predictor and the June-July-August 500-mb zonal wind throughout the globe. There are regions

of strong negative correlation throughout the equatorial Pacific, signifying easterly winds at 500-mb in those regions. Easterly winds over the equatorial Pacific cause easterly surface winds, which push cooler surface water westward. As a result of this, cooler waters from the east Pacific Ocean spread westward, causing cool La Niña conditions in the Pacific Ocean. The SST map for the same JJA period shows that La Niña conditions had in fact developed.

2. **South Pacific 500-mb Zonal Wind Predictor**. Figure 4.3 shows the correlation between the October-November 500-mb zonal wind in the South Pacific (25-35°S, 150-180°E) with several global fields. The most striking features in the 200-mb height correlation map are a strong negative correlation between the 500-mb zonal wind and 200-mb heights southeast of Australia and a strong positive correlation center adjacent to it.

   When correlated with the predictor, the 500-mb zonal wind field shows a strong positive correlation southeast of Australia and a negative correlation just to the south. The positive correlation was expected, as the predictor was correlated with itself in that region. The adjacency of the strong opposite centers indicates a cyclone in this part of the south Pacific.

   When the Oct/Nov sea level pressure map is correlated with the Oct/Nov South Pacific 500-mb Zonal Wind Predictor, the map shows lower pressure centered over Australia and relatively high pressure in the Eastern Pacific. This suggests that the Southern Oscillation is in its positive phase; however, this relationship is not clear. The positive phase of the Southern Oscillation is generally associated with La Niña conditions in the Pacific, but the Oct/Nov SLP correlation map appears to be reminiscent of a positive phase of the Southern Oscillation, but there is not a clear cut relationship. The SSTA map confirms this, as the equatorial Pacific Ocean shows near neutral conditions.

   When the Oct/Nov South Pacific 500-mb Zonal Wind Predictor is correlated with the JJA 200-mb geopotential height, high heights appear throughout the tropics (Fig.

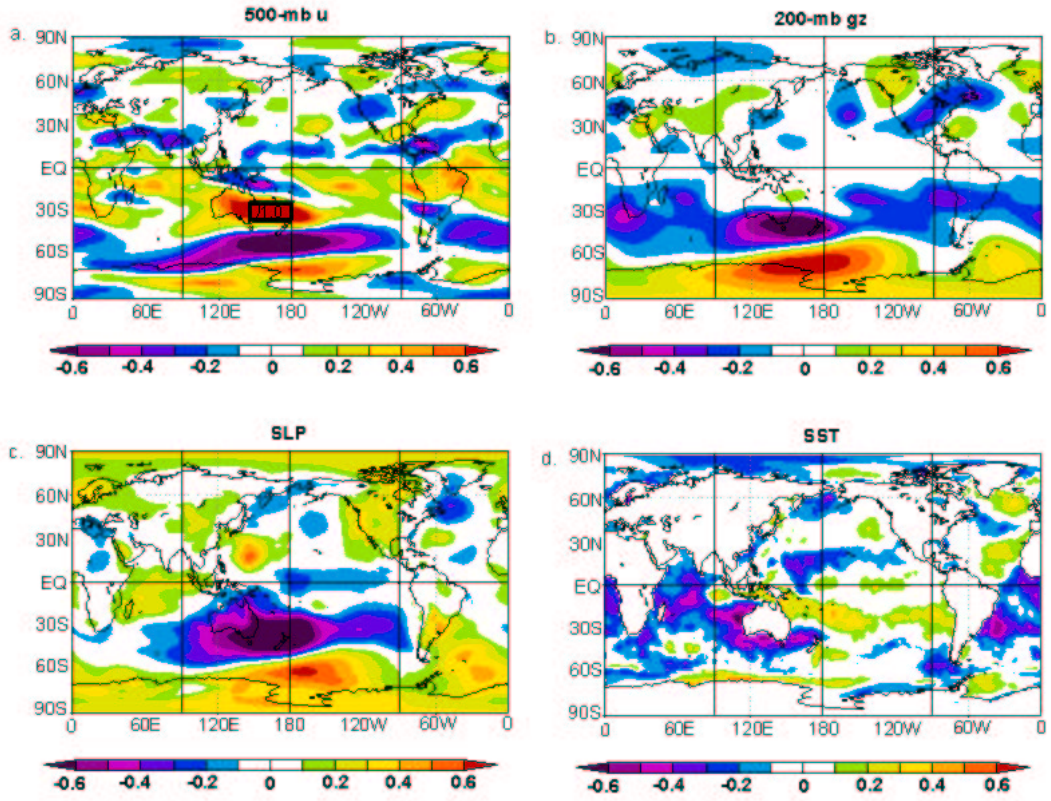

Figure 4.3: South Pacific Oct/Nov 500-mb zonal wind normalized anomalies in the region 25-35°S, 150-180°E (see black box in diagram a.) correlated with the **current Oct/Nov** global anomaly fields of a.) 500-mb u, b.) 200-mb gZ, c.) SLP, and d.) SST. Correlations based on 1950-1990 data.

4.4). High heights in this region indicate warm conditions in the Pacific Ocean. The Oct/Nov predictor is strongly correlated with atmospheric conditions that indicate an El Niño in JJA.

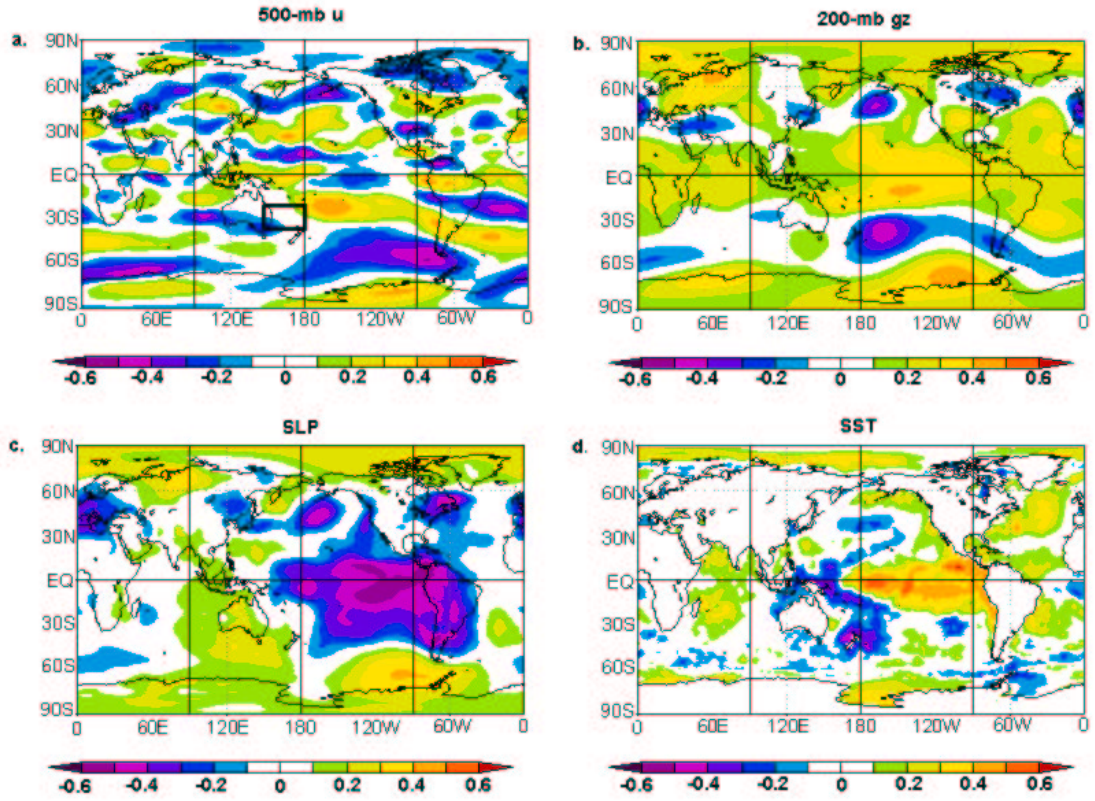

Figure 4.4: South Pacific Oct/Nov 500-mb zonal wind normalized anomalies in the region 25-35°S, 150-180°E (see black box in diagram a.) correlated with the **following year's JJA** global anomaly fields of a.) 500-mb u, b.) 200-mb gZ, c.) SLP, and d.) SST. Correlations based on 1950-1990 data.

The correlation between the 500-mb zonal winds and the South Pacific 500-mb Zonal Wind Predictor show that a positive correlation exists in the west Pacific, which means that westerly winds are present there. Westerly winds in this region mean that the warm pool is being shifted eastward, as occurs during El Niño events. Also note the strong correlation with westerly winds in the Southern Hemisphere from 15-30°S, 100-180°W. Although not on the equator, these westerly winds are often present during El Niño conditions.

3. **South Atlantic 200-mb gZ Predictor**. Figure 4.5 shows four Oct/Nov global fields correlated with the South Atlantic 200-mb Predictor, which appears to be strongly linked to global conditions typical of a warm ENSO event (Fig. 4.5). The 200-mb height correlation field shows that the predictor is correlated with high heights throughout the tropics. When warm conditions exist at the surface, as they do over the Pacific Ocean during an El Niño, the 200-mb heights tend to be anomalously high because the atmosphere is less dense where it is warmer.

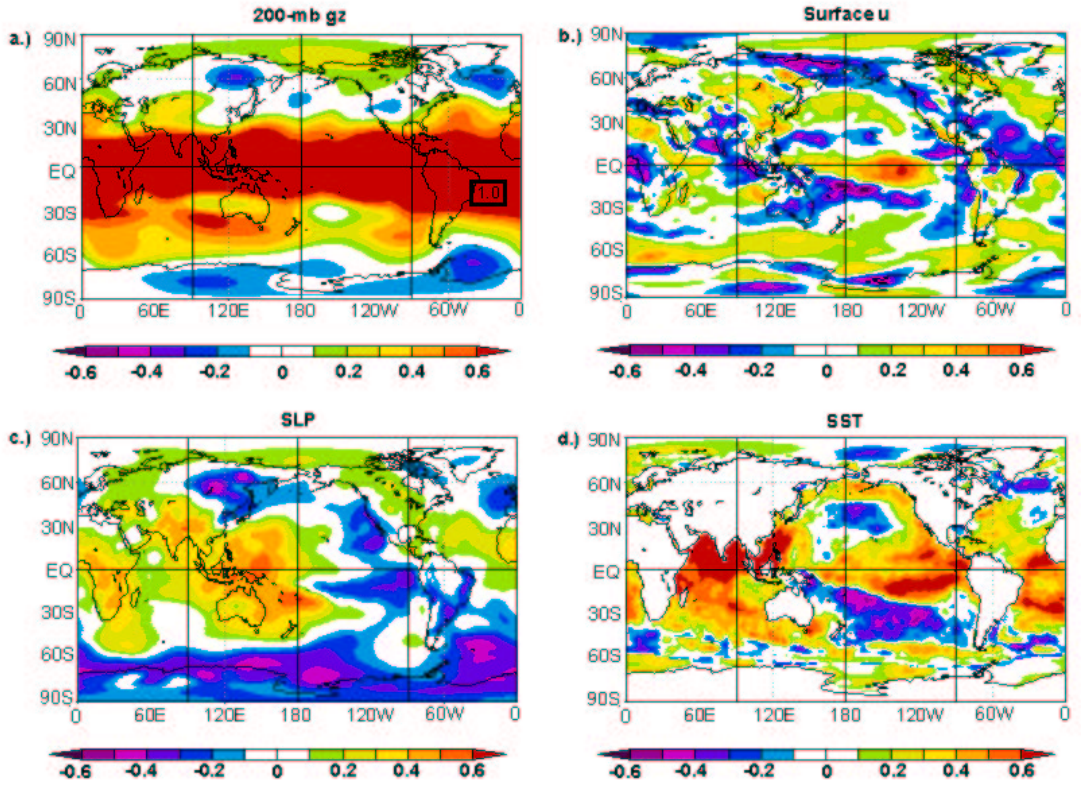

Figure 4.5: South Atlantic Oct/Nov 200-mb gZ normalized anomalies in the region 10-25°S, 10-40°W (see black box in diagram a.) correlated with the **current Oct/Nov** global anomaly fields of a.) 200-mb gZ, b.) surface u, c.) SLP, and d.) SST. Correlations based on 1950-1990 data.

The surface zonal wind field shows a strong positive correlation with the predictor along the equatorial Pacific. Anomalously strong westerly winds along the equator are indicative of El Niño conditions. Since the predictor is correlated with these

westerly surface zonal winds, it is also related to warm SSTAs in the equatorial Pacific.

The positive phase of the Southern Oscillation is strongly correlated with the Oct/Nov South Atlantic predictor, as the sea level pressure correlation map shows. This means that the 200-mb South Atlantic geopotential height is correlated with the positive phase of the Southern Oscillation in Oct/Nov, which is related to El Niño conditions.

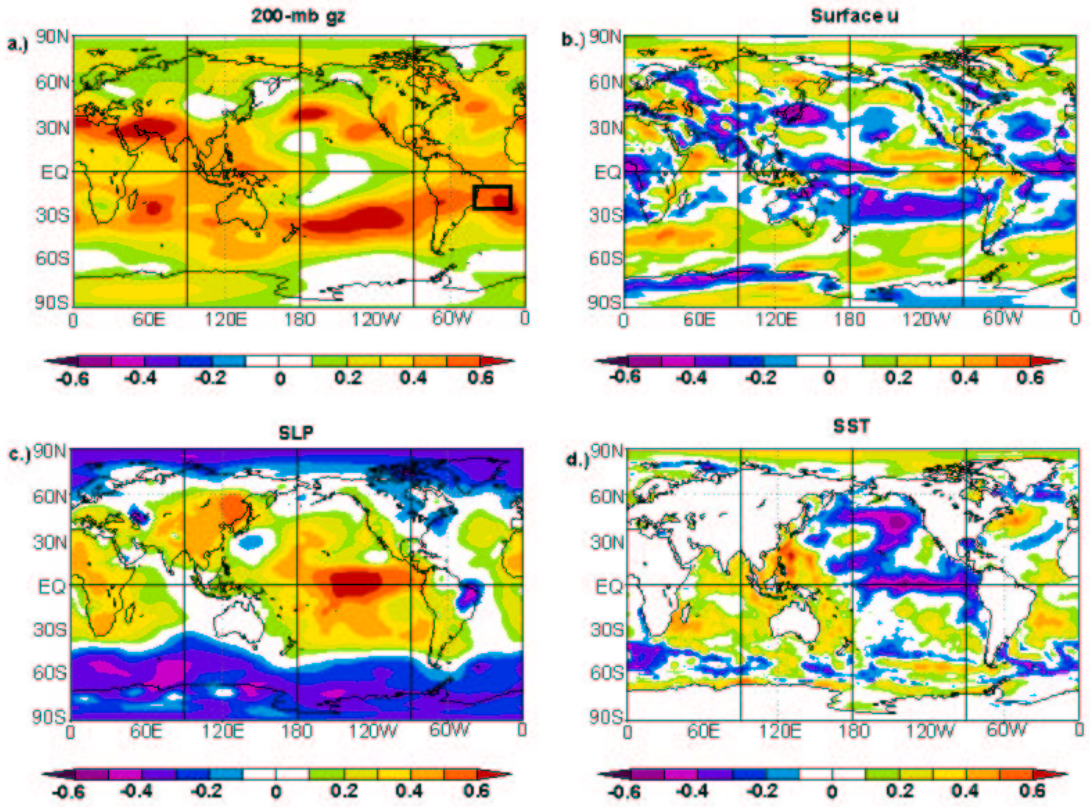

Figure 4.6: South Atlantic Oct/Nov 200-mb gZ normalized anomalies in the region 10-25°S, 10-40°W (see black box in diagram a.) correlated with the **following year's JJA** global anomaly fields of a.) 200-mb gZ, b.) surface u, c.) SLP, and d.) SST. Correlations based on 1950-1990 data.

The sea surface temperature map clearly shows that the Oct/Nov South Atlantic 200-mb gZ predictor is strongly correlated with warm SSTs throughout the Pacific, Atlantic, and Indian Oceans. A strong El Niño event is evident, as was expected from the conditions in the other fields.

The correlations between the Oct/Nov South Atlantic 200-mb gZ predictor and various JJA global fields suggest cool conditions in the Pacific (Fig. 4.6). The 200-mb height field shows that the heights have become since Oct/Nov, which suggests that the equatorial surface is not as warm as it was. As mentioned earlier, heights lag surface cooling by several months. The predictor is now correlated with easterly winds in the west Pacific, which are related to La Niña conditions. The SLP map also shows that the Oct/Nov predictor is correlated with higher pressure in the central and east Pacific. Anomalously high sea level pressures are related to cold surface temperatures, which come with La Niñas. As expected, the SSTA map shows that the Oct/Nov South Atlantic 200-mb gZ Predictor is strongly correlated with cold waters in the equatorial Pacific during the following JJA.

4. **Equatorial Pacific 500-mb Zonal Wind Predictor**. Figure 4.7 shows the correlations between the Oct/Nov 500-mb zonal wind predictor and four global fields. When the 500-mb Zonal Wind Predictor is correlated with the Oct/Nov 500-mb zonal wind, a strong positive correlation along the entire equatorial Pacific is evident. This positive correlation means that there are prevalent westerly winds throughout the region. As mentioned before, equatorial westerly winds are associated with El Niño events in the Pacific.

   The surface zonal wind field shows that the Oct/Nov predictor is strongly correlated with westerly winds over the central and eastern Pacific Ocean. Surface westerlies over the equatorial Pacific are a strong indicator of warm events, as they shift the warm pool eastward. The predictor is correlated with higher sea level pressure in the east Pacific and lower SLP in the south Pacific, which is the way the pressure dipole is set up during the positive phase of the Southern Oscillation. However, the correlation to the SO does not appear to be very strong. Neutral or slightly cooler conditions would be expected in the equatorial Pacific, since cool conditions have been linked with the positive phase of the SO. The SSTA field shows near neutral conditions in the Pacific, as anticipated.

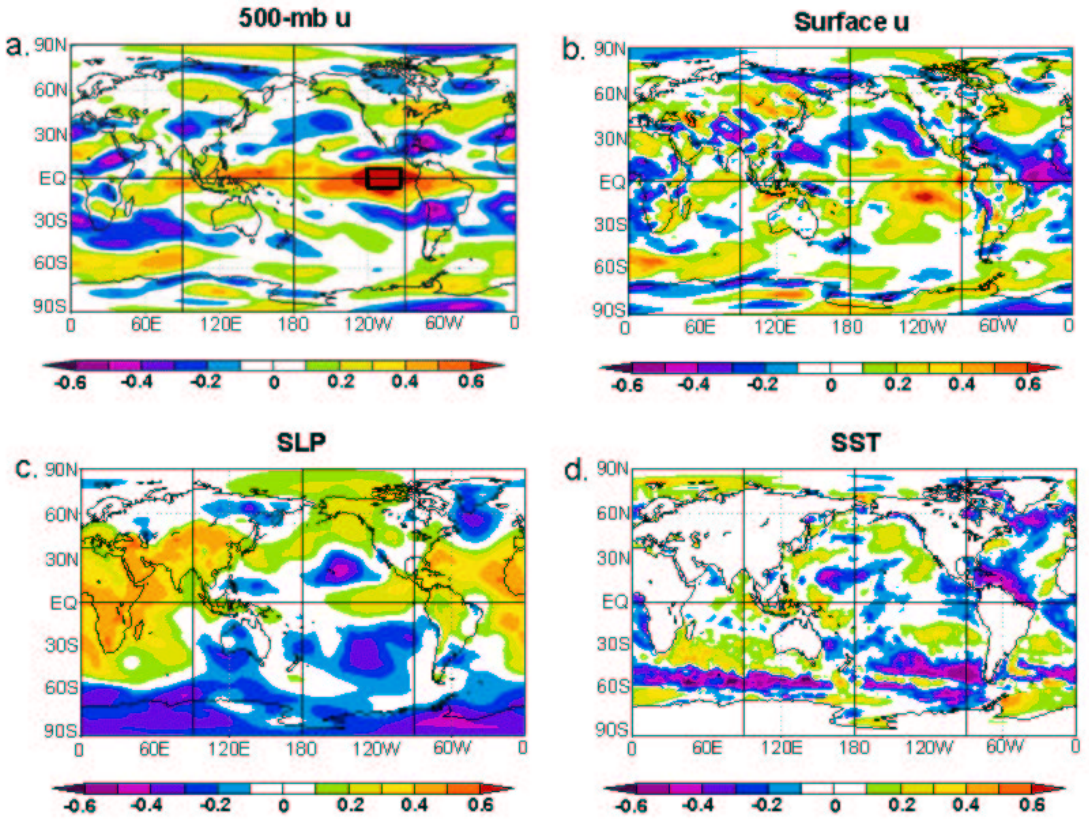

Figure 4.7: Equatorial Pacific Oct/Nov 500-mb zonal wind normalized anomalies in the region 5°N-5°S, 95-120°W (see black box in diagram a.) correlated with the **current Oct/Nov** global anomaly fields of a.) 500-mb u, b.) surface u, c.) SLP, and d.) SST. Correlations based on 1950-1990 data.

When the Oct/Nov Equatorial Pacific 500-mb Zonal Wind Predictor is correlated with the global JJA 500-mb zonal wind (Fig. 4.8), strong positive correlations appear throughout the equatorial Pacific, with strong centers over Indonesia and just west of South America along the equator. The positive correlations represent westerly winds, which are linked to El Niño conditions. Therefore, the Oct/Nov Equatorial Pacific 500-mb Zonal Wind Predictor is linked to El Niño conditions the following JJA.

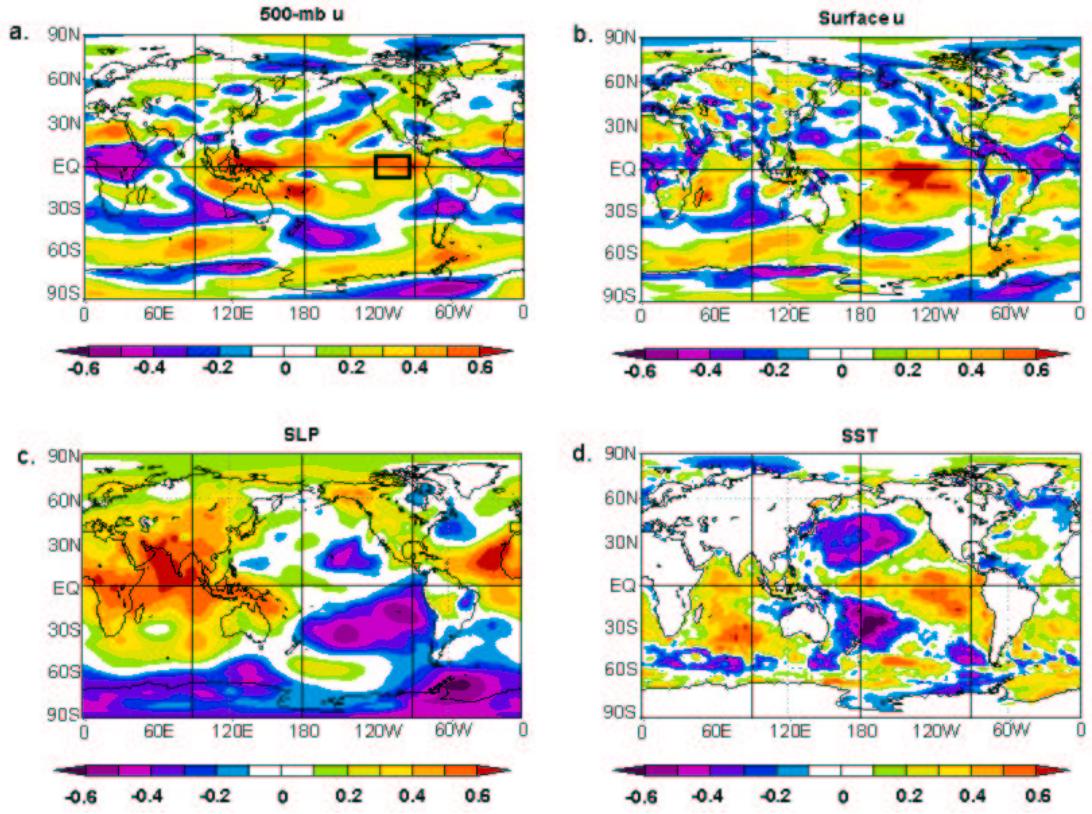

Figure 4.8: Equatorial Pacific Oct/Nov 500-mb zonal wind normalized anomalies in the region 5°N-5°S, 95-120°W (see black box in diagram a.) correlated with the **following year's JJA** global anomaly fields of a.) 500-mb u, b.) surface u, c.) SLP, and d.) SST. Correlations based on 1950-1990 data.

There is a strong positive correlation in the central equatorial Pacific between the Oct/Nov predictor and the JJA surface zonal wind. Surface westerly winds along the equator reduce upwelling causing warm SSTs. The 500-mb zonal wind is therefore correlated strongly with the surface zonal wind, which is related to El Niño events.

The sea level pressure correlation field shows high pressure in the west Pacific and Indian Ocean and low pressure in the east Pacific. This is the negative phase of the Southern Oscillation, which is generally in place when warm conditions exist along the equatorial Pacific.

5. **South Atlantic Surface Zonal Wind (5-15°S, 5-30°W)**. Figure 4.9 shows the correlation between the October-November surface zonal wind in the South Atlantic (5-15°S, 5-30°W) with several global fields for the same October-November period. The surface zonal wind correlation map shows that the predictor is correlated with a region of westerly winds along the central equatorial Pacific with some easterlies in the west and east equatorial Pacific. This mix of easterlies and westerlies along the equatorial Pacific does not specifically point to the development of warm or cool conditions. Similarly, the 200-mb gZ and SLP maps do not show any clear features that would be useful in predicting the following year's ENSO conditions.

   The correlation betwen the Oct/Nov South Atlantic surface zonal wind and the current Oct/Nov SST shows that there are positive correlations in the extreme west Pacific and the Indian Ocean, as well as in the South Atlantic. When the predictor is anomalously positive (westerly winds), the areas of positive correlation in the SST field also experience a positive (warm) anomaly. Overall, the Pacific shows neutral SST conditions.

   More useful are the maps that display correlations between the Oct/Nov South Atlantic surface zonal wind and the following year's JJA global fields (Fig. 4.10). When the Oct/Nov predictor is correlated with the following JJA surface zonal wind field, a strong negative correlation is apparent in the west equatorial Pacific and also the south Pacific. These regions indicate anomalous easterly winds when the predictor has an anomalously positive value. Easterly winds in these regions are associated with La Niña conditions in the Pacific.

   The 200-mb gZ map shows strong negative correlations between the Oct/Nov predictor and the following year's JJA 200-mb heights. Low upper level heights throughout

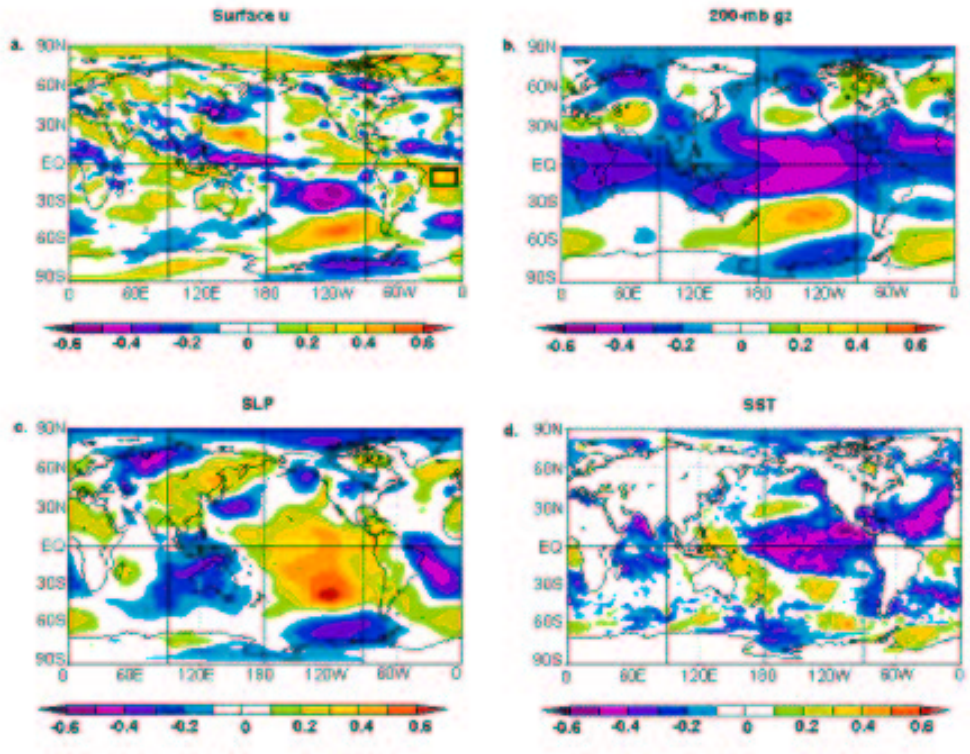

Figure 4.9: South Atlantic Oct/Nov 500-mb zonal wind normalized anomalies in the region 5-15°S, 5-30°W (see black box in diagram a.) correlated with the **current Oct/Nov** global anomaly fields of a.) surface u, b.) 200-mb gZ, c.) SLP, and d.) SST. Correlations based on 1950-1990 data.

the tropics are indicative of cool surface conditions, which typically occur during La Niña events. Note that the strongest negative correlation is centered over the central and east equatorial Pacific, where cool SSTAs are strongest.

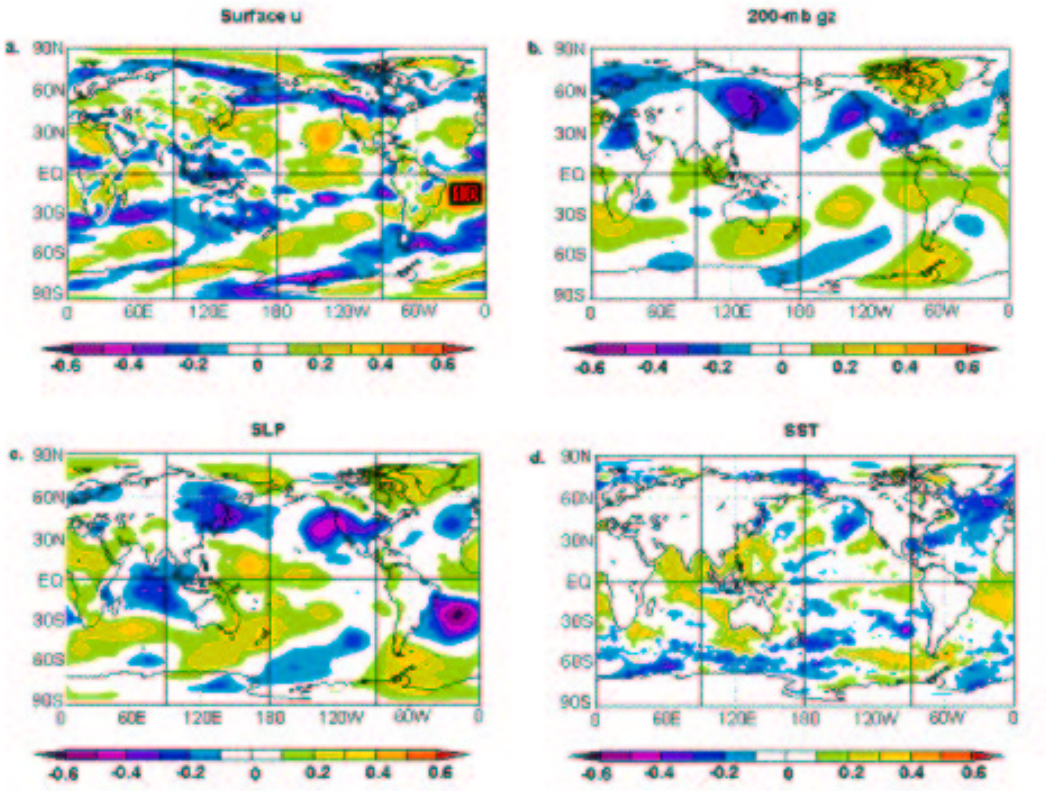

Figure 4.10: South Atlantic Oct/Nov 500-mb zonal wind normalized anomalies in the region 5-15°S, 5-30°W (see black box in diagram a.) correlated with the **following year's JJA** global anomaly fields of a.) surface u, b.) 200-mb gZ, c.) SLP, and d.) SST. Correlations based on 1950-1990 data.

The most striking feature in the SLP correlation map is the strong dipole between the east and west Pacific, indicative of a strong positive SO event. As previously explained, positive SO events, with high pressure in the east Pacific and low pressure in the west Pacific, are physically linked with La Niña events. The Oct/Nov predictor is strongly correlated with a physical feature that is related to ENSO and therefore, would likely be useful in predicting these events.

As expected from the previously examined fields, the SST field shows a strong negative correlation throughout the eastern and central Pacific. When the Oct/Nov South Atlantic surface zonal wind shows a positive anomaly (westerly wind), there is a negative anomaly (cool conditions) in the east and central Pacific. As this predictor is correlated strongly with JJA conditions typical of La Niña conditions, it would likely be useful in predicting ENSO events.

In summary, the best five predictors used to make the 1 December forecast for the JJA Niño SSTA are correlated with global climate features that are related to ENSO conditions. Therefore, these predictors are useful for forecasting these climatic events.

Chapter 5

SKILL OF THE 1 DECEMBER NIÑO 3.4 JJA FORECAST

In order to assess the skill of the ENSO forecasts presented in this thesis, comparisons must be made to ENSO-CLIPER. As mentioned previously, ENSO-CLIPER is regarded as a more rigorous baseline for determining forecast skill than persistence alone. The same forecast period and length will be used to evaluate each scheme (1 December forecast for JJA Niño 3.4). Variance explained will be evaluated for each forecast scheme as well as the standard error.

5.1 Variance Explained (r^2) by the JJA forecast

The forecast scheme presented in this paper explains more variance than ENSO-CLIPER does for the same forecast period (Table 5.1). For all years (1952-2002), SG explains 58 percent of the variance, while ENSO-CLIPER explains 14 percent. SG explains four times the variance of ENSO-CLIPER's for the period 1952-2002.

The comparison between the two schemes for 1992-2002 (the range of independent data years of SG) shows that SG has higher values of correlation and variance explained, regardless of the fact that ENSO-CLIPER's forecast for that period uses some dependent data (independent data years for ENSO-CLIPER are 1995-2002). The variance explained by SG (35 percent) for independent data years (1992-2002) is twice that of ENSO-CLIPER (18 percent).

Table 5.1: This table shows the variance explained (r^2) for SG and ENSO-CLIPER for various time periods.).

1 Dec. JJA Forecast	All Yrs. 1950-2002	Independent Yrs. 1992-2002	Dependent Yrs. (SG) 1950-1990
SG	58	35	69
ENSO-CLIPER	15	18	n/a

5.2 Examination of Error by Individual Years

Because the statistics for short ranges of years may not give a complete picture of the skill of this forecast, individual years will be examined and assessed for error. One striking feature in the plot of the standard error by year (Fig. 5.1) is that ENSO-CLIPER has more years with large, outlying error values (greater than 1.0) than SG. Also note that these outlying peaks in error seem to occur consistently for ENSO-CLIPER, whereas for SG, they have only occurred since the late 1990s. Figure 5.2 shows the JJA Niño 3.4 SSTA observations and predictions by the JJA SG and ENSO-CLIPER forecast schemes.

The ten worst years for SG's JJA forecast are listed in Table 5.2. In these years, the Niño 3.4 observations include both warm and cool phases of ENSO. These years consist of both large and small SSTA in the Niño 3.4 region, although the tendency is towards years with larger SSTAs. The average Niño 3.4 observations (without respect to sign) for the ten worst years for the SG scheme is 0.81, which is a large SSTA value.

The ten years with the worst standard errors for ENSO-CLIPER's JJA forecast are listed in Table 5.3. It should be noted that ENSO-CLIPER shares four of its ten worst years with SG (1997, 1987, 1975, and 1999). These years all exhibit a large SSTA in the Niño 3.4 region for JJA. The years with the highest RMSE scores for ENSO-CLIPER seem to be mostly years in which the SSTA exhibited large deviations. This is to be expected, since ENSO-CLIPER is heavily weighted by climatology and therefore does not handle extremes well.

The years with the lowest standard error for SG (ENSO-CLIPER) scheme are listed in Table 5.4 (Table 5.5) with their corresponding standard error and SSTA observation. On average, the smallest errors tend to occur in years when the SSTA is small. The average

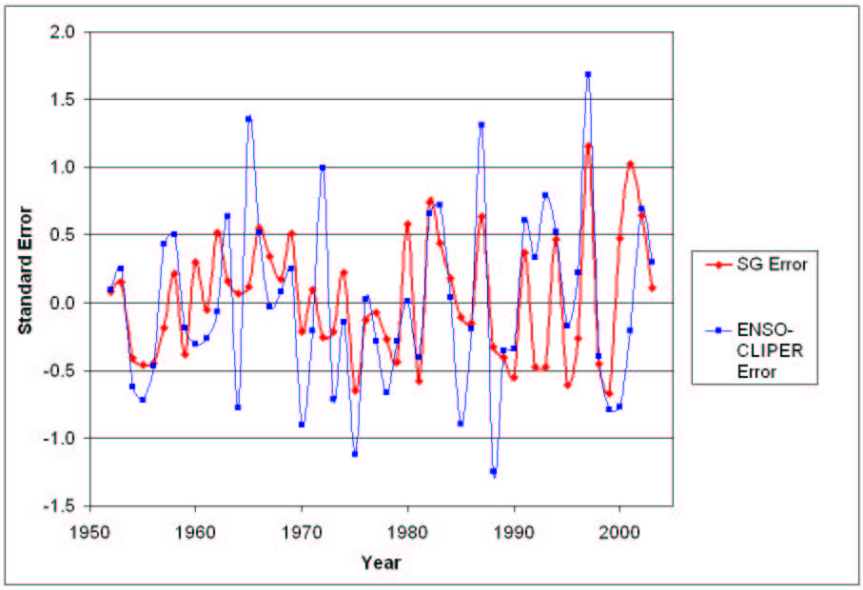

Figure 5.1: Shows the Standard Error (Observed-Predicted) for every year for JJA SG and ENSO-CLIPER Forecasts. Note that the SG scheme has few large errors.

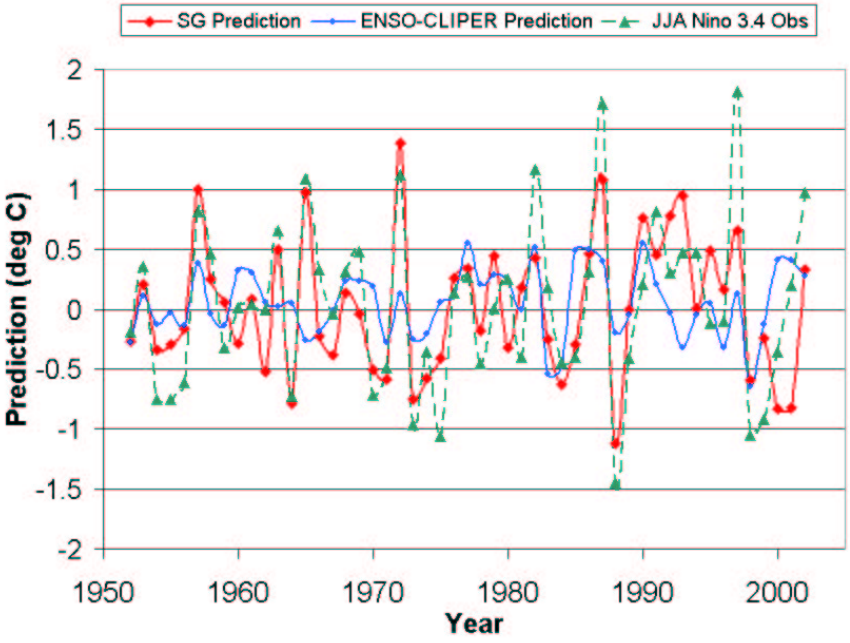

Figure 5.2: Shows the JJA Niño 3.4 SSTA observations and predictions by the JJA SG and ENSO-CLIPER schemes.

SSTA observations (without respect to sign) are 0.40 for SG and 0.21 for ENSO-CLIPER. Therefore, both models perform best when there are small SSTAs in the Niño 3.4 region.

Table 5.2: This table shows the **worst** years (largest error) for the **SG** 1 December forecast for JJA Niño 3.4 SSTA and the corresponding Niño 3.4 SSTA observations.

Worst Yrs. for SG	Niño 3.4 SSTA Obs	SG Prediction	Standard Error (Observed)-(Predicted)
1997	1.81	0.66	1.15
2001	0.20	-0.81	1.02
1982	1.17	0.42	0.74
1999	-0.92	-0.24	-0.67
1975	-1.06	-0.41	-0.65
2002	0.97	0.33	0.64
1987	1.71	1.08	0.63
1995	-0.12	0.48	-0.60
1981	-0.40	0.18	-0.58
1980	0.25	-0.32	0.57
Average with respect to sign	0.36	0.14	0.22
Average without respect to sign	0.86	0.49	0.73

5.3 Analysis of Largest Errors made by the 1 December SG Forecast for JJA Niño 3.4 SSTA

In an attempt to understand any physical explanations for why the SG forecast performs poorly for certain years, composites of various global fields were created for the JJA of the ten years with the largest errors. The JJA composites show the global conditions that the SG model had difficulty forecasting.

The composites of the global fields for the forecast years with largest errors all show El Niño conditions in the Pacific basin (Fig. 5.3). The surface wind field shows anomalous westerly winds along much of the equator, as well as a large region of strong westerlies in the South Pacific. These conditions are commonly associated with El Niño events. The composite of the 200-mb gZ of the worst forecast years shows anomalously high heights throughout most of the globe, particularly the tropics and subtropics. High upper-level heights are also linked with warm surface conditions. The SLP composite shows that the Southern Oscillation is in its negative phase, which is associated with El Niño conditions.

Table 5.3: This table shows the **worst** years (largest error) for the **ENSO-CLIPER** 1 December forecast for JJA Niño 3.4 SSTA and the corresponding Niño 3.4 SSTA observations.

Worst Yrs. for ENSO-CLIPER	Niño 3.4 SSTA Obs	ENSO-CLIPER Prediction	Standard Error (Observed)-(Predicted)
1997	1.81	0.13	1.68
1965	1.09	-0.26	1.35
1987	1.71	0.40	1.31
1988	-1.45	-0.20	-1.25
1975	-1.06	0.06	-1.12
1972	1.12	0.13	0.99
1970	-0.71	0.19	-0.90
1985	-0.40	0.49	-0.89
1993	0.47	-0.32	0.79
1999	-0.91	-0.13	-0.78
Average with respect to sign	0.17	0.05	0.11
Average without respect to sign	1.07	0.23	1.02

Table 5.4: This table shows the **best** years (smallest error) for the **SG** 1 December forecast for JJA Niño 3.4 SSTA and the corresponding Niño 3.4 SSTA observations.

Best Yrs. for SG	Niño 3.4 SSTA Obs	SG Prediction	Standard Error (Observed)-(Predicted)
1961	0.03	0.09	-0.06
1964	-0.72	-0.79	0.07
1977	0.26	0.34	-0.08
1952	-0.18	-0.27	0.09
1971	-0.48	-0.58	0.10
1985	-0.40	-0.29	-0.11
1965	1.09	0.97	0.12
1976	0.13	0.26	-0.13
1953	0.36	0.21	0.15
1986	0.31	0.46	-0.15
Average with respect to sign	0.04	0.04	-0.001
Average without respect to sign	0.40	0.43	0.10

Table 5.5: This table shows the **best** years (smallest error) for the **ENSO-CLIPER** 1 December forecast for JJA Niño 3.4 SSTA and the corresponding Niño 3.4 SSTA observations.

Best Yrs. for ENSO-CLIPER	Niño 3.4 SSTA Obs	ENSO-CLIPER Prediction	Standard Error (Observed)-(Predicted)
1980	0.25	0.24	0.01
1976	0.13	0.11	0.02
1967	-0.04	-0.01	-0.03
1984	-0.44	-0.48	0.04
1962	0.00	0.06	-0.06
1968	0.31	0.23	0.08
1952	-0.18	-0.28	0.10
1974	-0.35	-0.21	-0.14
1995	-0.12	0.05	-0.17
1959	-0.32	-0.14	-0.18
Average with respect to sign	-0.04	-0.04	-0.09
Average without respect to sign	0.08	0.18	0.22

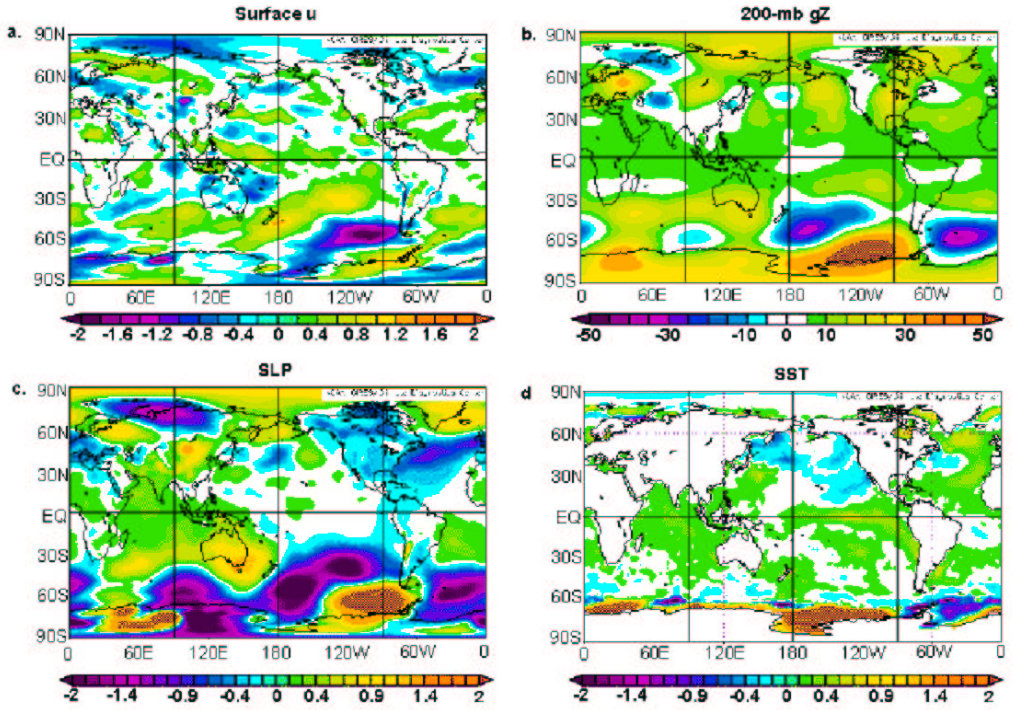

Figure 5.3: Composites of JJA global fields for the worst years for the 1 December SG Forecast. Worst years (listed in Table 5.2) are 1997, 2001, 1982, 1999, 1975, 2002, 1987, 1995, 1981, and 1980.

The SST composite shows slight El Niño conditions in the Pacific. The composite maps indicate that the SG model has some difficulties in forecasting warm ENSO conditions in the Pacific.

5.4 Examination of Forecast Error in Terms of Too Warm/Cold

To better understand why this model performs poorly in some years and well in others, the global conditions for the years in which the model performs well and poorly are separately examined for possible answers. Years in which the standard error (observation-prediction) is negative signifies a prediction that is too warm (over-prediction) compared to the Niño 3.4 SSTA for that year. Conversely, a prediction that is too cold occurs when the standard error is positive (under-prediction). Examining the cases that are too warm separately from the cases that are too cold may reveal some insight into the causes of error for this scheme.

Table 5.6: Years in which SG forecasts too warm/cold for JJA Niño 3.4 SSTA and the corresponding standard error (observation - prediction).

Forecast Too Warm (over-predicts)	Standard Error	Forecast Too Cold (under-predicts)	Standard Error
1949	-1.65	1997	1.15
1999	-0.67	2001	1.02
1975	-0.65	1982	0.74
1995	-0.60	2002	0.64
1981	-0.58	1987	0.63

The five years in which SG over-predicts the Niño 3.4 SSTA by the most are shown in Table 5.6. Composites of the JJA global conditions for the five years with errors that are too warm show conditions characterized by La Niña, such as cool SSTs in the east and central Pacific, easterly equatorial winds along the Pacific, and a positive SO pattern. To reduce redundancy, only the SST composite is shown in Figure 5.4. These conditions are logical to expect, as forecasts that err on the warm side expect conditions that are warmer than what occurs in reality. Conversely, the composite of the JJA global conditions for the years which err on the cold side show El Niño conditions (Fig. 5.5).

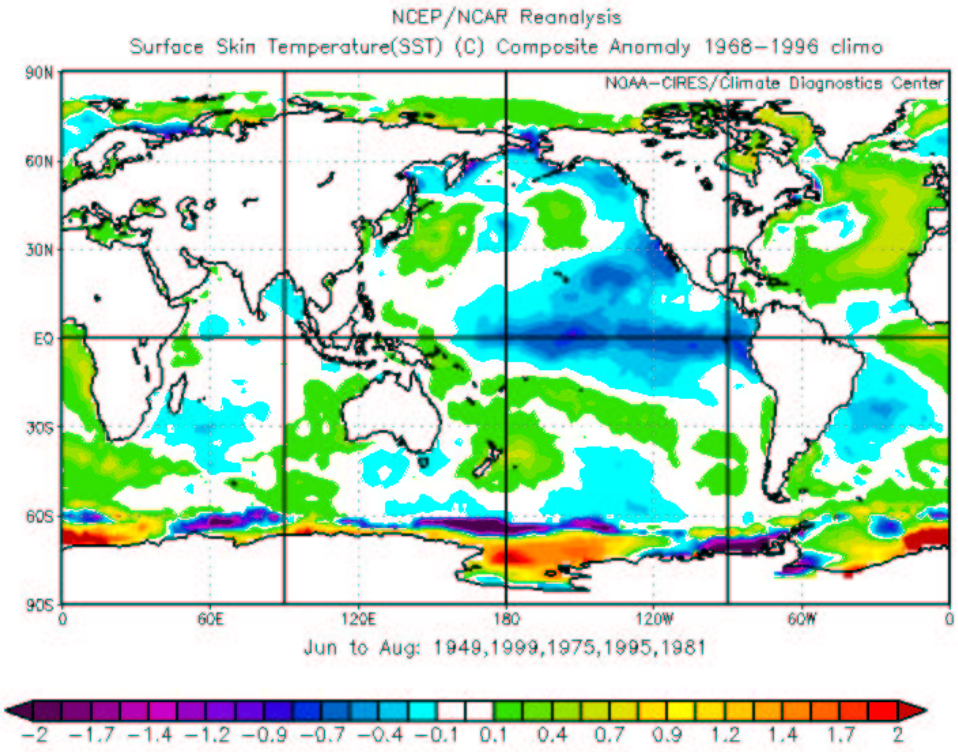

Figure 5.4: Composite of JJA SSTA field for the five years where the 1 Dec. SG forecast was **too warm** (over-predicts) compared to the Niño 3.4 observation. The "too warm" years are 1949, 1999, 1975, 1995 and 1981.

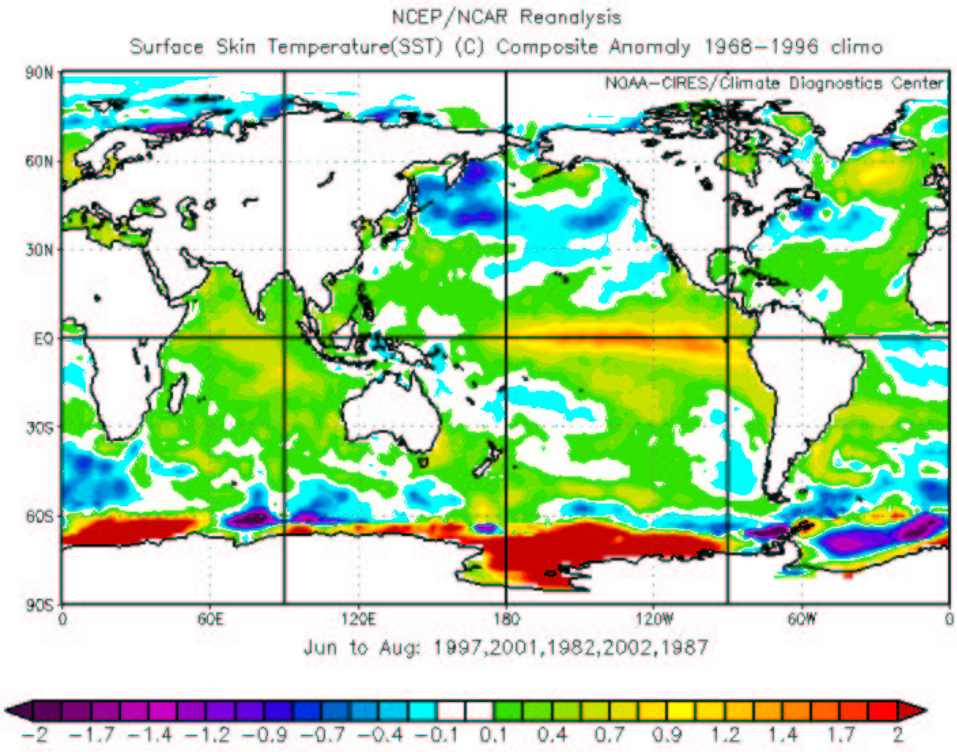

Figure 5.5: Composite of the JJA SSTA field for the five years where the 1 Dec. SG forecast was **too cold** (under-predicts) compared to the Niño 3.4 observation. The "too cold" years are 1997, 2001, 1982, 2002, and 1987.

Composite maps of the difference between the too warm and too cold years are shown in Fig. 5.5 (too warm - too cold). There appear to be large differences in the global fields of 500-mb gZ, SLP, SST, and surface zonal wind. This further shows that the global atmosphere and ocean are affected by the phases of ENSO.

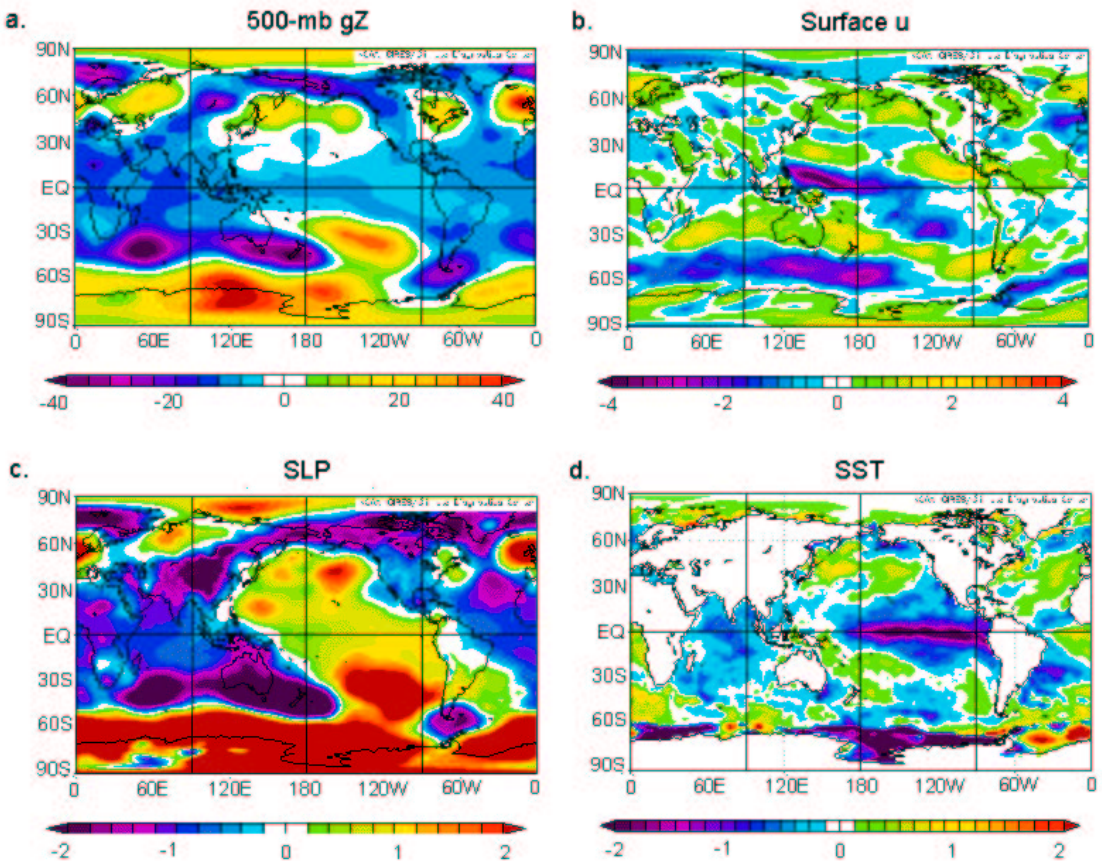

Figure 5.6: Composites of the difference between the years that SG forecast too warm and too cold (listed in Table 5.6) for the JJA forecast.

5.5 Degradation of the JJA Forecast Based on Removal of Predictors

The amount of variance explained by each forecast decreases upon removal of a predictor from the group of five best predictors used to make the forecast. By removing each of the best five predictors individually, the importance of the predictors can be inferred by the reduction in variance explained. Table 5.7 lists the removed predictors and the corresponding reduction in variance.

Table 5.7: This table shows the degradation in variance explained when each of the five best JJA predictors was separately removed. The predictors are numbered as follows: 1 = South Pacific 500-mb u, 2 = Equatorial Pacific 500-mb u, 3 = Lake Baikal 500-mb u, 4 = South Atlantic 200-mb gZ, 5 = South Atlantic Surface u. The largest degradation occurs with Predictor 2.

Predictor Removed	Percent Variance Explained	Percent Degraded
0	69	0
1	61	8
2	53	16
3	63	6
4	65	4
5	60	9
Average	60	9

The forecast for JJA was degraded the most by removal of Predictor 2, which is the Equatorial Pacific 500-mb zonal wind. In combination with the other predictors, this one explained the most variance and is therefore very important to the forecast. Predictor 5 contributes the second largest amount of degradation: removing it from the forecast reduces the variance explained by 9 percent. These two predictors may be most important to the forecast because they both cover regions in the tropics that are near to the ENSO event. Removal of Predictor 4 (South Atlantic 200-mb gZ) causes the percent variance to degrade the least, implying that this predictor does not contribute as much to the forecast as the others.

5.6 Summary

The analysis in this chapter shows that the SG forecast scheme explained more variance than the ENSO-CLIPER scheme and also showed a reduction in the number of large errors. Therefore, the five best Oct/Nov predictors selected for the 6-8 month SG prediction have indeed produced a skillful ENSO forecast.

Chapter 6

DISCUSSION OF 1 DECEMBER FORECAST FOR SON NIÑO 3.4 SSTA

6.1 Relation of SON Predictors to Global Fields

In an attempt to understand how the predictors are related to global fields and ENSO, correlation maps between each predictor and various fields were created. For each map, a time series for a specific predictor region was correlated with a global field 9-11 months later. For example, the Oct/Nov Lake Baikal SLP from 40-60°N, 90-120°E (the region of the predictor) was correlated with the global SST during September-October-November of the following year. On each map, red implies a strong positive correlation and on the other end of the spectrum, purple stands for a strong negative correlation. For the wind maps, reds indicate westerly winds, and purples indicate easterly winds. On height maps, reds stand for high heights and purples stand for low heights.

1. **Lake Baikal SLP Predictor (40-60°N, 90-120°E)**. Figure 6.1 shows the correlation between the October-November Lake Baikal region (see the black box in diagram a.) SLP correlated with the following year's SON global anomaly fields of: a.) SLP, b.) 200-mb gZ, c.) surface u, and d.) SST. The SLP map shows that the predictor is correlated with the negative phase of the Southern Oscillation, which is shown by the negative correlations in the east Pacific and the positive correlations over the west Pacific. Negative correlations mean that when the predictor is positive (i.e. the Lake Baikal Oct/Nov SLP is anomalously high), the heights in the east Pacific are low. The opposite is true for the regions of positive correlation: when the predictor is anomalously positive, these regions have positive anomalies (high heights) as well.

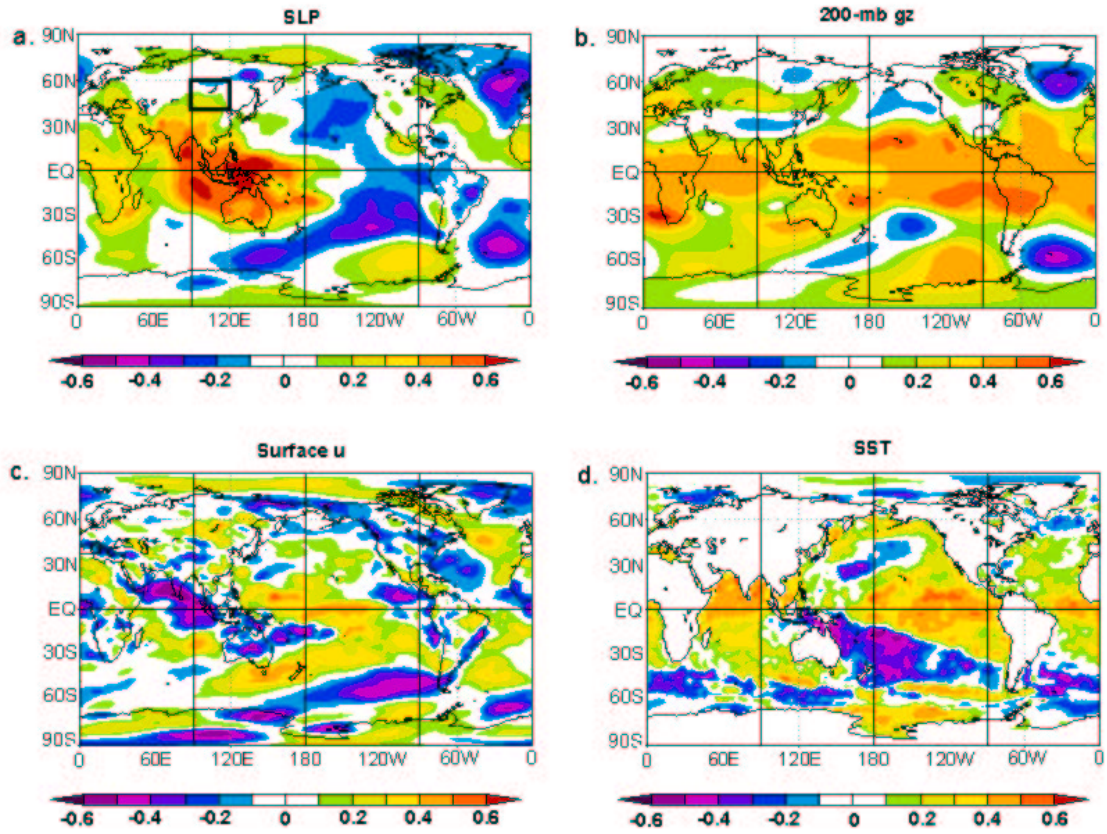

Figure 6.1: Lake Baikal Oct/Nov SLP normalized anomalies in the region 40-60°N, 90-120°E (see black box in diagram a.) correlated with the **following year's SON** global anomaly fields of a.) SLP, b.) 200-mb gZ, c.) surface u, and d.) SST. Correlations based on 1950-1990 data.

The 200-mb geopotential height map shows that the Lake Baikal area SLP is correlated with anomalously high heights throughout the tropics and subtropics. When the SLP in the Lake Baikal region is high, the 200-mb heights in the tropics and subtropics tend to be high. In the tropics, anomalously high heights at the 200-mb pressure level are associated with a warm surface, which occurs during El Niño events. Therefore, using the Oct/Nov Lake Baikal region SLP may be a useful predictor in forecasting the SON Niño 3.4 SSTA.

There is a strong positive correlation between the Oct/Nov Lake Baikal SLP and surface zonal winds in the central and western equatorial Pacific. This means that anomalously high SLP heights in the Lake Baikal region in Oct/Nov are correlated with westerly winds in the aforementioned region of the Pacific. Westerly winds along the equator are associated with El Niño events. Therefore, the Oct/Nov Lake Baikal SLP would appear to be useful in forecasting the SON Niño 3.4 SSTA, which is heavily influenced by equatorial surface winds.

The correlation between the Oct/Nov Lake Baikal region SLP and the following SON SSTA shows a strong positive correlation throughout not only the equatorial Pacific, but also the Indian and Atlantic Oceans. As was suspected from studying the previous fields, the predictor is correlated with an El Niño pattern warming in the Pacific. This suggests that the Oct/Nov Lake Baikal SLP values would be useful in forecasting the SON Niño 3.4 SSTA.

2. **South Atlantic 200-mb Geopotential Height (10-20°S, 15-40°W)**. Figure 6.2 shows the October-November South Atlantic 200-mb geopotential height (see the black box in diagram a.) correlated with the following year's SON global anomaly fields of: a.) 200-mb gZ, b.) surface u, c.) SLP, and d.) SST. Anomalously high 200-mb heights in Oct/Nov in the region of the South Atlantic predictor correlated well with high heights in the midlatitudes. In the tropics, however, the correlation is not as strong. From the Oct/Nov South Atlantic 200-mb gZ predictor alone, it is

difficult to determine whether it is correlated with a warm or cool ENSO event in the following SON.

There is a strong negative correlation between the Oct/Nov South Atlantic 200-mb predictor and the SON surface zonal wind in the equatorial west Pacific. The negative correlation implies that when there are high heights in Oct/Nov in the region of the predictor, there are easterly winds along the equator in the west Pacific. The surface winds in this region are critical in predicting ENSO events, as they influence the flow at the surface of the ocean. The anomalous easterly winds in this region are associated with La Niña events. Therefore, it would be expected that this Oct/Nov predictor is useful in determining the phase of an ENSO event.

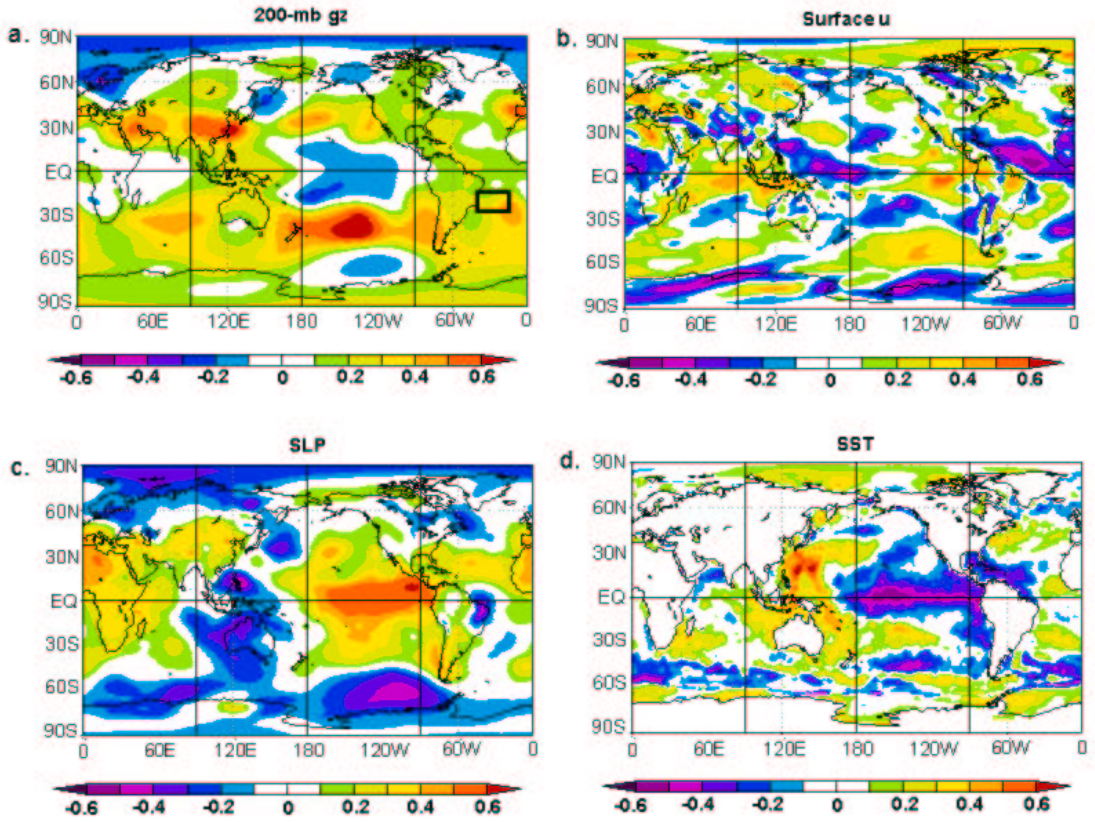

Figure 6.2: South Atlantic Oct/Nov 200-mb gZ normalized anomalies in the region 10-20°S, 15-40°W (see black box in diagram a.) correlated with the **following year's SON** global anomaly fields of a.) 200-mb gZ, b.) surface u, c.) SLP, and d.) SST. Correlations based on 1950-1990 data.

It is clear from the SLP map that there is a strong correlation between the Oct/Nov South Atlantic 200-mb gZ predictor and the positive phase of the Southern Oscillation. The Oct/Nov predictor value is correlated with high SLP in the east Pacific and low SLP in the west Pacific in the SON time period. As previously shown in a schematic figure, high SLP occurs over regions where cool surface waters reside. The positive phase of the SO is hence associated with La Niña conditions. Therefore, the Oct/Nov 200-mb heights in the South Atlantic may be useful in predicting the SON Niño 3.4 SSTA.

As expected from the previous correlation maps, the 200-mb gZ South Atlantic is correlated with cool conditions in the eastern and central Pacific Ocean. Also note that the predictor is positively correlated with SON SSTs in the west Pacific, which means there are anomalously warm temperatures there. This SST pattern is indicative of La Niña conditions, suggesting that the Oct/Nov South Atlantic 200-mb gZ predictor would be useful in forecasting the Niño 3.4 SSTA in the following SON.

3. **North Pacific SST Predictor (35-45°N, 150-170°W)**. Figure 6.3 shows that the Oct/Nov SST values in the North Pacific (35-45°N, 150-170°W) correlate positively with SSTs in the east Pacific (warm conditions) and correlate negatively with SSTs in the west Pacific (cool conditions). This SST pattern is indicative of a positive ENSO phase. Hence, the Oct/Nov predictor value may be useful in predicting the Niño 3.4 SSTA the following SON.

   The correlation between the North Pacific SST predictor and the surface zonal wind shows that the Oct/Nov predictor is correlated positively with the zonal winds in the west Pacific (westerly winds) and negatively in the east Pacific (easterly winds) in SON. This pattern of surface zonal wind suggests El Niño conditions in the Pacific, as the SST correlation map also shows.

   The SLP correlation map shows that the Oct/Nov predictor is negatively correlated with the SON SLP throughout the east and central Pacific. This means that warm

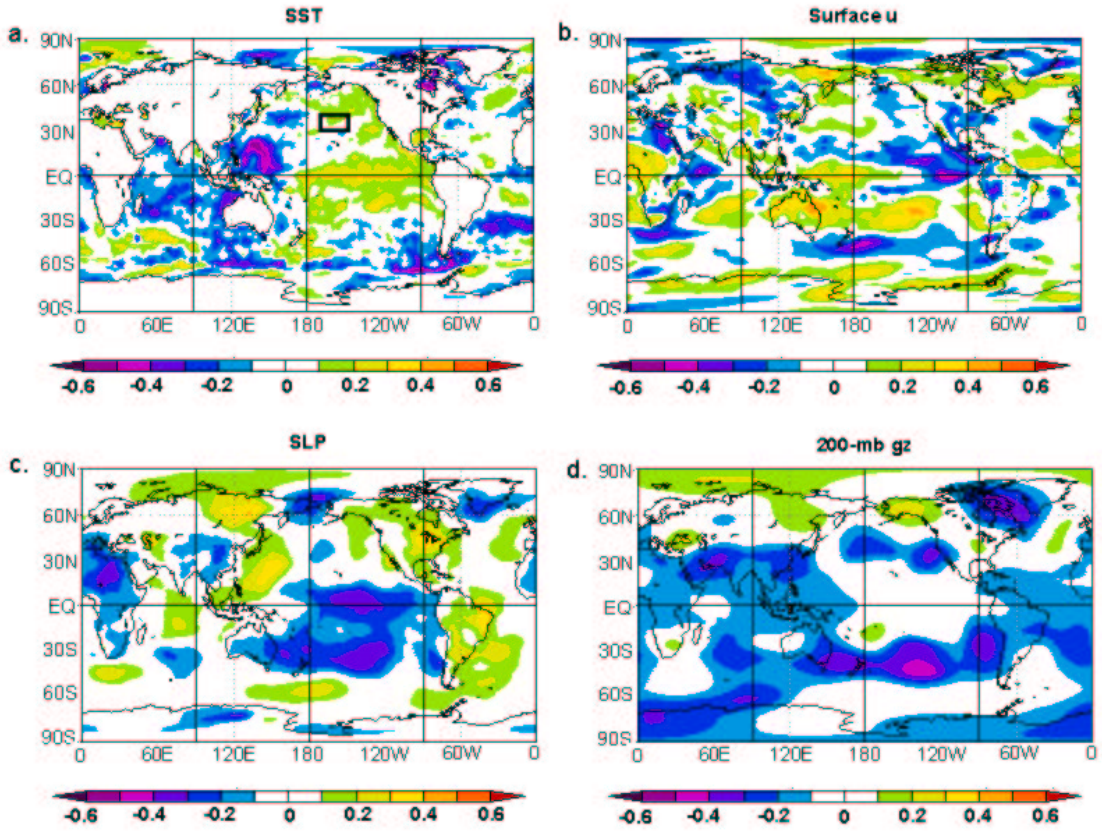

Figure 6.3: North Pacific Oct/Nov SST normalized anomalies in the region 35-45°N, 150-170°W (see black box in diagram a.) correlated with the **following year's SON** global anomaly fields of a.) SST, b.) surface u, c.) SLP, and d.) 200 mb gZ. Correlations based on 1950-1990 data.

conditions in the region of the predictor in Oct/Nov would suggest low SLP heights in the central and east Pacific during the following SON. Low SLP is an indicator of warm SSTs, so this predictor can give insight to what the Niño 3.4 SSTA will be the following year.

When correlated with the Oct/Nov SST predictor, the 200-mb gZ field shows generally low heights throughout much of the tropics and subtropics, but there is also a large region in the central and east Pacific where the heights are neutral or slightly positive. Low upper-level heights generally indicate cool SSTs in the east Pacific. However, these heights seem to be in transition to a higher state, based on what the other fields show. The 200-mb height field often shows a slight lag behind the surface fields, so it is sometimes difficult to interpret conditions with only a snapshot view of this predictor alone.

4. **South Pacific SLP Predictor (25-45°S, 160°E-160°W)**. Figure 6.4 shows the correlation between the October-November South Pacific region (see the black box in diagram a.) SLP correlated with the following year's SON global anomaly fields of: a.) SLP, b.) surface u, c.) 200-mb gZ, and d.) SST. The SLP map shows that the predictor is correlated with the positive phase of the Southern Oscillation, which is shown by the positive correlations in the east Pacific and the negative correlations over the west Pacific. The positive phase of the SO is linked with La Niña conditions in the Pacific, so this predictor may be useful, as it is correlated strongly with the SO.

   The correlation map between the Oct/Nov South Pacific SLP Predictor and surface u shows a region of negative correlation in the central and west Pacific, as well as a small region of positive correlation in the east Pacific. As previously discussed, easterly winds (indicated by negative correlation areas) are indicative of La Niña conditions. This predictor would likely be of use in determining wind direction along the equatorial Pacific, and hence give insight to ENSO conditions.

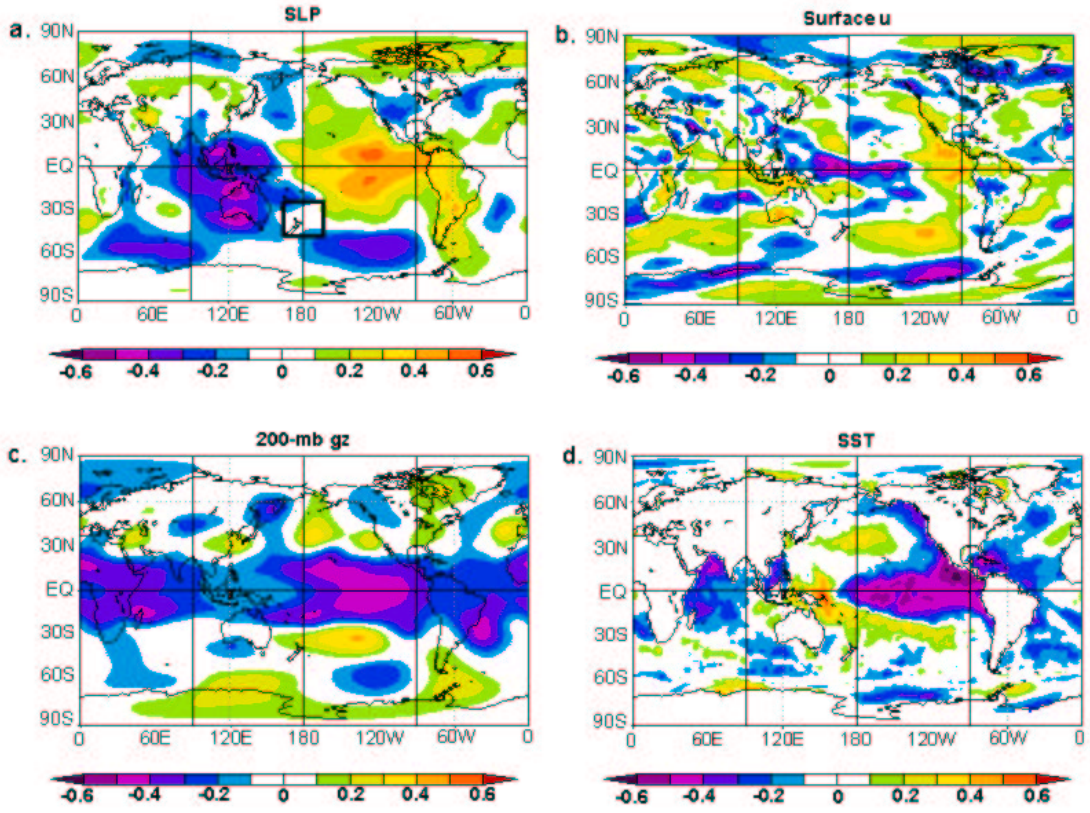

Figure 6.4: South Pacific Oct/Nov SLP normalized anomalies in the region 25-45°S, 160°E-160°W (see black box in diagram a.) correlated with the **following year's SON** global anomaly fields of a.) SLP, b.) surface u, c.) 200-mb gZ, and d.) SST. Correlations based on 1950-1990 data.

The 200-mb gZ is negatively correlated with the South Pacific SLP predictor throughout the entire tropics and subtropics. This means that when the predictor value is anomalously high, the heights in the tropics and subtropics will be low. As discussed previously, low heights throughout the tropics can indicate cool conditions at the surface. In this case, the Pacific is very cool, as reflected by the 200-mb gZ.

The Oct/Nov South Pacific SLP predictor is correlated with cool conditions in the central and eastern Pacific Ocean. Also note that the predictor is positively correlated with SON SSTs in the west Pacific, which means there are anomalously warm temperatures there. This SST pattern is indicative of La Niña conditions, suggesting that the Oct/Nov South Pacific SLP predictor would be useful in forecasting the Niño 3.4 SSTA in the following SON.

5. **PDO Index (SSTA in Pacific basin, poleward of 20°N)**. The PDO Index is composed of the values of the SSTA in the Pacific basin, poleward of 20°N. When the Oct/Nov value of this index is correlated with SSTA (Fig. 6.5), there is a strong positive correlation throughout the west Pacific and Indian Oceans, which means that a positive PDO value coincides with warm conditions there. There is a slight region of cool SSTs (negative correlation) along the central and eastern equatorial Pacific. These SST patterns are indicative of weak La Niña conditions.

   The correlation map of surface zonal wind shows that the Oct/Nov PDO predictor value is positively correlated with westerly winds in the east Pacific. These conditions typically are associated with El Niño conditions. This map is incongruent with the SST correlation map, which may suggest that ENSO is in transition, with westerly winds just beginning to change the conditions in the Pacific.

   Throughout much of the tropics, there is a positive correlation between the Oct/Nov PDO predictor and the following SON SLP. Because there is little difference between the SLP anomalies in the east and west Pacific, this predictor is not correlated with either phase of the SO and therefore, cannot be linked directly with either phase of ENSO.

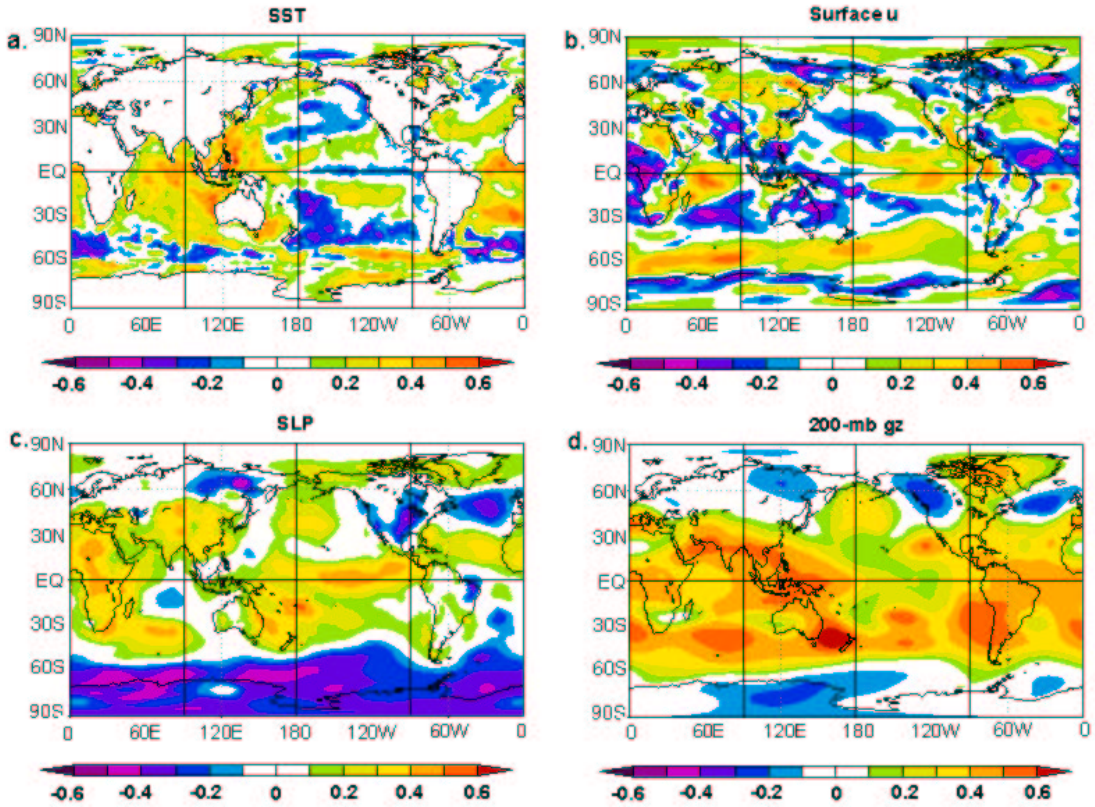

Figure 6.5: Oct/Nov Pacific Decadal Oscillation (PDO) Index correlated with the **following year's SON** global anomaly fields of a.) SST, b.) surface u, c.) SLP, and d.) 200-mb gZ. Correlations based on 1950-1990 data.

The correlation between the Oct/Nov PDO predictor and the following SON 200-mb gZ global field shows very strong positive correlations (high heights) extending from the tropics to mid-latitudes. These high heights are associated with warm surface conditions, which are not reflected in the SST correlation map. It is difficult with the PDO predictor alone to forecast the Niño 3.4 the following year, as the correlations between the predictor and the global fields the following SON are somewhat ambiguous.

Chapter 7

SKILL OF THE 1 DECEMBER NIÑO 3.4 SON FORECAST

The SON forecast scheme presented in this paper was compared with ENSO-CLIPER to establish skill. The variance explained and standard error of each scheme were evaluated to show forecast ability.

7.1 Variance explained (r^2) by the SON Forecast

The 1 December forecast for the SON Niño 3.4 SSTA showed reasonable improvement over ENSO-CLIPER for the forecast period. For all years (1952-2002), the SON forecast scheme explained 36 percent of the variance, while ENSO-CLIPER explained 25 percent of the variance. However, the combination of both schemes showed vast improvement over each scheme independently, explaining over 50 percent of the variance for this 9-11 month forecast. Therefore, the use of this SON forecast scheme and ENSO-CLIPER forecast together has the ability to produce a much better forecast for the Niño 3.4 region.

For the independent forecast years of 1992-2002, the forecast skill is reduced for this scheme as well as for the ENSO-CLIPER forecast. This scheme explains 23 percent of the variance, while ENSO-CLIPER explains only 15 percent. Again, the combination of the two schemes results in a much higher percentage of variance explained: 51 percent. This result is encouraging, as forecasting with independent data tends to yield slightly less skillful results then when hindcasting.

It is clear from the analysis of results that the combination of SG and ENSO-CLIPER provides a much more skillful forecast than either of the forecasts on their own. Each model appears to explain different portions of the variance, since the combination of variance explained is nearly equal to the sum of the variances from each model. ENSO-CLIPER

may add useful information from the Pacific basin that SG did not account for. For the 1 December forecast, ENSO-CLIPER uses three predictors: 1.) three month trend in Niño 4 SSTA (i.e., SON-JJA values), 2.) SON value of the SOI, and 3.) three month trend in SOI. These predictors clearly add some information that is useful and unique from the five SON predictors used by SG. While the combination of the two schemes did not improve skill for the JJA forecast, it is beneficial for the 1 December forecast for SON SSTA in Niño 3.4.

Table 7.1: This table gives the percent variance (r^2) explained for the three 1 December SON Niño 3.4 forecast schemes being evaluated.

Forecast Scheme	All Yrs. 1952-2002	Independent Yrs. 1992-2002	Dependent Yrs. 1950-1990
SG	36	23	73
ENSO-CLIPER	25	15	n/a
Combination	50	51	n/a

7.2 Examination of Error by Individual Years

Individual years were also examined to give insight into any large errors made by the forecast scheme. The standard error (observation - prediction) for each year can be found in Appendix A.2. The ten worst years in terms of standard error for the SG forecast for SON are listed in Table 7.2.

The extremely warm ENSO events of 1997 (the largest El Niño event ever recorded) and 1982 are two of the largest errors made by the SG forecast. Largest errors tended to be made in years that had anomalously strong ENSO events, with the exception of 1993. The unusual extended El Niño conditions that persisted throughout the early 1990s caused forecasting errors for most ENSO models.

The average standard error of the ten worst years of SG is 1.38°C. Comparatively, this is 13 percent lower than the average standard error of ENSO-CLIPER (1.53°C). The Combination forecast shows the lowest average of the ten largest errors, with a value that is 19 percent lower that that of ENSO-CLIPER (1.23°C). The combination of SG and ENSO-CLIPER shows a substantial reduction in the largest errors.

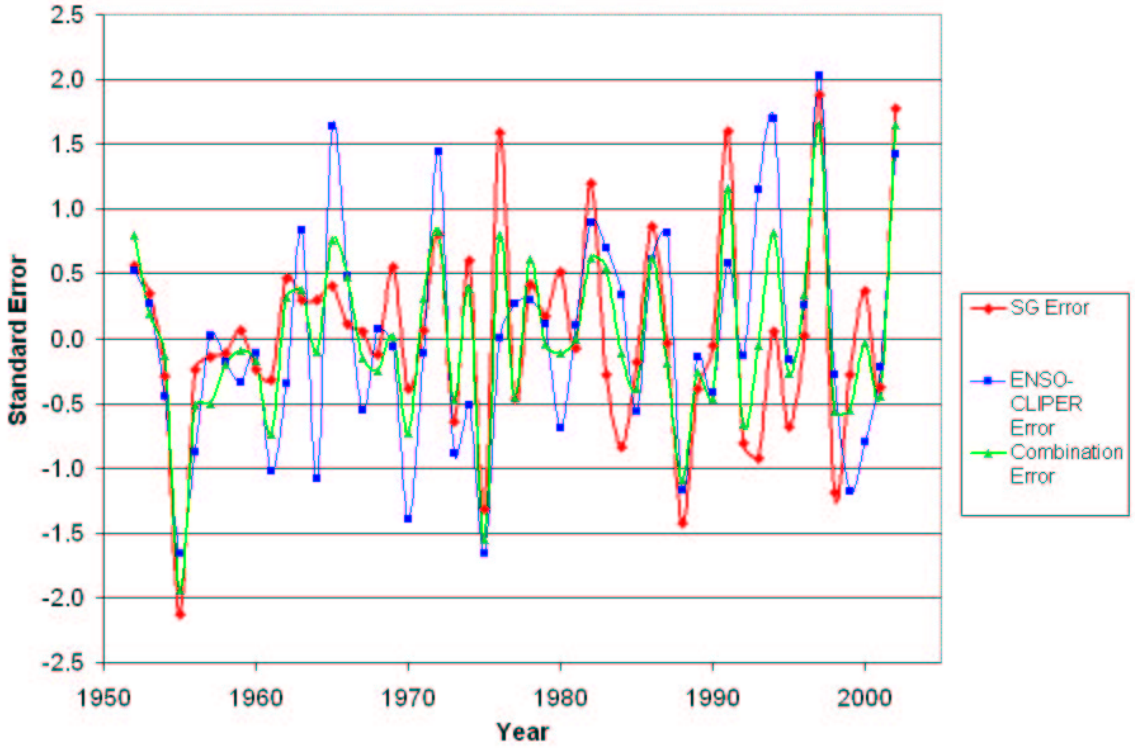

Figure 7.1: Shows the standard error (observation - prediction) by year for the three SON forecasts being evaluated (SG, ENSO-CLIPER, Combination).

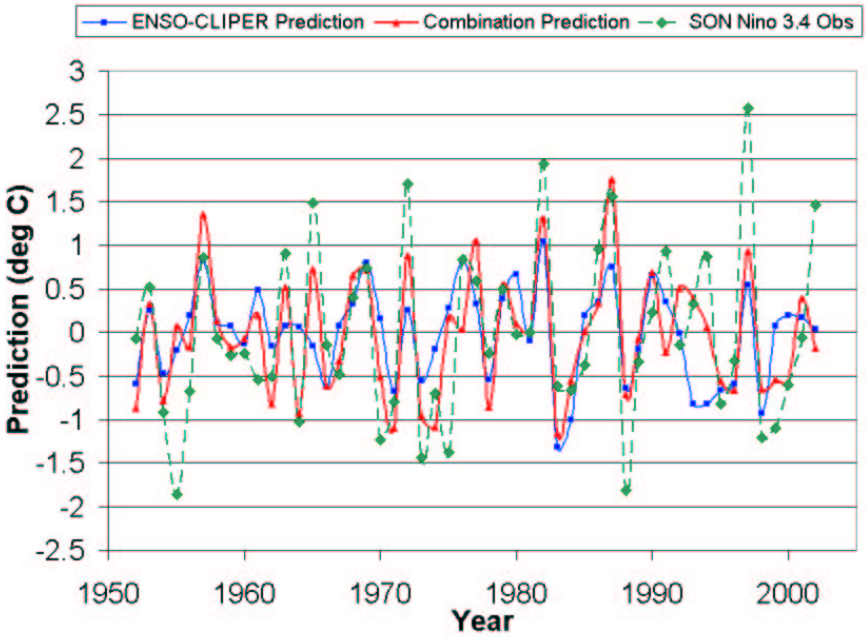

Figure 7.2: Shows the SON Niño 3.4 SSTA observations and predictions by the SON Combination and ENSO-CLIPER schemes.

The ten years with the worst standard errors for the ENSO-CLIPER SON forecast are listed in Table 7.3. The worst errors occur mainly in years with largest SST anomalies in the Niño 3.4 region.

The ten years with the worst standard errors for the Combination forecast (SG + ENSO-CLIPER) SON forecast are listed in Table 7.4. Years with large anomalies in the Niño 3.4 SST seem to be the years that the Combination forecast performs the poorest.

For comparison, the ten best years (lowest standard errors) are listed for each of the forecasts (SG Table 7.5, ENSO-CLIPER Table 7.6, Combination Table 7.7). The averages of the best ten years for each of the forecasts are all similarly close to zero.

7.3 Analysis of Largest Errors made by the 1 December SG Forecast for SON Niño 3.4 SSTA

In an attempt to understand any physical explanations for why the SG forecast performs poorly for certain years, composites of various global fields were created for the SON of the ten years with the largest errors. The SON composites show the global conditions that the SG model had difficulty forecasting.

Table 7.2: This table shows the ten **worst** years (largest errors) for the 1 Dec **SG** Forecast for SON Niño 3.4 SSTA.

Year	SON Niño 3.4 Obs	SG Prediction	SG Error (Observed)-(Predicted)
1997	2.58	0.69	1.88
2002	1.47	-0.31	1.77
1991	0.93	-0.66	1.60
1976	0.83	-0.76	1.59
1988	-1.81	-0.38	-1.43
1975	-1.38	-0.06	-1.32
1998	-1.21	-0.02	-1.19
1982	1.94	0.74	1.19
1993	0.33	1.26	-0.92
1986	0.96	0.09	0.87
Average with respect to sign	0.46	0.06	0.40
Average without respect to sign	1.34	0.50	1.38

Table 7.3: This table shows the ten **worst** years (largest errors) for the 1 Dec **ENSO-CLIPER** Forecast for SON Niño 3.4 SSTA.

Year	SON Niño 3.4 Obs	ENSO-CLIPER Prediction	ENSO-CLIPER Error (Observed)-(Predicted)
1997	2.58	0.55	2.03
1994	0.87	-0.82	1.69
1955	-1.86	-0.20	-1.66
1975	-1.38	0.28	-1.66
1965	1.49	-0.15	1.64
1972	1.70	0.26	1.44
2002	1.47	0.04	1.43
1970	-1.23	0.16	-1.39
1999	-1.10	0.08	-1.18
1988	-1.81	-0.64	-1.17
Average with respect to sign	0.07	-0.04	0.12
Average without respect to sign	1.55	0.32	1.53

Table 7.4: This table shows the ten **worst** years (largest errors) for the 1 Dec **Combination (SG + ENSO-CLIPER)** Forecast for SON Niño 3.4 SSTA.

Year	SON Niño 3.4 Obs	Combination Prediction	Combination Error (Observed)-(Predicted)
1955	-1.86	0.08	-1.94
1997	2.58	0.93	1.65
2002	1.47	-0.18	1.65
1975	-1.38	0.17	-1.55
1991	0.93	-0.23	1.16
1988	-1.81	-0.71	-1.10
1994	0.87	0.06	0.82
1972	1.70	0.88	0.82
1976	0.83	0.04	0.80
1952	-0.07	-0.87	0.80
Average with respect to sign	0.33	0.02	0.31
Average without respect to sign	1.35	0.42	1.23

Table 7.5: This table shows the ten **best** years (smallest errors) for the 1 Dec **SG** Forecast for SON Niño 3.4 SSTA.

Year	SON Niño 3.4 Obs	SG Prediction	SG Error (Observed)-(Predicted)
1987	1.57	1.60	-0.03
1996	-0.33	-0.36	0.03
1990	0.23	0.29	-0.05
1967	-0.48	-0.53	0.05
1994	0.87	0.82	0.06
1971	-0.79	-0.85	0.06
1959	-0.26	-0.33	0.07
1981	0.01	0.08	-0.07
1966	-0.15	-0.26	0.12
1958	-0.07	0.05	-0.12
Average with respect to sign	0.06	0.05	0.12
Average without respect to sign	0.48	0.52	0.07

Table 7.6: This table shows the ten **best** years (smallest errors) for the 1 Dec **ENSO-CLIPER** Forecast for SON Niño 3.4 SSTA.

Year	SON Niño 3.4 Obs	ENSO-CLIPER Prediction	ENSO-CLIPER Error (Observed)-(Predicted)
1976	0.83	0.83	0.00
1957	0.86	0.83	0.03
1969	0.74	0.80	-0.06
1968	0.41	0.33	0.08
1981	0.01	-0.10	0.11
1979	0.50	0.39	0.11
1971	-0.79	-0.68	-0.11
1960	-0.24	-0.13	-0.11
1992	-0.14	-0.01	-0.13
1989	-0.34	-0.19	-0.15
Average with respect to sign	0.18	0.21	-0.23
Average without respect to sign	0.49	0.43	0.09

Table 7.7: This table shows the ten **best** years (smallest errors) for the 1 Dec **Combination (SG + ENSO-CLIPER)** Forecast for SON Niño 3.4 SSTA.

Year	SON Niño 3.4 Obs	Combination Prediction	Combination Error (Observed)-(Predicted)
1981	0.01	0.01	0.00
1969	0.74	-0.50	0.02
2000	-0.60	-0.57	-0.03
1979	0.50	0.54	-0.04
1993	0.33	0.39	-0.06
1959	-0.26	-0.17	-0.09
1964	-1.02	-0.92	-0.10
1980	-0.02	0.10	-0.11
1984	-0.66	-0.55	-0.11
1954	-0.92	-0.78	-0.14
Average with respect to sign	-0.20	-0.25	0.07
Average without respect to sign	0.51	0.45	0.07

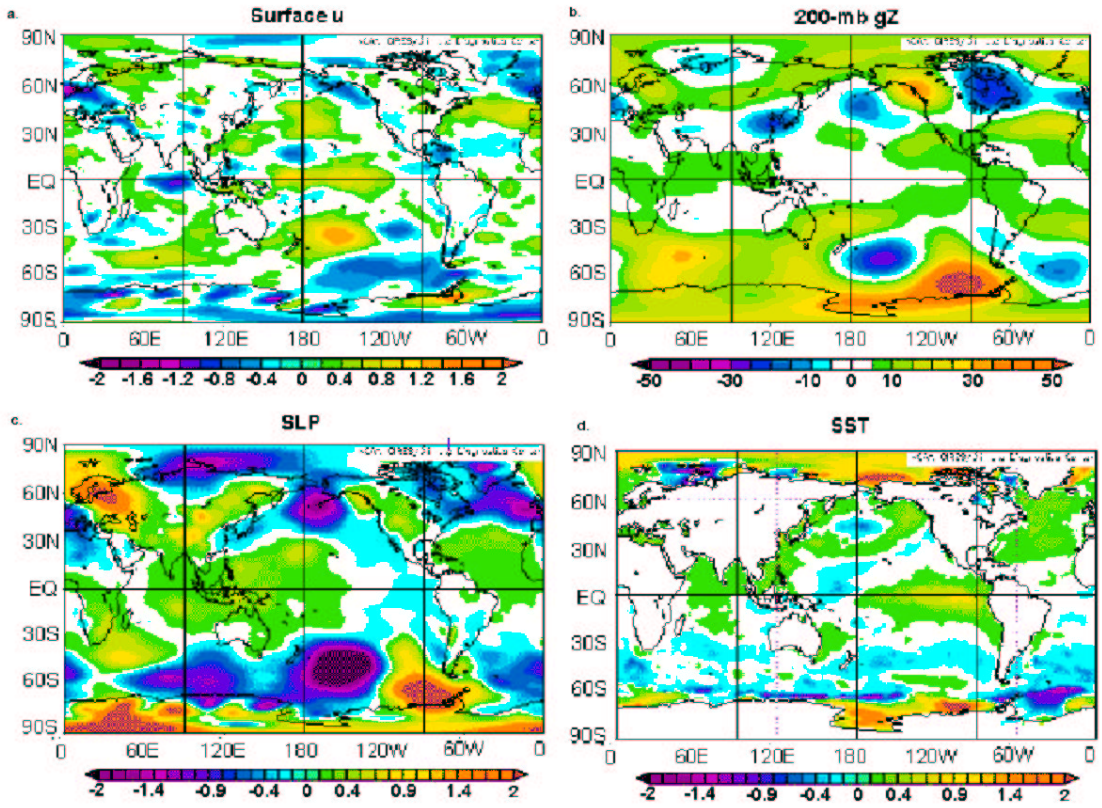

Figure 7.3: Composites of SON global fields for the **worst** years for the 1 December **SG** Forecast. Worst years (listed in Table 7.3) are 1997, 2002, 1991, 1976, 1988, 1975, 1998, 1982, 1993, and 1986.

The composites of the global fields for the SG forecast years with largest errors all show El Niño conditions in the Pacific basin (Figure 7.3). The surface wind field shows anomalous westerly winds along much of the equator, as well as a large region of strong westerlies in the South Pacific. These conditions are commonly associated with El Niño events. The composite of the 200-mb gZ of the worst forecast years shows a mix of neutral and high heights throughout the tropics. High upper-level heights are often found over warm conditions at the surface. The SLP composite shows that the Southern Oscillation is in its negative phase, which is associated with El Niño conditions. The SST composite shows warm waters in the east and central Pacific, which is indicative of El Niño conditions. The composite maps indicate that the SG forecast for SON Niño 3.4 has some difficulties in forecasting warm ENSO conditions in the Pacific.

Figure 7.4 displays composites for the ten years that the Combination forecast performed the worst. The surface zonal wind composite shows westerly winds in the equatorial west Pacific which implies El Niño conditions. The 200-mb gZ composite does not show any large anomalies in the tropics. A weak negative Southern Oscillation pattern in the SLP composite is related to El Niño conditions in the Pacific. The SST composites shows that the worst years, on average, were years that the Pacific was warm (El Niño years). On average, both the SG and the Combination forecasts seem to have difficulty with El Niño events.

7.4 Examination of Forecast Error in Terms of Too Warm/Cold

To gain insight as to why this model performs poorly in some years and well in others, the global conditions for the years in which the model performs well and poorly are separately examined for possible answers. Years in which the standard error (observation-prediction) is negative signifies a prediction that is too warm (over-prediction) compared to the Niño 3.4 SSTA for that year. Conversely, a prediction that is too cold occurs when the standard error is positive (under-prediction). Examining the cases that are too warm separately from the cases that are too cold may reveal some insight into the causes error for this scheme.

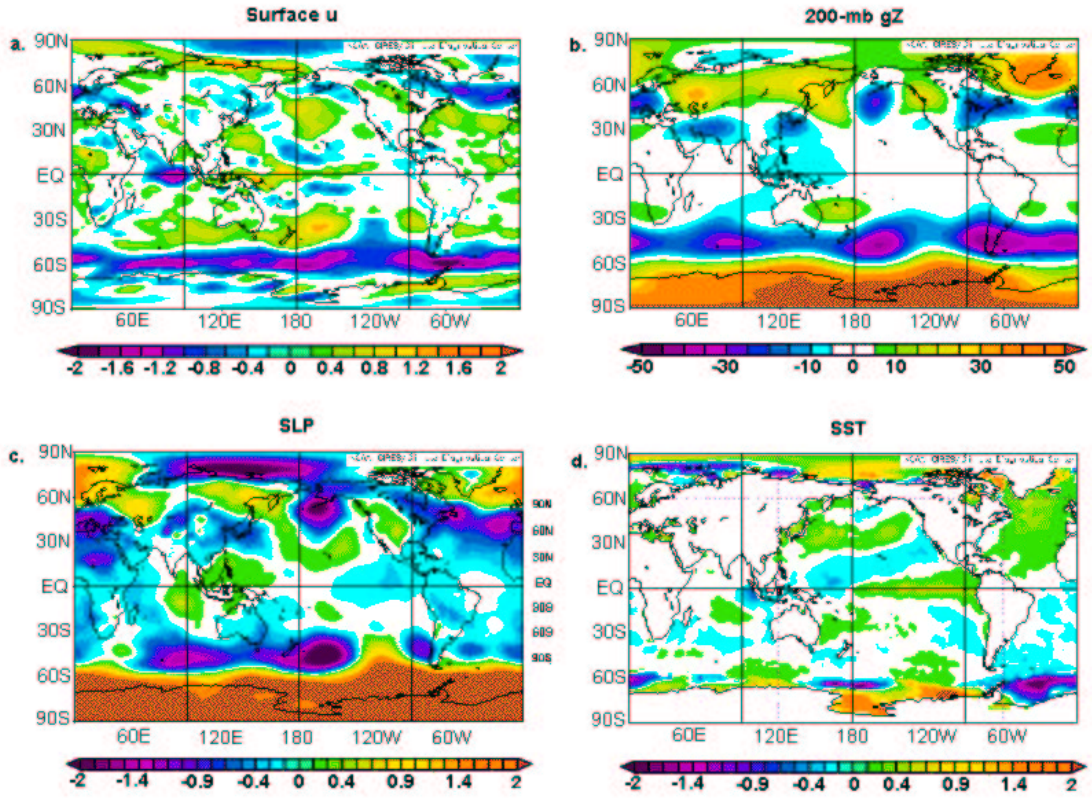

Figure 7.4: Composites of SON global fields for the **worst** years for the 1 December **Combination (SG + ENSO-CLIPER)** Forecast. Worst years (listed in Table 7.5) are 1955, 1997, 2002, 1975, 1991, 1988, 1994, 1972, 1976, and 1952.

The years in which the SG and Combination forecasts over- and under-predict are listed in Table 7.8 and Table 7.9, respectively. Composites for the years in which both models over-predicted are characterized by La Niña, such as cool SSTs in the east and central Pacific, easterly equatorial winds along the Pacific, and a positive SO pattern. The SST composites for the over-prediction years are shown in Figures 7.5 and 7.7 and the under-prediction years are shown in Figures 7.6 and 7.8. Conversely, the composite of the SON global conditions for the years which err on the cold side show El Niño conditions (Fig. 7.5). These results are logical, as a forecast that is too warm

Composite maps of the difference between the "too" warm and "too cold" years are shown in Figure 7.9 ("too warm" - "too cold"). There appear to be large differences in the global fields of 500-mb gZ, SLP, SST, and surface zonal wind. This further shows that the global atmosphere and ocean are affected by the phases of ENSO.

Table 7.8: Years in which SG forecasts too warm/cold for SON Niño 3.4 SSTA and the corresponding standard error (observation - prediction).

Forecast Too Warm (over-predicts)	Standard Error	Forecast Too Cold (under-predicts)	Standard Error
1955	-2.12	1982	1.19
1988	-1.43	1976	1.59
1975	-1.32	1991	1.60
1998	-1.19	2002	1.77
1993	-0.92	1997	1.88

Table 7.9: Years in which the Combination (SG + ENSO-CLIPER) forecast is too warm/cold for SON Niño 3.4 SSTA and the corresponding standard error (observation - prediction).

Forecast Too Warm (over-predicts)	Standard Error	Forecast Too Cold (under-predicts)	Standard Error
1955	-1.88	1997	1.75
1975	-1.50	2002	1.68
1988	-1.09	1991	1.18
1970	-0.73	1972	0.94
1961	-0.69	1994	0.89

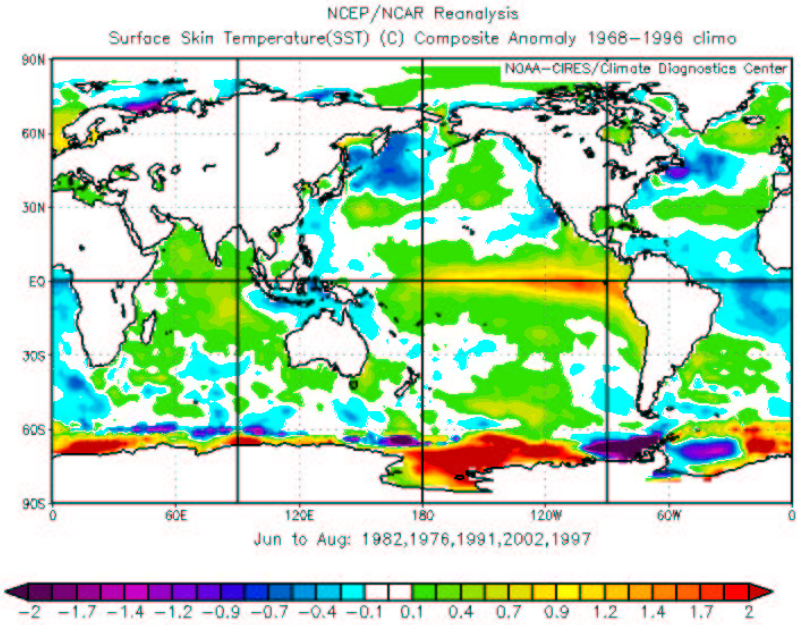

Figure 7.5: Composite of the SON SSTA field for the five years where the 1 Dec. SG forecast was **too cold** (under-predicts) compared to the Niño 3.4 observation. The "too cold" years are 1982, 1976, 1991, 2002, and 1997.

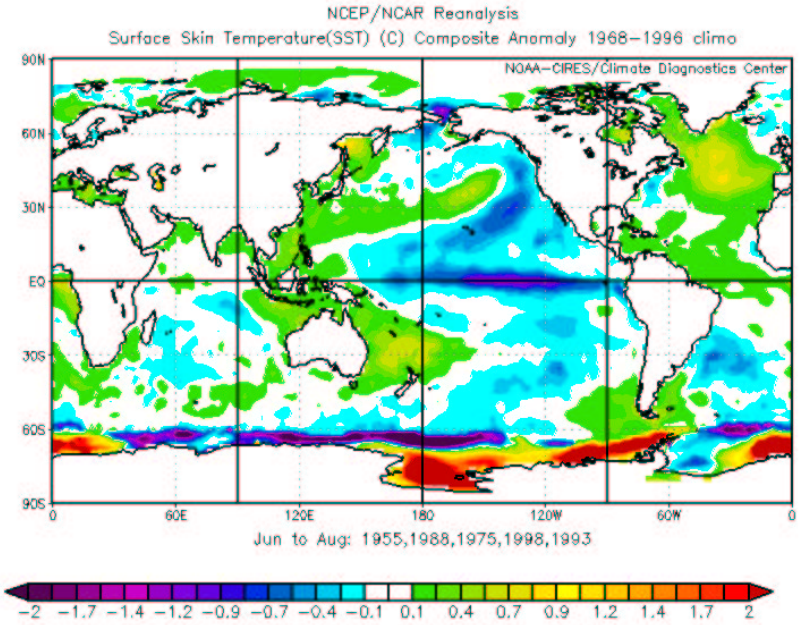

Figure 7.6: Composite of the SON SSTA field for the five years where the 1 Dec. SG forecast was **too warm** (over-predicts) compared to the Niño 3.4 observation. The "too warm" years are 1955, 1988, 1975, 1998, and 1993.

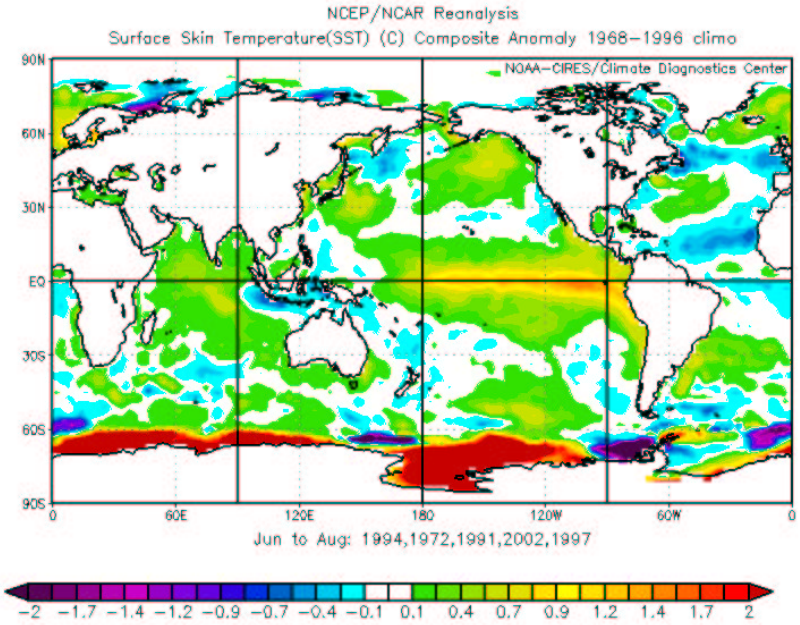

Figure 7.7: Composite of the SON SSTA field for the five years where the 1 Dec. Combination (SG + ENSO-CLIPER) forecast was **too cold** (under-predicts) compared to the Niño 3.4 observation. The "too cold" years are 1994, 1972, 1991, 2002, and 1997.

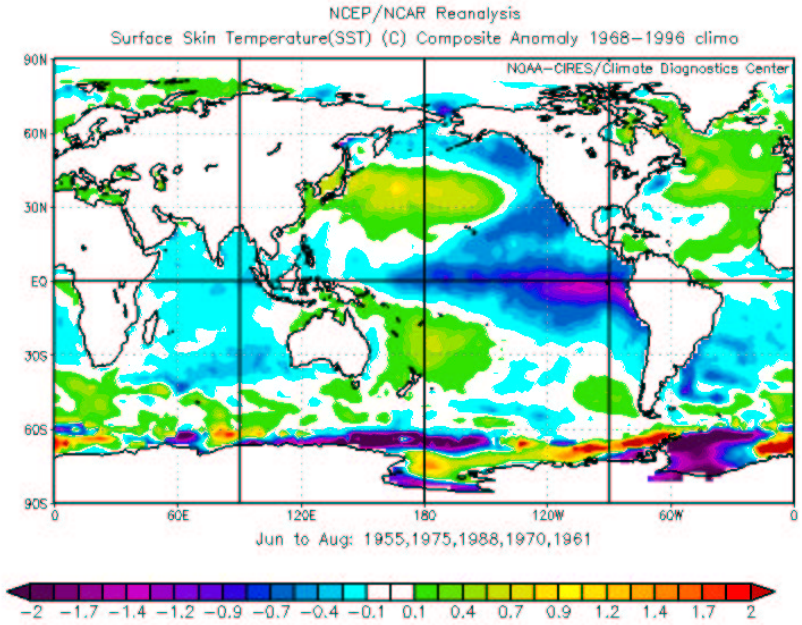

Figure 7.8: Composite of the SON SSTA field for the five years where the 1 Dec. Combination (SG+ENSO-CLIPER) forecast was **too warm** (over-predicts) compared to the Niño 3.4 observation. The "too warm" years are 1955, 1975, 1988, 1970, and 1961.

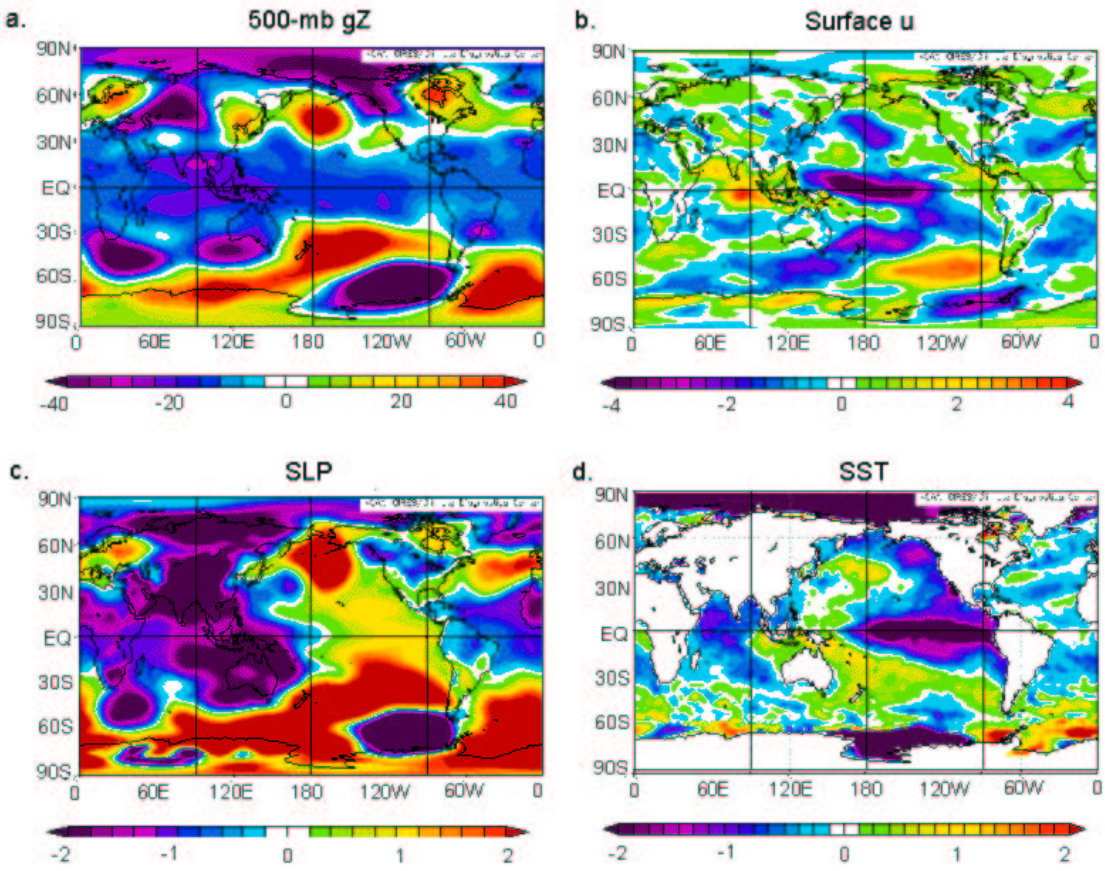

Figure 7.9: Composites of the difference between the years that SG forecast too warm and too cold (listed in Table 7.9) for the SON forecast.

7.5 Degradation of the SON Forecast Based on Removal of Predictors

The amount of variance explained decreases upon removal of a predictor from the group of five best predictors used to make the forecast. By removing each of the best five predictors individually, the importance of the predictors can be inferred by the reduction in variance explained. Table 7.10 lists the removed predictors and the corresponding reduction in variance.

Table 7.10: This table shows which SON predictor was removed, the percent variance explained with the remaining four predictors and the percent variance the forecast was degraded by upon the removal of the predictor. For clarity, the predictors are numbered as follows: 1 = South Atlantic 200-mb gZ, 2 = Lake Baikal SLP, 3 = South Pacific SLP, 4 = North Pacific SST, 5 = PDO Index.

Predictor Removed	Percent Variance Explained	Percent Degraded
0	73	0
1	63	10
2	61	12
3	66	7
4	71	1
5	57	16
AVG	64	9

The forecast for SON was degraded the most by removal of Predictor 5, the PDO Index. By itself, the PDO Index does not explain much variance of the SON Niño 3.4 SSTA. However, in combination with the other predictors, it explains the most variance and is therefore very important to the forecast. Removing Predictor 2 from the forecast reduces the variance explained by 12 percent, making it the second most predictor in the group of best five. These two predictors may be most important to the forecast because they both cover regions in the tropics that are near to the ENSO event. Removal of Predictor 4 (South Atlantic 200-mb gZ) causes the percent variance to degrade the least, implying that this predictor does not contribute as much to the forecast as the others.

7.6 Summary

While the SG forecast scheme explained a slightly larger amount of variance than the ENSO-CLIPER scheme, the combination of the two scheme explains almost twice as much as each scheme individually. Also, the combination showed a reduction in the number of large errors. Therefore, the five best Oct/Nov predictors selected for the 9-11 month SG prediction have indeed produced a skillful ENSO forecast.

Chapter 8

CONCLUSIONS AND FUTURE WORK

This study is based on a climate prediction methodology that makes use of the valuable long-term memory of the atmosphere and ocean. Signals in the climate several seasons in advance can be used for prediction of ENSO events. Accessing this data on a global scale has been difficult until the recent advances in technology. Now, the ease with which this data can be accessed makes it possible to scan the global data for these predictive signals. This forecast methodology assumes that the atmosphere-ocean system will continue to operate as it has in the past. As ENSO events influence the entire global circulation, it is likely that the global circulation also influences them. Studying past global associations allows forecasts to be made even though the full physics of such relations are not fully understood.

Many statistical models, such as ENSO-CLIPER, use only predictors local to the Pacific basin where the ENSO events occur. By only utilizing data from this restricted portion of the globe, these models exclude important global predictive signals in the entire atmosphere and ocean. Likewise, initial value models do not utilize the useful memory of the atmosphere for past parameter associations. Heavily based on equations modeled to simulate real-world physics, initial value numerical models have not shown skill in predicting long-term climate events.

This preliminary study in using global data to forecast ENSO events suggests that it is beneficial to use global data, not just data local to the Pacific, in forecasting these events. Results for the 6-8 month forecast (1 December to the following JJA) show that this forecast scheme explains more variance than that of ENSO-CLIPER over an extended period of time (51 years).

The results for the 9-11 month forecast (1 December to the following SON) show that SG only improves slightly upon ENSO-CLIPER (SG explained 36 percent; ENSO-CLIPER explained 25 percent). However, a combination of the two schemes (SG + ENSO-CLIPER) showed even more skill, explaining over 50 percent of the variance.

This research shows that the forecast presented in this thesis (SG) does indeed surpass the rigorous benchmark test of ENSO-CLIPER by exploiting the predictive signals in the global atmosphere and ocean data. The forecast must also be appreciated for the level of skill it shows at such an extended range (6-11 months) and the fact that it crosses the spring "predictability" barrier (Fig. 1.10).

8.1 Amendments to the Forecast

The SG forecast scheme employs a linear regression model which uses five predictors to make a precise ENSO forecast. Relying on this method does not allow any human interpretation or reasoning behind the forecast. Also, studying the conditions several years before the forecast period may offer additional information for making this forecast and should likely improve the forecast. Studying the progression of conditions in the equatorial Pacific over several years may be helpful in making a better forecast.

8.2 Future Work

Forecasting ENSO with past global atmospheric and oceanic data has been made much more feasible than ever before thanks to the improvement of technology in recent years. While many global predictors were tested for correlation with ENSO events, it is likely that there is a near unlimited number of predictors that might be helpful in predicting various aspects of the climate, such as monthly or seasonal rainfall, temperature, etc. Similar forecasts have also been made for Atlantic basin hurricane activity (Blake and Gray 2004, Gray and Klotzbach 2003, Klotzbach and Gray 2003, 2004).

The forecast schemes presented in this thesis are useful because they offer a skillful prediction for an extended-range. However, adjustments to this forecast might also be

made in early spring when more data is available and there is more insight as to whether conditions in the Pacific will change rapidly or not in the "predictability barrier" period.

ACKNOWLEDGEMENTS

I would like to thank my advisor William Gray for his guidance and support throughout this project. His encouragement and enthusiasm were an essential ingredient to the completion of this project. I would also like to thank Wayne Schubert and Paul Mielke for their input. I also appreciate information on ENSO-CLIPER from John Knaff. Additionally, I would like to thank project member Phil Klotzbach, who offered endless support and friendship during my time at CSU. Phil offered great insight and advice to this project, and I will be forever greatful for the help he gave me. Of course, great thanks goes to my family and friends who supported me during my time at CSU.

REFERENCES

Battisti, David S. and David D. Ovens, 1995: The Dependence of the low-level equatorial easterly jet on Hadley and Walker circulations. *J. of Atmos. Sci.*, 52, 3911-3931.

Barnston, Anthony G., He, Yuxiang, Glantz, Michael H., 1999: Predictive skill of statistical and dynamical climate models in SST forecasts during the 1997-98 El Niño episode and the 1998 La Niña onset. *Bull. Amer. Meteor. Soc.*, 80, 217-244.

Blake, E. and W. M. Gray, 2004: Prediction of August Atlantic basin hurricane activity. Being published in *Wea. and Forecasting*

Chan, Johnny C. L., Xu, Jianjun, 2000: Physical Mechanisms responsible for the transition from a warm to a cold state of the El Niño-Southern Oscillation. *J. Climate*, 13, 2056-2071.

Chen, Dake, Zebiak, Stephen E., and Mark A. Cane, 1997: Initialization and predictability of a coupled ENSO forecast model. *Mon. Wea. Rev.*, 125, 773-788.

Davey, M. K., Anderson, D. L. T., and S. Lawrence, 1996: A simulation of variability of ENSO forecast skill. *J. Climate*, 9, 240-246.

Deque, M. and J. Servain, 1989: Teleconnections between tropical Atlantic sea surface temperatures and midlatitude 50kPa heights during 1964-1986. *J. Climate*, 2, 929-944.

Enfield, David B. and Alberto M. Mestas-Nuñez, 1999: Multiscale variabilities in global sea surface temperatures and their relationships with tropospheric climate patterns. *J. Climate*: 12, 9, 2719-2733.

Gray, W. M., P. W. Mielke Jr., K. J. Berry and J. A. Knaff, 1994: Predicting ENSO 9-14 months in advance. *Conference in Trieste, Italy*, May 9-13

Gray, W. M. and P. J. Klotzbach, 2003: Extended range forecast of Atlantic seasonal hurricane activity and US landfall strike probability for 2004. Dept. of Atmos. Sci. Paper, Colo. State Univ., Ft. Collins, CO, 17 pp.

Hanley, Deborah E., Bourassa, Mark A., O'Brien, James J., Smith, Shawn R. and Elizabeth R. Spade, 2003: A quantitative evaluation of ENSO indices. *J. Climate*, 16, 1249-1258.

Hoerling, Martin P., Kumar, Arun, Zhong, Min. 1997: El Niño, La Niña, and the nonlinearity of their teleconnections. *J. Climate*: 10, 8, 1769-1786.

Horel, John D. and John M. Wallace, 1981: Planetary-scale atmospheric phenomena associated with the southern oscillation. *Mon. Wea. Rev.*, 109, 813-829.

Kalnay, E., Kanamitsu, M., Kistler, R., Collins, W., Deaven, D., Gandin, L., Iredell, M., Saha, S., White, G., Woollen, J., Zhu, Y., Leetmaa, A., Reynolds, B., Chelliah, M., Ebisuzaki, W., Higgins, W., Janowiak, J., Mo, K.C., Ropelewski, C., Wang, J., Jenne, Roy, Joseph, Dennis. 1996: The NCEP/NCAR 40-year reanalysis project. *Bull. Amer. Meteor. Soc.*: 77, 3, 437-472.

Klotzbach, P. J. and W. M. Gray, 2003: Forecasting September Atlantic basin tropical cyclone activity. *Wea. and Forecasting*, 18, 6, 1109-1128.

Knaff, John A. and Christopher W. Landsea, 1997: An El Niño-southern oscillation climatology and persistence (CLIPER) forecasting scheme. *Wea. Forecasting*, 12, 633-652.

Landsea, Christopher W. and John A. Knaff, 2000: How much skill was there in forecasting the very strong 1997-98 El Niño? *Bull. Amer. Meteor. Soc.*, 81, 2107-2119.

Larkin, Narasimhan K., Harrison, D. E., 2002: ENSO warm (El Niño) and cold (La Niña) dvent life cycles: Ocean surface anomaly patterns, their symmetries, asymmetries, and implications. *J. Climate*, 15, 1118-1140.

Larkin, Narasimhan K. and D. E. Harrison, 2001: Tropical Pacific ENSO cold events, 1946-95: SST, SLP, and surface wind composite anomalies. *J. Climate*, 14, 3904-3931.

Madden, Roland A. and Paul R. Julian, 1971: Detection of a 40-50 day oscillation in the zonal wind in the tropical Pacific. *J. Atmos. Sci.*, 28, 55, 702-708.

Mason, Simon J. and Gillian M. Mimmack, 2002: Comparison of some statistical methods of probabilistic forecasting of ENSO. *J. Climate*, 15, 8-29.

Rasmusson, Eugene M. and Thomas H. Carpenter, 1982: Variations in tropical sea surface temperature and surface wind fields associated with the southern oscillation/El Niño. *Mon. Wea. Rev.*, 110, 354-384.

Shapiro, Llyod J. and Stanley B. Goldenberg, 1993: Intraseasonal oscillations over the Atlantic. *J. Climate*, 6, 677-699.

Tomita, Tomohiko and Tetsuzo Yasunari, 1993: On the two types of ENSO. *Met. Soc. Japan*, 71, 273-283.

Trenberth, Kevin E., 1997: The definition of El Niño. *Bull. Amer. Meteor. Soc.*, 78, 2771-2777.

Trenberth, Kevin E., Branstator, Grant W., Karoly, David, Kumar, Arun, Lau, Ngar-Cheung, and Chester Ropelewski, 1998: Progress during TOGA in understanding and modeling global teleconnections associated with tropical sea surface temperatures. *J. Geophys. Res.*, 103, 14, 291-14, 324.

Wallace, John M. and David S. Gutzler, 1981: Teleconnections in the geopotential height field during the northern hemisphere winter. *Mon. Wea. Rev.*, 109, 784-812.

White, Warren B., Pazan, Stephen E., and Masamichi Inoue, 1987: Hindcast/forecast of ENSO events based upon the redistribution of observed and model heat content in the western tropical Pacific, 1964-86. *J. Phys. Oceanography*, 17, 264-280.

Wright, Peter B., Wallace, John M., Mitchell, Todd P., and Clara Deser, 1988: Correlation structure of the El Niño-southern oscillation phenomenon. *J. Climate*, 1, 609-625.

Xu, Jianjun, Chan, Johnny C. L., 2001: The Role of the Asian-Australian monsoon system in the onset time of El Niño events. *J. Climate*, 14, 418-433.

Appendix A

Table A.1: 1 DECEMBER FORECAST FOR JJA NIÑO 3.4 SSTA

Forecast Point	Forecast for:	SG Prediction	CLIPER Prediction	OBS	SG Error	CLIPER Error
Dec. 1, 1948	JJA 1949	1.30	n/a	-0.36	-1.66	n/a
Dec. 1, 1949	JJA 1950	-0.02	n/a	-0.59	-0.57	n/a
Dec. 1, 1950	JJA 1951	0.55	n/a	0.40	-0.15	n/a
Dec. 1, 1951	JJA 1952	-0.27	-0.28	-0.19	0.08	0.09
Dec. 1, 1952	JJA 1953	0.21	0.11	0.36	0.15	0.25
Dec. 1, 1953	JJA 1954	-0.34	-0.13	-0.75	-0.41	-0.62
Dec. 1, 1954	JJA 1955	-0.29	-0.03	-0.75	-0.46	-0.72
Dec. 1, 1955	JJA 1956	-0.16	-0.14	-0.61	-0.45	-0.47
Dec. 1, 1956	JJA 1957	0.99	0.38	0.81	-0.18	0.43
Dec. 1, 1957	JJA 1958	0.25	-0.04	0.46	0.21	0.50
Dec. 1, 1958	JJA 1959	0.06	-0.14	-0.32	-0.38	-0.18
Dec. 1, 1959	JJA 1960	-0.28	0.32	0.02	0.30	-0.30
Dec. 1, 1960	JJA 1961	0.09	0.30	0.04	-0.05	-0.26
Dec. 1, 1961	JJA 1962	-0.53	0.06	-0.01	0.52	-0.07
Dec. 1, 1962	JJA 1963	0.50	0.02	0.65	0.16	0.63
Dec. 1, 1963	JJA 1964	-0.79	0.05	-0.72	0.07	-0.77
Dec. 1, 1964	JJA 1965	0.97	-0.26	1.09	0.12	1.35
Dec. 1, 1965	JJA 1966	-0.22	-0.19	0.33	0.55	0.52
Dec. 1, 1966	JJA 1967	-0.39	-0.01	-0.04	0.34	-0.03
Dec. 1, 1967	JJA 1968	0.14	0.23	0.31	0.17	0.08
Dec. 1, 1968	JJA 1969	-0.04	0.23	0.48	0.51	0.25
Dec. 1, 1969	JJA 1970	-0.50	0.19	-0.71	-0.21	-0.90
Dec. 1, 1970	JJA 1971	-0.58	-0.28	-0.49	0.10	-0.21
Dec. 1, 1971	JJA 1972	1.38	0.13	1.12	-0.26	0.99
Dec. 1, 1972	JJA 1973	-0.75	-0.25	-0.96	-0.21	-0.71
Dec. 1, 1973	JJA 1974	-0.58	-0.21	-0.36	0.22	-0.15
Dec. 1, 1974	JJA 1975	-0.41	0.06	-1.06	-0.65	-1.12
Dec. 1, 1975	JJA 1976	0.26	0.11	0.13	-0.13	0.02
Dec. 1, 1976	JJA 1977	0.34	0.55	0.27	-0.07	-0.28
Dec. 1, 1977	JJA 1978	-0.18	0.21	-0.45	-0.27	-0.66
Dec. 1, 1978	JJA 1979	0.44	0.29	0.00	-0.44	-0.29
Dec. 1, 1979	JJA 1980	-0.32	0.24	0.25	0.58	0.01
Dec. 1, 1980	JJA 1981	0.18	0.00	-0.40	-0.58	-0.40
Dec. 1, 1981	JJA 1982	0.42	0.51	1.17	0.74	0.66
Dec. 1, 1982	JJA 1983	-0.25	-0.54	0.18	0.44	0.72
Dec. 1, 1983	JJA 1984	-0.63	-0.48	-0.44	0.18	0.04
Dec. 1, 1984	JJA 1985	-0.29	0.49	-0.40	-0.11	-0.89
Dec. 1, 1985	JJA 1986	0.46	0.50	0.31	-0.15	-0.19
Dec. 1, 1986	JJA 1987	1.08	0.40	1.71	0.63	1.31
Dec. 1, 1987	JJA 1988	-1.12	-0.20	-1.45	-0.33	-1.25
Dec. 1, 1988	JJA 1989	0.00	-0.05	-0.41	-0.40	-0.36
Dec. 1, 1989	JJA 1990	0.76	0.55	0.21	-0.55	-0.34
Dec. 1, 1990	JJA 1991	0.45	0.21	0.82	0.37	0.61
Dec. 1, 1991	JJA 1992	0.78	-0.03	0.30	-0.48	0.33
Dec. 1, 1992	JJA 1993	0.94	-0.32	0.47	-0.47	0.79
Dec. 1, 1993	JJA 1994	0.01	-0.05	0.47	0.47	0.52
Dec. 1, 1994	JJA 1995	0.48	0.05	-0.12	-0.60	-0.17
Dec. 1, 1995	JJA 1996	0.17	-0.32	-0.10	-0.27	0.22
Dec. 1, 1996	JJA 1997	0.66	0.13	1.81	1.15	1.68
Dec. 1, 1997	JJA 1998	-0.60	-0.65	-1.05	-0.45	-0.40
Dec. 1, 1998	JJA 1999	-0.24	-0.13	-0.92	-0.67	-0.79
Dec. 1, 1999	JJA 2000	-0.83	0.41	-0.36	0.47	-0.77
Dec. 1, 2000	JJA 2001	-0.82	0.41	0.20	1.02	-0.21
Dec. 1, 2001	JJA 2002	0.33	0.28	0.97	0.64	0.69
Dec. 1, 2002	JJA 2003	0.05	-0.14	-0.67	-1.31	-1.36
Dec. 1, 2003	JJA 2004	-0.48	-0.12	-	-	-
AVERAGE with respect to sign	-	0.05	0.05	0.03	-0.02	-0.01
AVERAGE without respect to sign	-	0.47	0.24	0.54	0.40	0.51

Table A.2: 1 DECEMBER FORECAST FOR SON NIÑO 3.4 SSTA

Forecast Point	Forecast for:	SG Forecast	CLIPER Forecast	Combo Forecast	OBS SON Niño 3.4	SG Error	CLIPER Error	Combo Error
Dec. 1, 1951	SON 1952	-0.63	-0.59	-0.87	-0.07	0.57	0.52	0.80
Dec. 1, 1952	SON 1953	0.17	0.25	0.33	0.52	0.35	0.27	0.19
Dec. 1, 1953	SON 1954	-0.63	-0.47	-0.78	-0.92	-0.29	-0.45	-0.14
Dec. 1, 1954	SON 1955	0.26	-0.20	0.08	-1.86	-2.12	-1.66	-1.94
Dec. 1, 1955	SON 1956	-0.44	0.20	-0.16	-0.68	-0.24	-0.88	-0.52
Dec. 1, 1956	SON 1957	1.00	0.83	1.36	0.86	-0.14	0.03	-0.50
Dec. 1, 1957	SON 1958	0.05	0.11	0.14	-0.07	-0.12	-0.18	-0.20
Dec. 1, 1958	SON 1959	-0.33	0.08	-0.17	-0.26	0.07	-0.34	-0.09
Dec. 1, 1959	SON 1960	-0.01	-0.13	-0.07	-0.24	-0.24	-0.11	-0.17
Dec. 1, 1960	SON 1961	-0.22	0.48	0.19	-0.55	-0.32	-1.03	-0.74
Dec. 1, 1961	SON 1962	-0.97	-0.16	-0.82	-0.51	0.47	-0.35	0.31
Dec. 1, 1962	SON 1963	0.61	0.07	0.53	0.90	0.30	0.83	0.38
Dec. 1, 1963	SON 1964	-1.32	0.06	-0.92	-1.02	0.29	-1.08	-0.10
Dec. 1, 1964	SON 1965	1.08	-0.15	0.73	1.49	0.41	1.64	0.76
Dec. 1, 1965	SON 1966	-0.26	-0.63	-0.62	-0.15	0.12	0.48	0.47
Dec. 1, 1966	SON 1967	-0.53	0.07	-0.33	-0.48	0.05	-0.55	-0.15
Dec. 1, 1967	SON 1968	0.53	0.33	0.65	0.41	-0.12	0.08	-0.25
Dec. 1, 1968	SON 1969	0.18	0.80	0.72	0.74	0.56	-0.06	0.02
Dec. 1, 1969	SON 1970	-0.85	0.16	-0.50	-1.23	-0.38	-1.39	-0.73
Dec. 1, 1970	SON 1971	-0.85	-0.68	-1.10	-0.79	0.06	-0.11	0.31
Dec. 1, 1971	SON 1972	0.90	0.26	0.88	1.70	0.81	1.44	0.82
Dec. 1, 1972	SON 1973	-0.79	-0.55	-0.96	-1.43	-0.64	-0.88	-0.48
Dec. 1, 1973	SON 1974	-1.31	-0.19	-1.09	-0.70	0.60	-0.51	0.39
Dec. 1, 1974	SON 1975	-0.06	0.28	0.17	-1.38	-1.32	-1.66	-1.55
Dec. 1, 1975	SON 1976	-0.76	0.83	0.04	0.83	1.59	0.00	0.80
Dec. 1, 1976	SON 1977	1.07	0.33	1.05	0.60	-0.47	0.27	-0.45
Dec. 1, 1977	SON 1978	-0.66	-0.54	-0.85	-0.24	0.41	0.30	0.61
Dec. 1, 1978	SON 1979	0.33	0.39	0.54	0.50	0.17	0.11	-0.04
Dec. 1, 1979	SON 1980	-0.53	0.67	0.10	-0.02	0.51	-0.69	-0.11
Dec. 1, 1980	SON 1981	0.08	-0.10	0.01	0.01	-0.07	0.11	-0.00
Dec. 1, 1981	SON 1982	0.74	1.04	1.31	1.94	1.19	0.90	0.62
Dec. 1, 1982	SON 1983	-0.34	-1.32	-1.16	-0.62	-0.28	0.70	0.54
Dec. 1, 1983	SON 1984	0.17	-1.00	-0.55	-0.66	-0.83	0.34	-0.11
Dec. 1, 1984	SON 1985	-0.19	0.19	0.01	-0.37	-0.18	-0.56	-0.39
Dec. 1, 1985	SON 1986	0.09	0.35	0.34	0.96	0.87	0.61	0.62
Dec. 1, 1986	SON 1987	1.60	0.75	1.75	1.57	-0.03	0.82	-0.19
Dec. 1, 1987	SON 1988	-0.38	-0.64	-0.71	-1.81	-1.43	-1.17	-1.10
Dec. 1, 1988	SON 1989	0.05	-0.19	-0.07	-0.34	-0.39	-0.15	-0.26
Dec. 1, 1989	SON 1990	0.29	0.65	0.69	0.23	-0.05	-0.42	-0.46
Dec. 1, 1990	SON 1991	-0.66	0.35	-0.23	0.93	1.60	0.58	1.16
Dec. 1, 1991	SON 1992	0.66	-0.01	0.51	-0.14	-0.81	-0.13	-0.66
Dec. 1, 1992	SON 1993	1.26	-0.82	0.39	0.33	-0.92	1.15	-0.06
Dec. 1, 1993	SON 1994	0.82	-0.82	0.06	0.87	0.06	1.69	0.82
Dec. 1, 1994	SON 1995	-0.14	-0.66	-0.55	-0.82	-0.68	-0.16	-0.27
Dec. 1, 1995	SON 1996	-0.36	-0.59	-0.66	-0.33	0.03	0.26	0.33
Dec. 1, 1996	SON 1997	0.69	0.55	0.93	2.58	1.88	2.03	1.65
Dec. 1, 1997	SON 1998	-0.02	-0.93	-0.65	-1.21	-1.19	-0.28	-0.56
Dec. 1, 1998	SON 1999	-0.82	0.08	-0.54	-1.10	-0.27	-1.18	-0.56
Dec. 1, 1999	SON 2000	-0.97	0.20	-0.57	-0.60	0.37	-0.80	-0.03
Dec. 1, 2000	SON 2001	0.33	0.17	0.39	-0.05	-0.38	-0.22	-0.44
Dec. 1, 2001	SON 2002	-0.31	0.04	-0.18	1.47	1.77	1.43	1.65
Dec. 1, 2002	SON 2003	0.88	-0.30	0.47	-0.47	-1.35	-0.17	-0.94
Dec. 1, 2004	SON 2004	0.22	-0.36	-0.07	-	-	-	-
Average with respect to sign	-	-0.05	-0.02	-0.02	-0.01	0.02	-0.01	0.00
Average without respect to sign	-	0.55	0.43	0.57	0.79	0.57	0.66	0.52

Table A.3: JJA POOL OF PREDICTORS

Predictor	Month	Latitude, Longitude	Correlation w/ JJA Niño 3.4 SSTA 1952-2002
500-mb u	Oct/Nov	25-35°S, 150°E-175°W	0.44
500-mb u	Oct/Nov	5°N-5°S, 95-120°W	0.38
500-mb u	Oct/Nov	15-25°N, 80-120°E	-0.29
500-mb u	Oct/Nov	45-55°N, 90-125°E	-0.34
500-mb u	Oct/Nov	25-40°N, 5-30°W	-0.37
Surface u	Oct/Nov	15-35°S, 160-180°E	0.41
Surface u	Oct/Nov	15-35°S, 125-150°E	0.35
Surface u	Oct/Nov	15-35°S, 160°E-125°W	0.43
Surface u	Oct/Nov	5-15°S, 5-30°E	-0.50
Surface u	Oct/Nov	45-55°S, 175°E-160°W	-0.42
SLP	Oct/Nov	35-55°N, 125-155°W	0.36
SLP	Oct/Nov	38-48°N, 130-145°W	0.38
SLP	Oct/Nov	40-55°N, 120-145°W	0.40
SLP	Oct/Nov	45-60°N, 100-120°E	0.43
SLP	Oct/Nov	45-60°N, 100-125°E	0.41
SLP	Oct/Nov	5-20°N, 160°E-160°W	-0.49
SLP	Nov	20-40°S, 120-160°W	-0.42
200-mb gZ	Oct/Nov	10-25°S, 10-40°W	-0.46
200-mb gZ	Nov	10-25°S, 20-50°W	-0.38
200-mb gZ	Nov	10-20°S, 20-45°W	-0.50
200-mb gZ	Oct/Nov	15°N-30°S, 60°E-100°W	-0.31
200-mb gZ	Oct/Nov	0-30°S, 60°E-120°W	-0.30
200-mb gZ	Oct/Nov	0-30°S, 0°E-80°W	-0.30
500-mb gZ	Oct/Nov	35-50°N, 10-30°W	0.28
700-mb gZ	Oct/Nov	25-45°S, 160°E-175°W	-0.48
700-mb gZ	Oct/Nov	30-45°S, 160-180°E	-0.48
PDO Index	Oct/Nov	Pac. basin poleward of 20°N	-0.05
SOI	Oct/Nov	-	0.04
SOI	May/June	-	0.40
Niño 3.4 SSTA	Oct/Nov	5°N-5°S, 120-170°W	-0.04
Niño 3.4 SSTA	JJA	5°N-5°S, 120-170°W	-0.14
SST	Oct/Nov	1°N-35°S, 0-35°W	-0.40
SST	Oct/Nov	5°N-5°S, 169°E-120°W	-0.01
SST	Oct/Nov	10.5°N-10.5°S, 85-120 °W	-0.23

Table A.4: SON POOL OF PREDICTORS

Predictor	Month	Latitude, Longitude	Correlation w/ SON Niño 3.4 SSTA 1952-2002
500-mb u	Oct/Nov	5°N-10°S, 100-160°W	0.39
500-mb u	Oct/Nov	5°N-5°S, 100-140 °W	0.44
500-mb u	Oct/Nov	45-55°N, 90-125 °E	-0.36
500-mb u	Oct/Nov	25-35°S, 110-180 °E	0.38
Surface u	Oct/Nov	15-30°S, 150°E-170 °W	0.41
Surface u	Oct/Nov	15-30°S, 140°E-120 °W	0.44
Surface u	Oct/Nov	5°N-15°S, 5-30°W	-0.47
200-mb gZ	Oct/Nov	10-20°S, 15-40°W	-0.45
200-mb gZ	Oct/Nov	10-20°S, 2-100°W	-0.33
500-mb gZ	Oct/Nov	28-40°S, 100°E-175°W	-0.43
500-mb gZ	Oct/Nov	50-65°N, 90-125°E	0.30
500-mb gZ	Oct/Nov	15-25°S, 80-100°W	-0.24
700-mb gZ	Oct/Nov	25-40°S, 100°E-175°W	-0.46
700-mb gZ	Oct/Nov	50-65°N, 90-125°E	0.38
PDO	Oct/Nov	SSTA in Pacific, poleward of 20°N	-0.05
SLP	Oct/Nov	40-60°N, 90-120°E	0.43
SLP	Oct/Nov	25-45°S, 160 E-160°W	-0.44
SST	Oct/Nov	10.5°N-10.5°S, 80-110°W	-0.32
SST	Oct/Nov	35-45°N, 150-170°W	0.25
SST	Oct/Nov	5-30°N, 90-126°E	-0.31
SST	Oct/Nov	5°N-30°S, 2-35°W	-0.37
SST	Oct/Nov	1°N-14°S, 139-159°E	0.29

Appendix B

Table B.1: FORECAST SKILL FOR YEARS WITH LARGE JJA SST ANOMALIES: ENSO events are marked by large SST anomalies in the east and central Pacific. Forecasting these events with skill is very important and useful.

Year	JJA Niño 3.4 Obs	SG Error	CLIPER Error
1988	-1.45	-0.33	-1.25
1975	-1.06	-0.65	-1.12
1998	-1.05	-0.45	-0.40
1973	-0.96	-0.21	-0.71
1999	-0.92	-0.67	-0.79
1954	-0.75	-0.41	-0.62
1955	-0.75	-0.46	-0.72
1964	-0.72	0.07	-0.77
1970	-0.71	-0.21	-0.90
1956	-0.61	-0.45	-0.47
AVG with resp. to sign	-0.90	-0.38	-0.78
AVG without resp. to sign	0.90	0.39	0.78
1963	0.65	0.16	0.63
1957	0.81	-0.18	0.43
1991	0.82	0.37	0.61
2002	0.97	0.64	0.69
1965	1.09	0.12	1.35
1972	1.12	-0.26	0.99
1982	1.17	0.74	0.66
1987	1.71	0.63	1.31
1997	1.81	1.15	1.68
AVG with resp. to sign	1.13	0.37	0.93
AVG without resp. to sign	1.13	0.47	0.93

Table B.2: FORECAST SKILL FOR YEARS WITH LARGE SON SST ANOMALIES: ENSO events are marked by large SST anomalies in the east and central Pacific. Forecasting these events with skill is very important and useful.

Year	SON Niño 3.4 Obs	SG Error	CLIPER Error	Combination Error
1955	-1.86	-2.12	-1.66	-1.94
1988	-1.81	-1.43	-1.17	-1.10
1973	-1.43	-0.64	-0.88	-0.48
1975	-1.38	-1.32	-1.66	-1.55
1970	-1.23	-0.38	-1.39	-0.73
1998	-1.21	-1.19	-0.28	-0.56
1999	-1.10	-0.27	-1.18	-0.56
1964	-1.02	0.29	-1.08	-0.10
1954	-0.92	-0.29	-0.45	-0.14
1995	-0.82	-0.68	-0.16	-0.27
1971	-0.79	0.06	-0.11	0.31
1974	-0.70	0.60	-0.51	0.39
1956	-0.68	-0.24	-0.88	-0.52
1984	-0.66	-0.83	-0.34	-0.11
1983	-0.62	-0.28	0.70	0.54
2000	-0.60	0.37	-0.80	-0.03
1961	-0.55	-0.32	-1.03	-0.74
1962	-0.51	0.47	-0.35	0.31
AVG with resp. to sign	-0.99	-0.46	-0.70	-0.40
AVG without resp. to sign	0.99	0.66	0.81	0.58

Table B.3: FORECAST SKILL FOR YEARS WITH LARGE SON SST ANOMALIES: ENSO events are marked by large warm SST anomalies in the east and central Pacific. Forecasting these events with skill is very important and useful.

Year	SON Niño 3.4 Obs	SG Error	CLIPER Error	Combination Error
1979	0.50	0.17	0.11	-0.04
1953	0.52	0.35	0.27	0.19
1977	0.60	-0.47	0.27	-0.45
1969	0.74	0.56	-0.06	0.02
1976	0.83	1.59	0.00	0.80
1957	0.86	-0.14	0.03	-0.50
1994	0.87	0.06	1.69	0.82
1963	0.90	0.30	0.83	0.38
1991	0.93	1.60	0.58	1.16
1986	0.96	0.87	0.61	0.62
2002	1.47	1.77	1.43	1.65
1965	1.49	0.41	1.64	0.76
1987	1.57	-0.03	0.82	-0.19
1972	1.70	0.81	1.44	0.82
1982	1.94	1.19	0.90	0.62
1997	2.58	1.88	2.03	1.65
AVG with resp. to sign	1.15	0.68	0.79	0.52
AVG without resp. to sign	1.15	0.76	0.79	0.67

Appendix C

Table C.1: ADDITIONAL STATISTICS FOR THE JJA FORECAST: Original statistics and equations were computed based on the Ordinary Least Squares (OLS) technique. This Appendix lists some additional statistics (based on the same 1950-1990 forecast data) computed by the Least Absolute Distance (LAD) method as suggested by Professor P. Mielke.

For the JJA Forecast: Measure of Agreement between x and y: 0.55
Variance Explained: 0.63

For the SON Forecast: Measure of Agreement between x and y: 0.53
Variance Explained: 0.53

PROJECT REPORTS FROM W. M. GRAY'S FEDERALLY SUPPORTED RESEARCH (SINCE 1967)

CSU Dept. of Atmos. Sci. Report No.	Report Title, Author, Date, Agency Support
104	The Mutual Variation of Wind, Shear and Baroclinicity in the Cumulus Convective Atmosphere of the Hurricane (69 pp.). W. M. Gray. February 1967. NSF Support.
114	Global View of the Origin of Tropical Disturbances and Storms (105 pp.). W. M. Gray. October 1967. NSF Support.
116	A Statistical Study of the Frictional Wind Veering in the Planetary Boundary Layer (57 pp.). B. Mendenhall. December 1967. NSF and ESSA Support.
124	Investigation of the Importance of Cumulus Convection and ventilation in Early Tropical Storm Development (88 pp.). R. Lopez. June 1968. ESSA Satellite Lab. Support.
Unnumbered	Role of Angular Momentum Transports in Tropical Storm Dissipation over Tropical Oceans (46 pp.). R. F. Wachtmann. December 1968. NSF and ESSA Support.
Unnumbered	Monthly Climatological Wind Fields Associated with Tropical Storm Genesis in the West Indies (34 pp.). J. W. Sartor. December 1968. NSF Support.
140	Characteristics of the Tornado Environment as Deduced from Proximity Soundings (55 pp.). T. G. Wills. June 1969. NOAA and NSF Support.
161	Statistical Analysis of Trade Wind Cloud Clusters in the Western North Pacific (80 pp.). K. Williams. June 1970. ESSA Satellite Lab. Support.
No. 19-70	A Climatology of Tropical Cyclones and Disturbances of the Western Pacific with a Suggested Theory for Their Genesis/Maintenance (225 pp.). W. M. Gray. NAVWEARSCHFAC Tech. Paper No. 19-70. November 1970. (Available from US Navy, Monterey, CA). US Navy Support.
179	A diagnostic Study of the Planetary Boundary Layer over the Oceans (95 pp.). W. M. Gray. February 1972. Navy and NSF Support.
182	The Structure and Dynamics of the Hurricane's Inner Core Area (105 pp.). D. J. Shea. April 1972. NOAA and NSF Support.
188	Cumulus Convection and Larger-scale Circulations, Part I: A Parametric Model of Cumulus Convection (100 pp.). R. E. Lopez. June 1972. NSF Support.
189	Cumulus Convection and Larger-scale Circulations, Part II: Cumulus and Meso-scale Interactions (63 pp.). R. E. Lopez. June 1972. NSF Support.
190	Cumulus Convection and Larger-scale Circulations, Part III: Broadscale and Meso-scale Considerations (80 pp.). W. M. Gray. July 1972. NOAA-NESS Support.
195	Characteristics of Carbon Black Dust as a Tropospheric Heat Source for Weather Modification (55 pp.). W. M. Frank. January 1973. NSF Support.
196	Feasibility of Beneficial Hurricane Modification by Carbon Black Seeding (130 pp.). W. M. Gray. April 1973. NOAA Support.

CSU Dept. of Atmos. Sci. Report No.	Report Title, Author, Date, Agency Support
199	Variability of Planetary Boundary Layer Winds (157 pp.). L. R. Hoxit. May 1973. NSF Support.
200	Hurricane Spawned Tornadoes (57 pp.). D. J. Novlan. May 1973. NOAA and NSF Support.
212	A Study of Tornado Proximity Data and an Observationally Derived Model of Tornado Genesis (101 pp.). R. Maddox. November 1973. NOAA Support.
219	Analysis of Satellite Observed Tropical Cloud Clusters (91 pp.). E. Ruprecht and W. M. Gray. May 1974. NOAA/NESS Support.
224	Precipitation Characteristics in the Northeast Brazil Dry Region (56 pp.). R. P. L. Ramos. May 1974. NSF Support.
225	Weather Modification through Carbon Dust Absorption of Solar Energy (190 pp.). W. M. Gray, W. M. Frank, M. L. Corrin, and C. A. Stokes. July 1974.
234	Tropical Cyclone Genesis (121 pp.). W. M. Gray. March 1975. NSF Support.
No. 16-75	Tropical Cyclone Genesis in the Western North Pacific (66 pp.). W. M. Gray. March 1975. US Navy Environmental Prediction Research Facility Report. Tech. Paper No. 16-75. (Available from the US Navy, Monterey, CA). Navy Support.
241	Tropical Cyclone Motion and Surrounding Parameter Relationships (105 pp.). J. E. George. December 1975. NOAA Support.
243	Diurnal Variation of Oceanic Deep Cumulus Convection. Paper I: Observational Evidence, Paper II: Physical Hypothesis (106 pp.). R. W. Jacobson, Jr. and W. M. Gray. February 1976. NOAA-NESS Support.
257	Data Summary of NOAA's Hurricanes Inner-Core Radial Leg Flight Penetrations 1957-1967, and 1969 (245 pp.). W. M. Gray and D. J. Shea. October 1976. NSF and NOAA Support.
258	The Structure and Energetics of the Tropical Cyclone (180 pp.). W. M. Frank. October 1976. NOAA-NHEML, NOAA-NESS and NSF Support.
259	Typhoon Genesis and Pre-typhoon Cloud Clusters (79 pp.). R. M. Zehr. November 1976. NSF Support.
Unnumbered	Severe Thunderstorm Wind Gusts (81 pp.). G. W. Walters. December 1976. NSF Support.
262	Diurnal Variation of the Tropospheric Energy Budget (141 pp.). G. S. Foltz. November 1976. NSF Support.
274	Comparison of Developing and Non-developing Tropical Disturbances (81 pp.). S. L. Erickson. July 1977. US Army Support.
No. 77-01	Tropical Cyclone Research by Data Compositing (79 pp.). W. M. Gray and W. M. Frank. July 1977. US Navy Environmental Prediction Research Facility Report. Tech. Paper No. 77-01. (Available from the US Navy, Monterey, CA). Navy Support.
277	Tropical Cyclone Cloud and Intensity Relationships (154 pp.). C. P. Arnold. November 1977. US Army and NHEML Support.

CSU Dept. of Atmos. Sci. Report No.	Report Title, Author, Date, Agency Support
297	Diagnostic Analyses of the GATE A/B-scale Area at Individual Time Periods (102 pp.). W. M. Frank. November 1978. NSF Support.
298	Diurnal Variability in the GATE Region (80 pp.). J. M. Dewart. November 1978. NSF Support.
299	Mass Divergence in Tropical Weather Systems, Paper I: Diurnal Variation; Paper II: Large-scale Controls on Convection (109 pp.). J. L. McBride and W. M. Gray. November 1978. NOAA-NHEML Support.
No. 78-01	New Results of Tropical Cyclone Research from Observational Analysis (108 pp.). W. M. Gray and W. M. Frank. June 1978. US Navy Environmental Prediction Research Facility Report. Tech. Paper No. 78-01. (Available from the US Navy, Monterey, CA). Navy Support.
305	Convection Induced Temperature Change in GATE (128 pp.). P. G. Grube. February 1979. NSF Support.
308	Observational Analysis of Tropical Cyclone Formation (230 pp.). J. L. McBride. April 1979. NOAA-NHEML, NSF and NEPRF Support.
No. CR-79-06	Tropical Cyclone Origin, Movement and Intensity Characteristics Based on Data Compositing Techniques (124 pp.). W. M. Gray. August 1979. US Navy Environmental Prediction Research Facility Report. Tech. Paper No. CR-79-06. (Available from the US Navy, Monterey, CA). Navy Support.
No. CR-81-02	Further Analysis of Tropical Cyclone Characteristics from Rawinsonde Compositing Techniques (129 pp.). W. M. Gray. March 1981. US Navy Environmental Prediction Research Facility Report. Tech. Paper No. CR-81-02. (Available from the US Navy, Monterey, CA). Navy Support.
333	Tropical Cyclone Intensity Change–A Quantitative Forecasting Scheme. K. M. Dropco. May 1981. NOAA Support.
Unnumbered	Recent Advances in Tropical Cyclone Research from Rawinsonde Composite Analysis (407 pp.). WMO Publication. W. M. Gray. 1981.
340	The Role of the General Circulation in Tropical Cyclone Genesis (230 pp.). G. Love. April 1982. NSF Support.
341	Cumulus Momentum Transports in Tropical Cyclones (78 pp.). C. S. Lee. May 1982. ONR Support.
343	Tropical Cyclone Movement and Surrounding Flow Relationships (68 pp.). J. C. L. Chan and W. M. Gray. May 1982. ONR Support.
346	Environmental Circulations Associated with Tropical Cyclones Experiencing Fast, Slow and Looping Motions (273 pp.). J. Xu and W. M. Gray. May 1982. NOAA and NSF Support.
348	Tropical Cyclone Motion: Environmental Interaction Plus a Beta Effect (47 pp.). G. J. Holland. May 1982. ONR Support.
Unnumbered	Tropical Cyclone and Related Meteorological Data Sets Available at CSU and Their Utilization (186 pp.). W. M. Gray, E. Buzzell, G. Burton and Other Project Personnel. February 1982. NSF, ONR, NOAA, and NEPRF Support.
352	A Comparison of Large and Small Tropical Cyclones (75 pp.). R. T. Merrill. July 1982. NOAA and NSF Support.

CSU Dept. of Atmos. Sci. Report No.	Report Title, Author, Date, Agency Support
358	On the Physical Processes Responsible for Tropical Cyclone Motion (200 pp.). Johnny C. L. Chan. November 1982. NSF, NOAA/NHRL and NEPRF Support.
363	Tropical Cyclones in the Australian/Southwest Pacific Region (264 pp.). Greg J. Holland. March 1983. NSF, NOAA/NHRL and Australian Government Support.
370	Atlantic Seasonal Hurricane Frequency, Part I: El Nino and 30 mb QBO Influences; Part II: Forecasting Its Variability (105 pp.). W. M. Gray. July 1983. NSF Support.
379	A Statistical Method for One- to Three-Day Tropical Cyclone Track Prediction (201 pp). Clifford R. Matsumoto. December, 1984. NSF/NOAA and NEPRF support.
No. CR 84-08	Varying Structure and Intensity Change Characteristics of Four Western North Pacific Tropical Cyclones. (100 pp.). Cecilia A. Askue and W. M. Gray. October 1984. US Navy Environmental Prediction Research Facility Report No. CR 84-08. (Available from the US Navy, Monterey, CA). Navy Support.
No. CR 84-11	Characteristics of North Indian Ocean Tropical Cyclone Activity. (108 pp.). Cheng-Shang Lee and W. M. Gray. December 1984. US Navy Environmental Prediction Research Facility Report No. CR 84-11. (Available from the US Navy, Monterey, CA). Navy Support.
391	Typhoon Structural Variability. (77 pp.). Candis L. Weatherford. October, 1985. NSF/NOAA Support.
392	Global View of the Upper Level Outflow Patterns Associated with Tropical Cyclone Intensity Change During FGGE. (126 pp.). L. Chen and W. Gray. October, 1985. NASA support.
394	Environmental Influences on Hurricane Intensification. (156 pp.). Robert T. Merrill. December, 1985. NSF/NOAA Support.
403	An Observational Study of Tropical Cloud Cluster Evolution and Cyclogenesis in the Western North Pacific. (250 pp.). Cheng-Shang Lee. September, 1986. NSF/NOAA support.
No. CR 87-10	Recent Colorado State University Tropical Cyclone Research of Interest to Forecasters. (115 pp.). William M. Gray. June, 1987. US Navy Environmental Prediction Research Facility Contractor Report No. CR 87-10. Available from US Navy, Monterey, CA. Navy support.
428	Tropical Cyclone Observation and Forecasting With and With and Without Aircraft Reconnaissance. (105 pp.) Joel D. Martin. May, 1988. USAF, NWS, ONR support.

CSU Dept. of Atmos. Sci. Report No.	Report Title, Author, Date, Agency Support
429	Investigation of Tropical Cyclone Genesis and Development Using Low-level Aircraft Flight Data. (94 pp.) Michael G. Middlebrooke. May, 1988. USAF, NSF support.
436	Environmental and convective influence on tropical cyclone development vs. non–development. (105 pp.) Patrick A. Lunney. December, 1988.
446	The structural evolution of typhoons. (198 pp.). Candis Weatherford. September, 1989. NSF/NOAA and ONR Support
457	Relationships between tropical cyclone deep convection and the radial extent of damaging winds. (109 pp.) Daniel N. Shoemaker. October, 1989. AFGL Support.
468	Associations between West Pacific equatorial zonal winds and East Pacific SST anomalies. (103 pp.) Christopher C. Collimore. May, 1990. NSF Support.
480	An observational analysis of tropical cyclone recurvature. (124 pp.). Stephen J. Hodanish. May, 1991. ONR Support.
484	West African monsoonal rainfall and intense hurricane associations. (270 pp.). Christopher W. Landsea. October, 1991. NSF Support.
508	Tropical cyclone motion and recurvature in TCM-90. (80 pp.). Michael E. Fitzpatrick. September, 1992. ONR Support.
520	Evidence of a stratospheric QBO modulation of tropical convection. (91 pp.). John A. Knaff. January, 1993. NSF and NOAA Support.
598	Understanding and forecasting tropical cyclone intensity change. (346 pp.). Patrick J. Fitzpatrick. March, 1996. AF Support.
Unnumbered	The outer radius tangential winds of tropical cyclones. Stephen B. Cocks. MS Thesis. Spring 1998.
Unnumbered	Multi-platform exploration of the inner-core intensity change for hurricane Marilyn (1995) (132 pp). Kelly Marie Carpenter. MS Thesis. August, 1999.
683	Instrument wetting errors in hurricanes and a re-examination of inner-core thermodynamics (203 pp.). Matthew D. Eastin. August 1999. NSF and NOAA/CIRA Support.
Unnumbered	Hurricane inner-core structure as revealed by GPS dropwindsondes. (56 pp.) Robert N. LeeJoice. MS Thesis. Summer, 2000. Air Force and NSF Support.
Unnumbered	Variability of tropical cyclone wind-pressure relationships. (110 pp.) Steven E. Vilpors. MS Thesis. Summer, 2001. Air Force and NSF Support.
719	Prediction of August Atlantic basin hurricane activity. (80 pp.) Eric S. Blake. MS Thesis. Spring, 2002. NSF, USAA, and State Farm Support
Unnumbered	Forecasting September Atlantic basin tropical cyclone activity at zero and one month lead times. (pp.). Philip J. Klotzbach. MS Thesis. Summer, 2002. NSF Support.